R005-01
Zoom meeting C ：11/1 AM1 (9:00-10:30)
9:00〜9:15

極冠域プラズマホールの生成について

#小原 隆博 [1)]
(1 東北大 惑星プラズマ

Formation of Polar Cap Plasma Hole

#Takahiro Obara[1)]
(1PPARC, Tohoku University

In the night side polar cap region, the low density of the ionospheric plasma, called the polar cap plasma hole, was first studied in 1978. The formation of the polar hole is more often connected to the prolonged recombination in darkness. During the magnetically quiet condition, the polar hole forms as a result of slow anti-sunward convection across the dark polar cap. Vertical sounder experiment, which was carried out by Ohzora satellite in 1985, revealed that the polar hole structure appeared in the night side polar cap, extending down to the peak height (˜200km) of the ionosphere. In cases of noon-night passes, plasma density monotonically decreased from the noon side to the night side, forming deep plasma hole just poleward of the night side auroral oval. By using the gradient of the slope, we have evaluated loss time constant of O+. Results demonstrated that the loss time constant is at about 2,000 sec, assuming the weakened convection speed (˜0.1 km/sec) across the polar cap.

夜側の極冠域電離層に, プラズマ密度が極端に少ない領域（ホール）が生成される事が,1978 年に発見されている. 日照が無い夜側の極冠域では, 昼側からの供給が乏しい時, プラズマの消失が続き, ホールになると考えられた.1985 年に, おおぞら衛星が, 極冠域を昼側から夜側に横切って, 電離層の立体構造を観測したが, 幾つかのパスにおいて, ホールが観測された. それらの観測では, プラズマ密度が昼側から夜側に向かって緩やかに減少し, プラズマ密度の極小が, 夜側のオーロラオーバル境界に出現していた. プラズマ密度の傾斜は, 極冠の対流速度の減少によるとして, 対流速度を秒速 0.1km とした場合, 電離層プラズマ消失の時定数は,2000 秒と求められた. 講演では, ホールの出現特性や, プラズマの不規則構造の同時発生についても, 詳しく報告する.

R005-02
Zoom meeting C ：11/1 AM1 (9:00-10:30)
9:15〜9:30

Improvement of the Auroral Computed Tomography analysis method for each aurora type

#Yoshimasa Tanaka[1)],Yasunobu Ogawa[2)],Mizuki Fukizawa[3)],Takeshi Sakanoi[4)],Keisuke Hosokawa[5)],Takuo Tsuda[5)],Akira Kadokura[6)]
([1]NIPR/ROIS-DS/SOKENDAI,([2]NIPR,([3]Graduate School of Science, Tohoku University,([4]PPARC, Grad. School of Science, Tohoku Univ.,([5]UEC,([6]ROIS-DS/NIPR

Auroral Computed Tomography (ACT) is a method to reconstruct the three-dimensional (3-D) spatial distribution of the auroral luminosity and the energy distribution of the precipitating electrons from auroral images taken simultaneously at multiple observation sites. So far, the ACT method has been mainly applied to discrete auroras, and has been clarified to be effective in estimating their altitude profiles and the energy spectra of the precipitating electrons. It is generally difficult to reconstruct the 3-D distribution of faint auroral phenomena, such as pulsating auroras, by the ACT analysis. Due to the development of high-sensitivity imagers, however, there is a growing demand for the use of ACT analysis for the pulsating auroras. The improvement the ACT method and analysis procedures is required to reconstruct the 3-D distribution of the pulsating aurora.

In this study, we summarize the ACT analysis method and its key points separately for the discrete auroras and pulsating auroras. In particular, we focus on the following points: (1) the reduction of the effect of the diffuse auroras, (2) the estimation of the relative sensitivity between imagers, (3) the determination of the hyper-parameters of the regularization term, and (4) the validation of the reconstruction results using model auroras. We have also extended the ACT method to more generalized one, the G-ACT method, which retrieve the 3-D spatial distribution of the aurora (and ionospheric electron density) and the energy distribution of the precipitating electrons by combining multiple auroral images with ionospheric electron density observed by radars. We also show the points to be considered when combining optical data and ionospheric electron density data in this G-ACT analysis.

R005-03
Zoom meeting C ：11/1 AM1 (9:00-10:30)
9:30〜9:45

オーロラコンピュータトモグラフィによる脈動オーロラの3次元構造と降下電子の再構成

#吹澤 瑞貴[1)], 坂野井 健[2)], 田中 良昌[3)], 小川 泰信[4)]
([1] 東北大・理,[2] 東北大・理・PPARC,[3] 国立極地研究所/ROIS-DS/総研大,[4] 極地研,[5] ノルウェー北極大学 - トロムソ大学,[6] フィンランド気象研究所,[7] 欧州非干渉散乱レーダー科学協会,[8] オウル大学ソダンキラ地球物理観測所,[9] スウェーデン宇宙物理学研究所

Reconstruction of the three-dimensional structure and precipitating electrons of pulsating auroras by Aurora Computed Tomography

#Mizuki Fukizawa[1)],Takeshi Sakanoi[2)],Yoshimasa Tanaka[3)],Yasunobu Ogawa[4)],Bjorn Gustavsson[5)],Kirsti Kauristie[6)],Carl-Fredrik Enell[7)],Alexander Kozlovsky[8)],Tero Raita[8)],Urban Brandstrom[9)],Tima Sergienko[9)]
([1]Graduate School of Science, Tohoku University,[2]PPARC, Grad. School of Science, Tohoku Univ.,[3]NIPR/ROIS-DS/SOKENDAI,[4]NIPR,[5]UiT - The Arctic University of Norway,[6]Finnish Meteorological Institute,[7]EISCAT Scientific Association,[8]Sodankyla Geophysical Observatory, University of Oulu,[9]Swedish Institute of Space Physics

Aurora Computed Tomography (ACT) is an inversion analysis method to reconstruct the three-dimensional (3-D) distribution of auroral luminosity and the energy and spatial distributions of precipitating electrons from monochromatic auroral images obtained with multiple ground-based optical instruments (e.g., Aso et al., EPS, 1998). The ACT method has been applied to discrete auroras (e.g., Tanaka et al., Ann. Geophys., 2011). On the other hand, it is relatively difficult to reconstruct the 3-D structure of pulsating auroras (PsAs) by ACT since PsAs generally have low contrast and faint structures. Therefore, there have been no reports of 3-D reconstruction of PsAs so far.

This study aims (1) to reconstruct the 3-D distribution of the PsA emission intensity and the energy and spatial distribution of precipitating electrons and (2) to estimate the 3-D distribution of the ionospheric electron density from the reconstructed volume emission rate.

We used monochromatic auroral images obtained with three all-sky imagers in Skibotn (69.35 degrees north, 18.82 degrees east), Kilpisjarvi (69.05 degrees north, 20.36 degrees east), and Abisko (68.36 degrees north, 18.82 degrees east) during the substorm recovery phase in 0-2 UT on 18 February 2018. The observation wavelength is 427.8 nm and temporal resolution is 2 s. We selected PsA patches observed at the observation point of the EISCAT radar in Tromsoe (69.58 degrees north, 19.23 degrees east).

We applied ACT to the PsA patches and obtained the 3-D distribution of the volume emission rate from the auroral images. The background diffuse auroral emission was subtracted from the auroral images as uniform emission to reduce noises before conducting ACT. The peak altitudes of the reconstructed volume emission rates were 92-96 km and the full widths at half maximum were 18-22 km.

The horizontal distributions of the reconstructed precipitating electrons' average energy were high at the edge of the PsA patches. The total energy flux of the reconstructed precipitating electrons was proportional to the square of the average energy. This relationship indicates that the precipitating electrons are accelerated by a filed-aligned electric potential drop at the edge of the PsA patches (Ono and Morishima, GRL, 1994). To confirm whether these distributions are artifacts from the ACT analysis, ACT was applied to the pseudo images obtained by solving the forward problem assuming that the precipitating electrons have a uniform total and average energy distributions on the horizontal plane. The horizontal distribution of the reconstructed precipitating electrons' average energy was uniform and not high at the edge of the PsA patch. This indicates that ACT could solve the inversion problem correctly and that the result obtained from observation data would not be artifacts.

The 3-D distribution of ionospheric electron density was derived from the reconstructed precipitating electrons by solving the continuity equation for electron density with the steady state assumption. We compared the reconstruction results with the EISCAT radar data.. The error between them was small when the PsA emission intensity was large. However, the derived electron density was underestimated compared to that observed by the EISCAT radar as the PsA emission intensity attenuated. Therefore, the electron density was obtained by solving the continuity equation by the Runge-Kutta method without the steady state assumption. The error at the time when the PsA emission intensity attenuated became smaller. This result indicates that it is necessary to consider the time constant of recombination between electrons and ions when deriving the electron density from the volume emission rate of 427.8 nm especially for PsAs having quasi-periodic temporal modulations.

Through this study, we were able to reconstruct the energy and spatial distribution of precipitating electrons that cause PsA and the 3-D distribution of volume emission rate from auroral images with a wavelength of 427.8 nm observed from three points on the ground. It is expected that more realistic reconstruction results can be obtained by combining the auroral images and the 3D observation data of the ionospheric electron density by EISCAT_3D radar, which will start observation in the late 2022.

オーロラコンピュータトモグラフィ（ACT）は地上多地点に設置された単一波長のオーロラ画像から逆問題を解く

ことによってオーロラ発光強度の 3 次元分布や降下電子のエネルギー・空間分布を再構成する手法である (e.g., Aso et al., EPS, 1998)。これまで ACT はディスクリートオーロラに適用されてきた (e.g., Tanaka et al., Ann. Geophys., 2011)。一方、脈動オーロラはディスクリートオーロラよりも構造のコントラストが低く暗い発光であるため、発光強度の 3 次元構造を ACT により再構成することが難しい。このために脈動オーロラの 3 次元構造の報告例はなかった。

本研究は、ACT 解析により、（1）脈動オーロラパッチの体積放射率の 3 次元分布と降下電子のエネルギー・空間分布を再構成すること、さらに、（2）再構成された体積放射率から電離圏電子密度の 3 次元分布を推定することを目的とする。

観測データは北欧の 3 地点（Skibotn（69.35°N、18.82°E)、Kilpisjarvi（69.05°N、20.36°E)、Abisko（68.36°N、18.82°E））に設置された全天カメラによって 2018 年 2 月 18 日 0 - 2 UT のサブストーム回復相に取得された画像を使用した。観測波長は 427.8 nm であり、時間分解能は 2 秒である。これら 3 つの全天画像の視野内の内、Tromsø(69.58° N, 19.23° E) に設置された EISCAT UHF レーダー観測点上で観測された脈動オーロラパッチに対して ACT を行った。

脈動オーロラの背景で発光しているディフューズオーロラ発光を一様な発光と仮定して観測画像から差し引くことで、3 地点の観測画像から ACT により脈動オーロラの 3 次元体積放射率と降下電子のエネルギー・空間分布を再構成することができた。再構成された体積放射率のピーク高度は 92-96 km, 発光層の半値全幅は 18-22 km であった。

再構成された降下電子の平均エネルギーの水平面分布は脈動オーロラパッチのエッジで高くなっていた。再構成された降下電子フラックスの全エネルギーは平均エネルギーの 2 乗に比例し、この関係は脈動オーロラパッチのエッジにおいて降下電子が沿磁力線電位降下によって加速された可能性を示唆する (Ono and Morishima, GRL, 1994)。この構造が　ACT　解析によるエラーでないか確かめるために、水平面に一様な全エネルギーと平均エネルギーの分布を持った降下電子から順問題を解くことで得た擬似画像に対して　ACT　を行った。その結果、再構成された降下電子の平均エネルギーの水平面分布はエッジで高くならず、一様な分布が得られた。この結果は、観測画像からの再構成で得られた、パッチのエッジで降下電子の平均エネルギーが高い構造は　ACT　解析によるエラーではないことを示唆する。

また、定常状態を仮定して電子密度の連続の式を解くことで、再構成された体積放射率から電子密度を求めた。その結果、脈動オーロラが発光している最中は EISCAT レーダー観測データとよく似た高度分布が得られた。しかし、脈動オーロラの発光強度が減衰していくと観測データよりも過小評価となった。そこで、定常状態を仮定せずに連続の式をルンゲ・クッタ法により解くことで電子密度を求めたところ、オーロラ発光強度が減衰した時間でも観測データに近い高度分布が得られた。この結果は、427.8 nm 発光と電子密度の時間変動には時間差があることを意味し、特に脈動オーロラのように準周期的な変動を伴う 427.8 nm の体積放射率から電子密度を求める際には、電子とイオンとの再結合の時定数を考慮する必要があることを示す。

本研究により、地上 3 地点から観測された波長 427.8 nm のオーロラ画像を用いて脈動オーロラを発光させる降下電子のエネルギー・空間分布と体積放射率の 3 次元分布を再構成することができた。2022 年度後半から観測が始まる EISCAT 3D レーダーによる電離圏電子密度の 3 次元観測データと多点のオーロラ画像を組み合わせて再構成を行うことで、より現実を反映した信頼性のある再構成結果が得られることが期待される。

R005-04
Zoom meeting C ：11/1 AM1 (9:00-10:30)
9:45〜10:00

#川村 美季[1)], 坂野井 健[1)], 吹澤 瑞貴[1)], 三好 由純[2)], 細川 敬祐[3)], 土屋 史紀[1)], 加藤 雄人[1)], 小川 泰信[4)], 浅村 和史[5)], 齊藤 慎司[6)], スペンス ハラン[7)], ジョンソン アルロ[8)], 大山 伸一郎[2)], ウルバン ブランドストローム[9)]
([1 東北大学,([2 名大 ISEE,([3 電通大,([4 極地研,([5 宇宙研,([6 情報通信研究機構,([7 ニューハンプシャー大学,([8 モンタナ大学,([9 スウェーデン宇宙物理研究所

Simultaneous pulsating aurora and microburst observations with ground-based fast auroral imagers and CubeSat FIREBIRD-II

#Miki Kawamura[1)],Takeshi Sakanoi[1)],Mizuki Fukizawa[1)],Yoshizumi Miyoshi[2)],Keisuke Hosokawa[3)],Fuminori Tsuchiya[1)],Yuto Katoh[1)],Yasunobu Ogawa[4)],Yasunobu Ogawa[5)],Shinji Saito[6)],Harlan Spence[7)],Arlo Johnson[8)],Shin'ichiro Oyama[2)],Brandstorm Urban[9)]

([1TU,([2ISEE, Nagoya Univ.,([3UEC,([4NIPR,([5ISAS/JAXA,([6NICT,([7Univ. New Hampshire,([8Montana State University,([9Swedish Institute of Space Physics

We report the relationship between pulsating aurora and relativistic electron microburst using simultaneous observation of ground-based fast auroral imagers and the FIREBIRD-II CubeSat for the first time.

Miyoshi et al. (2020)has proposed that both of the 10 keV electron that generates pulsating aurora and microburst (high-speed modulation of MeV electron at 1 Hz or higher) are caused by chorus waves propagating along the field line. However, simultaneous pulsating aurora and microbursts were not reported so far. In this study, we examined the data taken by ground optical auroral EMCCD imagers (100 FPS, BG3 grass filter) at two locations (Sodankyla (67.37 degree north, 26.63 degree east) and Tjautjas (67.31 degree north, 20.73 degree east)) and high-energy electron data (˜220 keV to >1 MeV) obtained by a low-altitude (433 ˜632 km) satellite FIREBIRD-II CubeSat Flight Unit 4 (FU4) to clarify the relationship between pulsating aurora and microburst. We found one event when FU4 passed over the pulsating auroral patch at latitude 67.1 degree north and longitude 23.1 degree east (L = 5.4) during the period from 00:28:16 UT to 00:28:19 UT on October 8 ,2018. FU4 observed the energy-dispersed precipitating electrons, i.e., sub-relativistic/relativistic microburst, from ˜210eV to ˜MeV. On the other hand, all-sky imagers observed pulsating auroral variations with a typical period of 2 sec with internal modulations of 300ms (˜3Hz). Similar 3Hz modulations were also seen in the high-energy electron precipitations obtained with FU4. We carried out detailed analysis of the timings of the electron precipitations in the energy range higher than ˜220 keV the timing of the pulsating auroral emission. We found that the start time of the pulsating auroral emission was ˜585 ms later than those of the electron precipitations in the energy range higher than ˜220 keV. We calculated the velocity dispersion of precipitating electrons, which have been theoretically derived in Miyoshi et al.(2010,2020) and Saito et al.(2012), at L = 5.4 to explain the delays estimated above. In this analysis, we assumed that the electron density n of 10 /cmˆ3 is constant along the same field line, the sweep rate of the rising tone element to 2 kHz/s, and used the dipole magnetic field model. The time accuracy of FIREBIRD and EMCCD to the Universal Time is ± 55 ms and ± 10 ms respectively. The estimated velocity dispersion curves reproduce overall trend of the observed energy dispersion by FU4 and EMCCD. The results confirmed for the first time the theoretical prediction by Miyoshi et al.(2020) that the relativistic electron microburst is a high-energy tail of the pulsating aurora electrons, and show that the chorus waves propagating from the magnetic equator to the high-latitudes cause wide energy electron scattering from a few keV to MeV.

本研究では、FIREBIRD-IICubeSat 衛星と地上全天イメージャーによる脈動オーロラとマイクロバーストの同時観測結果について報告する。

脈動オーロラを発生させる˜10keV 電子とマイクロバースト（MeV 電子の 1 Hz 以上の高速変調) はともに磁気赤道付近のコーラス波により引き起こされるモデルが提唱されているが、両者が同時に観測された例はまだ無く実証されていない。そこで、本研究では北欧の Sodankyla(北緯 67.37 ° 東経 26.63 °) と Tjautjas(北緯 67.31 °、東経 20.73 °) の 2 地点に設置された EMCCD イメージャー（サンプリング周波数 100Hz、BG3 ガラスフィルター）による全天オーロラ観測と、低高度（高度 433 - 632km）衛星 FIREBIRD-II CubeSat Flight Unit4 (FU4) による˜ 220 keV から˜ MeV の高エネルギー電子観測との同時観測による脈動オーロラとマイクロバーストのイベント解析を実施した。2018 年 10 月 8 日 00:28:16-00:28:19 UT において、地上イメージャーにより捉えられた北緯 67.1 ° 東経 23.1 ° (L = 5.4) 近傍の脈動オーロラのパッチ上空を FU4 が通過した。このとき、˜220 keV から˜MeV の範囲に速度分散構造をもつマイクロバーストが観測された。地上イメージャーでは、脈動オーロラ発光の 2 秒周期の主脈動内に 1 秒以下の内部変調が観測された。一方で、FU4 の高エネルギー電子にも同様の 1 秒以下の周期の変調が見られた。この脈動オーロラとマイクロバーストの同時観測は世界初である。また、FU4 が観測した 220 keV 以上の電子降下と脈動オーロラの発光の立ち上がりの時間差は、約 585ms 高エネルギーの電子降下のほうが先行していた。この観測結果に対して、Miyoshi et al. (2010, 2020) や Saito et al. (2012) で示された磁気赤道から高緯度に伝搬するコーラス波動により、磁力線上の異なる緯度で電子が散乱されたことにより生じる Time-of-flight(TOF) モデル計算を行い、観測された降下電子の速度分散を検証した。この TOF モデルでは、L=5.4 の地点において、磁力線上での密度 n=10 /(cm)ˆ3、双極子磁場モデル、また、

コーラスエレメントの Sweep rate を 2 kHz/s と仮定した。FIREBIRD と EMCCD の時間精度はそれぞれ± 55ms と± 10ms であるが、想定されたパラメータを使用した TOF モデルは FU4 および EMCCD によって観測されたエネルギー分散の全体的な傾向を再現した。この結果は、Miyoshi et al.(2020) が提案した脈動オーロラと相対論的マイクロバーストの起源が同一であるというモデルを実証するものでありコーラス波動が脈動オーロラからマイクロバーストまでの広いエネルギー帯の電子降下が同時に引き起こすことを示すものである。

R005-05
Zoom meeting C ：11/1 AM1 (9:00-10:30)
10:00〜10:15

カナダ･アサバスカにおけるサブオーロラ帯オーロラアーク分離の統計解析:STEVEに関する新しい考察

#ヤダフ スネア [1)], 塩川 和夫 [1)], 大塚 雄一 [1)],Connors Martin[2)]
[(1] 名大宇地研,[(2]Center for Science, Athabasca Univ.

Statistical study of subauroral arc detachment at Athabasca, Canada: new insights on STEVE

#SNEHA YADAV[1)],Kazuo Shiokawa[1)],Yuichi Otsuka[1)],Martin Connors[2)]
[(1]ISEE, Nagoya Univ.,[(2]Center for Science, Athabasca Univ.

In the past, individual statistical study of SAR (stable auroral red) arc and STEVE (strong thermal emission velocity enhancement) have been carried out at subauroral latitudes (Takagi et al., 2018 and Gallardo Lacourt et al., 2018). However, detailed comparative statistical study of geomagnetic conditions for different subauroral arcs at a single station is missing from the literature. A statistical study of subauroral arc with simultaneous emission in red and green-line also remains unexplored. The comparative statistical study of different arcs is important to understand the specific geomagnetic conditions under which the arcs develop as red arc, red+green arc, and STEVE. In this study, we present the first comparative statistical study of subauroral arc detachment from the main auroral oval at Athabasca (magnetic latitude = 61.5 N), Canada, for three different types of subauroral arcs: pure red arc, red arc with simultaneous emission in green-line (red+green arc), and STEVE. Based on 15-years (2006-2020) of all-sky imaging observations, this study not only uncovers the occurrence characteristics of different arcs but also provides important insights into the specific geomagnetic conditions under which STEVE develops. Red arc was the most common subauroral arc (139 events), followed by red+green arc (44 events), and STEVE (26 events) was a rare phenomenon. The detachment rate of red and red+green arcs exhibits dependence on both the solar flux and geomagnetic activity. The detachment rate of STEVE was higher during premidnight, whereas red and red+green arcs were higher around the midnight sector. The geomagnetic activity was relatively higher for STEVE, the decrease in the AL index and local X-component magnetic variations were ˜2-3 times higher for STEVE as compared to other arcs. STEVE shows a strong association with asymmetric ring current in terms of prominent bay-like enhancement in ASY-H index prior to the STEVE detachment. Such bay-like enhancement was ˜4 times higher for STEVE as compared to other arcs. STEVE events were accompanied by dispersionless injection for both electron and proton flux at the geosynchronous orbit. These results unambiguously suggest that STEVE develops after the substorm associated energy injection and significant intensification of asymmetric ring current in the dusk sector.

R005-06
Zoom meeting C ：11/1 AM2 (10:45-12:30)
10:45〜11:00

Effects of CIR- and CME-driven magnetic storm on ion upflows in the low-altitude polar ionosphere

#Masayoshi Takada[1)],Kanako Seki[2)],Yasunobu Ogawa[3)],Kunihiro Keika[4)]
([1]Earth and Planetary Science, Tokyo Univ.,([2]Dept. Earth & Planetary Sci., Science, Univ. Tokyo,([3]NIPR,([4]University of Tokyo

Molecular ions (O_2^+/NO^+/N_2^+) in the ring current of the terrestrial magnetosphere have been observed during the magnetic storms [e.g., Klecker et al., 1986; Seki et al., 2019]. These ions originate from the low-altitude ionosphere. In the ionosphere, upward ion transports (upflows) supply sources of the ions outflowing to the magnetosphere. Since the molecular ions usually exist in the low-altitude (<300 km) ionosphere and can be affected by neutral winds, the generation mechanisms and properties of ion upflows to transport molecular ions are different from those of O^+ [e.g., Ogawa et al., 2010; Yamazaki et al., 2017]. In particular, their dependence on solar activities is one of the important properties to understand formation mechanisms of the ion upflows. In a previous study by Ogawa et al. [2019], the characteristics of O^+ ion upflows in the polar ionosphere were investigated during CIR- and CME-driven magnetic storms by using EISCAT radars. They reported that the upflows during CIR- and CME-driven storms have different dependence on magnetic local time. For the CIR-driven storms, upward ion flux around noon was pronounced, while it was enhanced around midnight during the CME-driven storms. Their study focused on the ion upflows in the altitude range between 400 and 500 km, where O^+ is the dominant species, and responses of the ion upflows to the different type of magnetic storms in the low-altitude ionosphere, where molecular ions exist, are far from understood. The purpose of this study is thus to understand effects of CIR- and CME-driven magnetic storms on ion upflows in the low-altitude ionosphere based on long-term observations of the EISCAT radars.

We used data from the EISCAT UHF radar at Tromso and Svalbard radar at Longyearbyen from January 1, 1996 to January 1, 2016, and investigated statistical properties of ion upflows and ionospheric conditions during CIR- and CME-driven magnetic storms. We used 5-minute time resolution data when the radar was looking along the local magnetic field line. The ionospheric parameters such as electron density, ion velocity, and ion and electron temperatures were averaged over 250-350 km altitudes. We screened data to exclude unrealistic values with the following criteria: Absolute value of ion velocity was less than 1500 m/s, ion and electron temperatures were less than 10000 K, and electron density was more than 10^{10} m^{-3} and less than 10^{13} m^{-3}. To understand the similarity and difference between low- and high- altitude upflows, we compared data at different altitude ranges using results from the previous study [Ogawa et al., 2019]. The results show that the upward velocity in the nightside at Tromso increased with increasing altitude in the main phase of both CIR- and CME-driven magnetic storms. On the other hand, the upward flux in the nightside at Longyearbyen was not enhanced at any altitude after CIR-driven storms, whereas it increased from the low-altitude region after CME-driven storms. It was also confirmed that any effect of the magnetic storms that was remarkable at the higher altitudes reported in the previous study [Ogawa et al., 2019] was not seen in the dayside low-altitude ionosphere at Longyearbyen. In the presentation, we will also discuss dependence of the low-altitude upflows on ion/electron temperature and density.

References:

[1] B. Klecker et al., Discovery of energetic molecular ions (NO+ and O2+) in the storm time ring current, Geophys. Res. Lett., 13, 632-635, 1986

[2] K. Seki et al., Statistical Properties of Molecular Ions in the Ring Current Observed by the Arase (ERG) Satellite, Geophys. Res. Lett., 46, 8643-8651, 2019

[3] Y. Ogawa et al., Solar activity dependence of ion upflow in the polar ionosphere observed with the European Incoherent Scatter (EISCAT) Tromso UHF radar, J. Geophys. Res., 115, A07310, 2010

[4] Y. Yamazaki et al., Average field-aligned ion velocity over the EISCAT radars, J. Geophys. Res. Space Physics, 122, 5630-5642, 2017

[5] Y. Ogawa et al., Characteristics of CME- and CIR-driven ion upflows in the polar ionosphere, J. Geophys. Res. Space Physics, 124, 3637-3649, 2019

R005-07
Zoom meeting C ：11/1 AM2 (10:45-12:30)
11:00〜11:15

Statistical investigation of polar mesosphere winter echoes by the PANSY radar: Superposed epoch analysis to substorm activities

#Kiyoka Murase[1)],Takanori Nishiyama[1,2)],Ryuho Kataoka[1,2)],Yoshimasa Tanaka[1,2,4)],Kaoru Sato[3)],Masaki Tsutsumi[1,2)], Yasunobu Ogawa[1,2)]
([1]Polar Science, SOKENDAI,([2]NIPR,([3]Graduate School of Science, Univ. of Tokyo,([4]ROIS-DS

One of the interesting aspects of the polar atmosphere is the effect of geomagnetic activities on the neutral atmosphere. Polar mesosphere winter echo (PMWE) is a coherent echo observed by VHF radars in the polar region during the winter period. The enhancement of echo power is influenced by not only the existence of the atmospheric turbulence (Yamamoto et al., 1986) but also the ionization due to energetic particle precipitation (EPP) during geomagnetically disturbed periods (Nishiyama et al., 2018). Recent studies reported enhancements of PMWE during substorms corresponding to EPP in a shorter timescale from several minutes to hours (Kataoka et al, 2019; Tanaka et al., 2019).

In this study, we statistically investigated the dependence of PMWE appearance on EPP during substorms. We used the data of the mesospheric echo power observed by the PANSY radar (Sato et al., 2014) at Syowa station (39.6E, 69.0S; CGMLAT=-66.5) in the Antarctic region in two austral winter seasons from 2017. The substorm activity is categorized by the amplitude of the southward excursion of the local magnetic field at Syowa station, which is a proxy of the amplitude of auroral electrojets. The timing of the minimum values of the north-south component (H_{min}) is used as zero epoch time, and the altitude-resolved echo powers are superposed.

First, positive dependencies of PMWE duration to the substorm activities are found during nighttime. The cosmic noise absorption at Syowa station is larger on average for larger activities, suggesting statistical dependencies of PMWE on ionization due to EPP during substorms. PMWE is enhanced at 75-85 km on average for any activity level, while they reach 70 km before and after the zero epoch time for larger substorms, where H_{min} is less than -600 nT (shown in the figure). On the other hand, PMWE in the daytime does not show clear dependence against substorm activities in terms of intensity and duration. It is suggested that the variation of electron density by EPP, which is much smaller than the background electron density during the daytime, does not have significant effects on the appearance of PMWE. In this presentation, we will also discuss the contribution of EPP to PMWE appearance by comparing our analysis to an empirical model for electron density in the mesosphere.

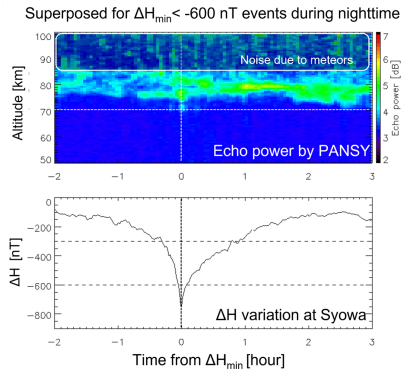

R005-08
Zoom meeting C ：11/1 AM2 (10:45-12:30)
11:15〜11:30

昭和基地で観測された中間圏カルシウムイオン層の挙動

#江尻 省 [1,2], 西山 尚典 [1,2], 津田 卓雄 [3], 堤 雅基 [1,2], 阿保 真 [4], 津野 克彦 [5], 川原 琢也 [6], 小川 貴代 [7], 和田 智之 [7], 中村 卓司 [1,2]
([1] 極地研,[2] 総研大,[3] 電通大,[4] 都立大・システムデザイン,[5] 理研,[6] 信州大・工,[7] 理化学研究所基幹研

Behavior of Ca+ layer in the mesosphere observed with a resonance scattering lidar at Syowa Station

#Mitsumu K Ejiri[1,2],Takanori Nishiyama[1,2],Takuo Tsuda[3],Masaki Tsutsumi[1,2],Makoto Abo[4],Katsuhiko Tsuno[5],Takuya Kawahara[6],Takayo Ogawa[7],Satoshi Wada[7],Takuji Nakamura[1,2]
([1]NIPR,[2]SOUKENDAI,[3]UEC,[4]System Design, Tokyo Metropolitan Univ.,[5]RIKEN,[6]Faculty of Engineering, Shinshu University,[7]ASI, RIKEN

Layers of metal ions in the mesosphere and lower-thermosphere (MLT) are produced by meteoric ablation. The meteoric metal ions have relatively long chemical life time in the MLT region and behave as plasma affected by neutral atmosphere dynamics. In the mid-latitude, the meteoric metal ions, including Calcium ion (Ca^+), in the MLT region are generally accepted as key species for generation of sporadic E (E_s) layer in the wind shear theory. Thin Ca^+ layer related with the E_s layer was often observed at the mid-latitude [Raizada et al., 2012; Ejiri et al., 2019a; 2019b]. Such thin Ca^+ layer usually descends in the MLT region while rare cases stay at an altitude of about 100 km for a long time. In contrast, thin Ca^+ layer was observed at Syowa Station (69S, 40E) only one night of 6 nights. One of thin Ca^+ layers was staying around 90 km altitude more than 3 hours while Ca^+ chemical lifetime was minutes to a few tens minutes estimated by previous studies at the midlatitude. We estimate a Ca^+ lifetime from observation and compare with a lifetime calculated using number density of neutral atmosphere over Syowa Station by NRLMSISE-00 Atmosphere Model. We will show the results and discuss the Ca^+ lifetime and behavior of the Ca^+ layer by background wind in case that number density profile of neutral atmosphere changes.

References

Raizada, S., C. A. Tepley, B. P. Williams, and R. Garcia (2012), Summer to winter variability in mesospheric calcium ion distribution and its dependence on Sporadic E at Arecibo, J. Geophys. Res., 117, A02303, doi:10.1029/2011JA016953.

Ejiri, M. K., Nakamura, T., Tsuda, T. T., Nishiyama, T., Abo, M., She, C. -Y., et al. (2019). Observation of synchronization between instabilities of the sporadic E layer and geomagnetic field line connected F region medium-scale traveling ionospheric disturbances. Journal of Geophysical Research: Space Physics, 124, 4627-4638. https://doi.org/10.1029/2018JA026242

Ejiri, M. K., Nakamura, T., Tsuda, T. T., Nishiyama, T., Abo, M., Takahashi, T., et al. (2019). Vertical fine structure and time evolution of plasma irregularities in the Es layer observed by a high-resolution Ca^+ lidar. Earth, Planets and Space, 71(1), 3. https://doi.org/10.1186/s40623-019-0984-z

R005-09
Zoom meeting C ：11/1 AM2 (10:45-12:30)
11:30〜11:45

観測との比較による GAIA 極域改良版の再現性評価

#垰 千尋 [1)], 陣 英克 [1)], 新堀 淳樹 [2)], 品川 裕之 [1)], 三好 勉信 [3)], 藤原 均 [4)]
[1 情報通信研究機構,[2 名古屋大学宇宙地球環境研究所,[3 九大・理・地球惑星,[4 成蹊大・理工

Evaluation of GAIA polar variable model compared with observations

#Chihiro Tao[1)],Hidekatsu Jin[1)],Atsuki Shinbori[2)],Hiroyuki Shinagawa[1)],Yasunobu Miyoshi[3)],Hitoshi Fujiwara[4)]
[1NICT,[2ISEE, Nagoya Univ.,[3Dept. Earth & Planetary Sci, Kyushu Univ.,[4Faculty of Science and Technology, Seikei University

We are extending the GAIA, Ground-to-Topside Model of Atmosphere and Ionosphere for Aeronomy, to include the magnetospheric variation via electric field deposition and auroral electron precipitation at the polar region and penetration of the electric field toward mid-to-low latitude. In order to validate the revised model performance in variation of total electron content (TEC), we compared model outputs with observation results from Global Navigation Satellite System (GNSS) in both event detail and statistical behavior.

We simulated and analyzed a geomagnetic storm event on September 27-28, 2017. TEC variation and distributions at the mid-to-low latitude due to penetrating electric field and disturbance dynamo shows good agreement with observations. On the other hand, there are difference in TEC value and profiles in the polar region between model outputs and observation. Superposed epoch analysis of TEC during magnetic storm events over 2019-2020 also shows the similar similarity and difference with the observation results.

We confirmed that the improvement of the TEC profile in the high latitudes using an electric potential map based on SuperDARN observations instead of the Wemer empirical model. In this presentation, we will discuss the effect of assumed auroral energy distribution and improvements.

対流圏から熱圏までの全球の大気圏と電離圏の主要な大気物理・化学過程を解くモデルである GAIA(Ground-to-Topside Model of Atmosphere and Ionosphere for Aeronomy) に、太陽圏や磁気圏の変動の効果を含めるよう改良を行ってきた。具体的には、極域電場およびオーロラ降込み総量を経験モデルに基づいて太陽風および地磁気指数に応じて変化させ、中低緯度への電場侵入効果を含めている。この改良版モデルによる電離圏電子密度分布の再現性を評価するために、GNSS(Global Navigation Satellite System) による全電子数 (TEC) をはじめとする観測と、事例および統計の両観点で比較を行った。

事例比較に用いたのは 2017 年 9 月 27-28 日の磁気嵐イベントである。中低緯度の電場侵入およびダイナモ擾乱に伴う全電子数変動と分布は、よい再現性を示した。他方、極域の TEC 値や分布のずれといった違いがあることが分かった。2019˜2020 年の計算結果から磁気嵐時の TEC 応答を super-posed epoch 解析して観測と比較した結果も、事例比較と同様に、中低緯度の TEC のよい再現性の反面、極域 TEC の値および分布に相違が見られた。

極域の TEC 分布に対しては、Weimer 経験モデルではなく SuperDARN 観測のポテンシャルマップの利用による再現性向上が確認された。発表では、オーロラエネルギー分布の仮定の影響とその改善等、議論する予定である。

R005-10
Zoom meeting C ：11/1 AM2 (10:45-12:30)
11:45〜12:00

フィンランド・ニロラの630nm大気光イメージャによって観測された極域型の中規模伝搬性電離圏擾乱の初期解析

#佐藤 雅紀[1)], 塩川 和夫[1)], 大山 伸一郎[1)], 大塚 雄一[1)]
[1)] 名大 ISEE

Preliminary analysis of polar-type MSTIDs observed by a 630-nm airglow imager at Nyrola, Finland

#Masaki Sato[1)],Kazuo Shiokawa[1)],Shin ichiro Oyama[1)],Yuichi Otsuka[1)]
[1)]ISEE, Nagoya Univ.

Medium-scale traveling ionospheric disturbances (MSTIDs) are ionospheric plasma density structures with scale sizes of 100-1000 km and are observable through 630-nm airglow imagers. Shiokawa et al. (2012) and Yadav et al. (2020) reported high-latitude MSTIDs which move associated with auroral brightenings, based on airglow imaging observation at Tromsoe (69.6 N, 19.2 E; magnetic latitude: 66.7 N), Norway. Here we call such MSTIDs as “polar-type MSTIDs”. However, the lower-latitude boundary of the polar-type MSTIDs has not been clearly observed. In this study, we analyzed the MSTIDs observed at Nyrola (62.3 N, 25.5 E; magnetic latitude: 59.4 N), Finland, which is located equatorward of Tromsoe, during the period from January 23, 2017 to April 29, 2017, and August 18, 2017 to December 30, 2017, using an airglow imager deployed by the PWING project. The association of geomagnetic disturbances with the MSTIDs was clarified by using the geomagnetic field data obtained by the IMAGE magnetometer chain (https://space.fmi.fi/image/www/index.php?page=home). As the result, we found three polar-type MSTID events. The two of them show clear equatorward boundary of MSTIDs over Nyrola, while the other one shows a possibility that the MSTIDs expand further lower latitudes. In the presentation we will report results with longer observation interval and discuss the equatorward boundary of polar-type MSTIDs.

References:
Yadav et al. (2020), https://doi.org/10.1029/2019JA027598
Shiokawa et al. (2012), https://doi.org/10.1029/2012JA017928

波長 630nm の大気光撮像を通して波長 100-1000km スケールの電離圏のプラズマ密度の変動である中規模伝搬性電離圏擾乱（MSTID）を観測することができる。S hiokawa et al. (2012) と Yadav et al.(2020) は、オーロラ帯の緯度に位置するノルウェーの Tromsø(69.6 ゜N, 19.2 ゜E; 磁気緯度：6 6.7 ゜N) で、オーロラの増光に伴って動きが変化する MSTIDの観測を報告している。ここではこのような MSTID を極域型の MSTID と呼ぶ。しかし、この極域型の MSTID が低緯度方向にどこまで拡がっているかはわかっていない。そこで今回は、極域型の MSTID の低緯度側の境界をとらえるために、ノルウェーの Tromsø の低緯度側に位置するフィンランドの Nyrola（6 2.3 ゜N, 2 5.5 ゜E ; 磁気緯度：5 9.4 ゜ N）で、P WING プロジェクトによる大気光イメージャによって MSTID を観測した。これまで解析した期間は、2 017年 1 月 23 日から 2017 年 4 月 29 日、2 017 年 8 月 18 日から 2017 年 12 月 30 日までの期間である。さらに、I MAGE magnetometer chain（h ttps://space.fmi.fi/image/www/index.php?page=home）によって提供された地磁気データを用いることで、MSTID の動きとサブストームなどの地磁気擾乱との関係を明確にした。その結果、これまで 3 例の極域型の MSTID を見出し、そのうち 2 例は、ニロラの上空で低緯度方向の境界がはっきり観測され、残りの 1 例はより低緯度まで拡がっている可能性があることが分かった。講演では、より観測期間を増やした解析結果とその考察を報告する予定である。

References:
Yadav et al. (2020), https://doi.org/10.1029/2019JA027598
Shiokawa et al. (2012), https://doi.org/10.1029/2012JA017928

R005-11
Zoom meeting C ：11/1 AM2 (10:45-12:30)
12:00〜12:15

地上とあらせ衛星による夜間中規模伝搬性電離圏擾乱の複数例同時観測

#川合 航輝[1)], 塩川 和夫[1)], 大塚 雄一[1)], 門倉 昭[2)], 田中 良昌[2)],Martin Connors[3)],Shevtsov Boris[4)],Poddelsky Igor[4)], 笠原 禎也[5)], 笠羽 康正[6)], 土屋 史紀[6)], 熊本 篤志[6)], 新堀 淳樹[1)], 松岡 彩子[7)], 篠原 育[8)], 三好 由純[1)]
([1] 名大 ISEE,[2] 国立極地研究所,[3]Athabasca Univ.,[4]IKIR,[5] 金沢大,[6] 東北大,[7] 京都大,[8] 宇宙研／宇宙機構

Multi-event study of simultaneous observation of nighttime MSTIDs from the ground and the Arase satellite

#Kouki Kawai[1)],Kazuo Shiokawa[1)],Yuichi Otsuka[1)],Akira Kadokura[2)],Yoshimasa Tanaka[2)],Connors Martin[3)],Boris Shevtsov[4)], Igor Poddelsky[4)],Yoshiya Kasahara[5)],Yasumasa Kasaba[6)],Fuminori Tsuchiya[6)],Atsushi Kumamoto[6)],Atsuki Shinbori[1)],Ayako Matsuoka[7)],Iku Shinohara[8)],Yoshizumi Miyoshi[1)]
([1]ISEE, Nagoya Univ.,[2]National Institute of Polar Research,[3]Athabasca Univ.,[4]IKIR,[5]Kanazawa Univ.,[6]Tohoku Univ., [7]Kyoto Univ.,[8]ISAS/JAXA

Traveling ionospheric disturbances (TIDs) are wavelike structures of electron density in the ionosphere. TIDs are classified as small, medium, and large scale [Hunsucker, 1982]. The interhemispheric propagation of nighttime medium-scale TIDs (MSTIDs) has been confirmed by simultaneous observations of ground airglow imagers in both hemispheres [Otsuka et al., 2004]. Otsuka et al. [2004] suggested that the conjugacy of the electric field along the magnetic field lines played an important role in the MSTID generation. However, the conjugacy of the electric field associated with MSTID had not been reported by satellites in the magnetosphere. We have firstly reported simultaneous observation of the nighttime MSTIDs with an airglow imager at Gakona (62.39 N, 214.78 E) and the Arase satellite on November 3, 2018 [Kawai et al., 2021]. In this event, the electron density fluctuation and the electric field variation measured by Arase were clearly associated with the MSTIDs. Here, we investigate more simultaneous observations of nighttime MSTIDs with the airglow imagers installed at high latitudes and the Arase satellite for 4 years from April 2017 to April 2021. We analyze electromagnetic fields and plasma densities obtained by Arase and compare them with several MSTID events observed by airglow imagers at 10 stations (Athabasca, Gakona, Kapsukasing, Istok, Zhigansk, Husafell, Magadan, Nyrola, Tromsoe, and Paratunka) deployed by the PWING project [Shiokawa et al., 2017]. In most cases, we found no clear correlation between MSTIDs and variations of electromagnetic fields and plasma densities observed by Arase. This result contradicts the fact that most MSTIDs have conjugation at middle latitudes [Otsuka et al., 2004; Shiokawa et al., 2005; Martinis et al., 2017]. We discuss the possibility that there is less propagation of MSTID structures from the ionosphere at high than at middle latitudes.

References:
Hunsucker, Rev. Geophys., 1982, https://doi.org/10.1029/RG020i002p00293
Kawai et al., J. Geophys. Res., 2021, https://doi.org/10.1029/2020JA029086
Martinis et al., Adv. Space Sci., 2017, https://doi.org/10.1016/j.asr.2017.07.021
Otsuka et al., Geophys. Res. Lett., 2004, http://doi.org/10.1029/2004GL020262
Shiokawa et al., Earth Planets Space, 2017, http://doi.org/10.1186/s40623-017-0745-9
Shiokawa et al., J. Geophys. Res., 2005, https://doi.org/10.1029/2004JA010845

伝搬性電離層擾乱 (TID) は電離圏の電子密度の波状構造である。TID はスケールの大きさにより小規模、中規模、大規模に分類される [Hunsucker et al., 1982]。夜間の中規模伝搬性電離圏擾乱 (MSTID) の半球間伝搬は、両半球の地上大気光イメージャを使用した同時観測により確認されている [Otsuka et al., 2004]。Otsuka et al. [2004] は地上の大気光画像の解析から MSTID の地磁気共役性を示し、磁力線を介した電場の共役性が MSTID 発生で重要な役割を果たしていることを示唆した。しかし MSTID に付随する電場が磁気圏で観測された報告はない。我々は初めて、Gakona (62.39 ° N、214.78 ° E) の大気光イメージャとあらせ衛星を用いて、2018 年 11 月 3 日に夜間 MSTID の同時観測を報告した [Kawai et al., 2021]。この観測例では、あらせ衛星により磁気圏で測定された電子密度変動と電場変動が、明白に MSTID と関連していた。本研究では、高緯度に設置された大気光イメージャとあらせ衛星を用いて、2017 年 4 月から 2021 年 4 月までの 4 年間、夜間の MSTID の同時観測例を調査する。あらせ衛星により観測された電磁場・プラズマデータを解析し、PWING プロジェクト [Shiokawa et al., 2017] で展開している 10 観測点 (Athabasca, Gakona, Kapsukasing, Istok, Zhigansk, Husafell, Magadan, Nyrola, Tromsø, and Paratunka) の大気光画像と比較している。いくつかの同時観測例を解析した結果、ほとんどの場合、MSTID とあらせ衛星により観測された電磁場・プラズマ密度の変動の間に明確な相関は見られなかった。この結果は、中緯度ではほとんどの MSTID は共役性を有するというこれまでの結果 [Otsuka et al., 2004; Shiokawa et al., 2005; Martinis et al., 2017] と一致しない。本講演では、これらの結果に基づいて、高緯度では中緯度に比べ MSTID の特徴が電離圏から磁気圏へ伝播しにくくなる要因について議論する。

R005-12
Zoom meeting C ：11/1 PM1 (13:45-15:30)
13:45〜14:00

Statistical analysis of nighttime MSTIDs characteristics using the mid-latitude SuperDARN radars

#Wataru Hazeyama[1)],Nozomu Nishitani[1)],Tomoaki Hori[1)],Takuji Nakamura[2)],SEPTI PERWITASARI[3)]
([1]ISEE, Nagoya Univ.,([2]NIPR,([3]NICT

We analyze the characteristics of nighttime medium-scale traveling ionospheric disturbances (MSTIDs) using the mid-latitude Super Dual Auroral Radar Network (SuperDARN) radars installed in Japan and the United States. We examine the longitudinal difference of the relationship between MSTID and solar activity by analyzing long-term data for 11 years, corresponding to one solar cycle. We find that the propagation direction is mainly southwestward and rotates clockwise with progressing local time in Japan and North America. This tendency can be explained by the Perkins instability, which is considered to be associated with the growth of nighttime MSTIDs and the change in the direction of nighttime mid-latitude neutral winds. In addition, we reveal a negative correlation between the nighttime MSTIDs amplitude and the solar F10.7 index. This negative correlation can also be explained by the linear growth late of the Perkins instability, which is inversely proportional to (H_n, ν _in, and then to the) solar activity. This study is the first to show the global solar activity dependence of the nighttime mid-latitude MSTIDs using the SuperDARN data.

R005-13
Zoom meeting C ：11/1 PM1 (13:45-15:30)
14:00〜14:15

HF ドップラー観測と GPS-TEC による異なる高度の MSTID の伝搬特性

#西山 祐樹 [1)], 中田 裕之 [2)], 大矢 浩代 [3)], 細川 敬祐 [4)], 津川 卓也 [5)], 西岡 未知 [5)]
[(1] 千葉大学大学院,[(2] 千葉大・工,[(3] 千葉大・工・電気,[(4] 電通大,[(5] 情報通信研究機構

Propagation characteristics of MSTIDs of different altitudes Obtained by HF Doppler sounding and GPS-TEC

#Yuki Nishiyama[1)],Hiroyuki Nakata[2)],Hiroyo Ohya[3)],Keisuke Hosokawa[4)],Takuya Tsugawa[5)],Michi Nishioka[5)]
[(1]Graduate School of Chiba Univercity,[(2]Grad. School of Eng., Chiba Univ.,[(3]Engineering, Chiba Univ.,[(4]UEC,[(5]NICT

We analyze medium scale traveling ionospheric disturbances (MSTIDs), which frequently occur during daytime in winter and during nighttime in summer. The period of the MSTIDs is about 15 to 60 minutes. Although it is known that the MSTIDs are caused by Perkins instability and atmospheric gravity waves, there are some unknown characteristics about the altitudinal distributions of the MSTIDs. In this study, we examined the characteristics of the MSTIDs using HF Doppler sounding utilized by the University of Electro-Communications（UEC）and TEC data from the GNSS Earth Observation Network (GEONET) of the Geospatial Information Authority of Japan (GSI). The HF Doppler sounding observes the ionosphere at the altitudes of 150km to 250 km, using 5.006 MHz and 8.006 MHz radio waves transmitted from the UEC Chofu campus. The TEC observation, on the other hand, observes fluctuations of the plasma distribution of the altitude around 300 km. By using these data, we analyzed the MSTID that occurred on January 24, 2015. In this study, Doppler frequency data received at seven sites were used; Iitate, Sugadaira, Kakioka, Oarai, Sugito, Fujisawa, and Kyoto.

In the HF Doppler observation, similar waveforms were observed at these seven sites for both 5.006MHz and 8.006MHz during 00:00UT to 06:00UT. Here, we examined the propagation characteristics of MSTIDs using the Doppler frequency data of 8.006MHz. We calculated the correlation coefficient of Doppler data for any two sites every one hour and determined the time delay of MSTIDs at each location by identifying the time when the correlation coefficient was the maximum. As a result, we found that the wave propagated from northwest to southwest.

We also examined the temporal variation of the TEC disturbance, and found that the TEC disturbance also propagated from northwest to southwest, which is consistent with the propagation characteristics of the HF Doppler observation.

These results indicate that the propagation characteristics at altitudes of 150km and 300 km are similar each other. In the presentation, we would like to mention the three-dimensional distributions of MSTIDs by comparing 5.006 MHz and 8.006 MHz.

R005-14
Zoom meeting C ：11/1 PM1 (13:45-15:30)
14:15〜14:30

Relationship between Es and MSTIDs: Comparison of Doppler shift from HFD and GPS-TEC from GEONET

#Ryo Matsushima[1)],Keisuke Hosokawa[1)],Jun Sakai[1)],Yuichi Otsuka[2)],Mitsumu K Ejiri[3)],Michi Nishioka[4)],Takuya Tsugawa[4)]

([1]UEC,[2]ISEE, Nagoya Univ.,[3]NIPR,[4]NICT

Sporadic-E (Es) is a thin layer in the E-region ionosphere (˜100 km) which is mainly composed of dense metallic ions and electrons. Es is known to appear in the mid-latitude region during summer months. Recent theoretical studies and numerical simulations have suggested that Es plays an important role in generating wave-like structures at F-region altitudes in summer nighttime, which are known as Medium-Scale Traveling Ionospheric Disturbances (MSTIDs). However, there have been only a few studies investigating the simultaneous observations of Es and MSTIDs at two different altitudes; thus, the coupling of these two phenomena has not yet been fully confirmed. To overcome this limitation, we employed data from the HF Doppler (HFD) sounder network in Japan to detect Es and tried to evaluate the E-F coupling, i.e., Es in the E-region and MSTIDs in the F-region. The HFD system is composed of a transmitting station in Chofu, Tokyo (35.7N, 139.5E) and receiving stations at 11 places in Japan. Based on these multipoint observations, we derived the dynamical characteristics, such as propagation speed and direction. A statistical analysis of the propagation characteristics of Es and MSTID was performed using a combination of HFD and Total Electron Content (TEC) data from GEONET GPS receivers for four years from 2014 to 2017. The statistical results demonstrate that the propagation characteristics of Es and MSTIDs were similar to each other, suggesting the occurrence of E-F coupling. However, it has not been confirmed if the variations in the HFD data actually reflect the behavior of Es (i.e., if the reflection actually takes place at the E-region altitude).

In this paper, we used the Doppler frequency data from HFD to estimate the reflection height of the possible Es traces in the HFD data. We employed data from Sugito, Saitama (36.0N, 139.7E) obtained in four summer seasons from 2014 to 2017. At the times of the possible Es reflections in the HFD data, the Doppler frequency plotted in the format of dynamic spectra showed a train of diagonal lines extending from upper left to lower right across the zero line. The figure shows an example of the HFD data when Es was observed. The upper panel shows the Doppler frequency for time at 8 MHz and the lower panel shows the Doppler frequency for time at 5 MHz. These diagonal traces, traversing from positive to negative Doppler frequency, indicated that the length of the ray-path became shorter first and then, after the crossing across the zero line, it again got longer. In most cases, the slope of such diagonal lines is too small to be explained only by the vertical motion of the Es layer; thus, the change in the Doppler frequency represents the change of the ray-path due to the horizontal motion of Es structures. Clear signatures of diagonal traces were identified in 79 cases out of 122 events where Es and MSTIDs occurred at the same time. On the other hand, there were only 66 cases of diagonal traces in 193 events where only Es were observed, and many of the diagonal lines in those cases were relatively unclear. These facts imply that the existence of the diagonal traces in the HFD data can be used as a proxy for the discreteness of the structures of Es and MSTIDs (i.e., how the E-F coupling is effectively working for producing clear spatial structures in both the altitudes). The duration of most of the diagonal structures ranges from 5 to 15 min; the corresponding spatial scale of the structure relatively smaller than the wavelength of MSTIDs. This suggests that the diagonal traces are manifestation of small-scale Es structures which have been observed in the past as QP echoes in the coherent VHF radars. In the presentation, we will show the altitude of reflection estimated from the slope of the diagonal traces in order to further confirm the E-F coupling seen in the statistics.

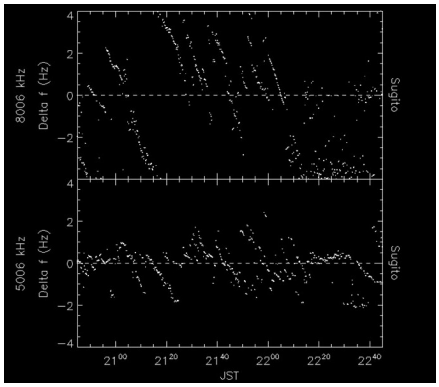

R005-15
Zoom meeting C ：11/1 PM1 (13:45-15:30)
14:30〜14:45

機械学習を用いた日本上空の中規模伝搬性電離圏擾乱の統計解析

#劉 鵬 [1)], 横山 竜宏 [1)], 山本 衛 [2)]
[(1] 京大生存研,[(2] 京大・生存圏研

Statistical analysis of Medium Scale Traveling Ionospheric Disturbances over Japan based on machine learning

#Peng LIU[1)],Tatsuhiro Yokoyama[1)],Mamoru Yamamoto[2)]
[(1]RISH, Kyoto Univ.,[(2]RISH, Kyoto Univ.

Medium Scale Traveling Ionospheric Disturbances (MSTIDs) are observed as wavelike perturbations of electron density in the ionospheric F region. One typical MSTIDs observation method is detrended Total Electron Content (TEC) map where TEC is calculated by signal transmission delay via GPS ground receiver network. However, there is still no automatic process method for these detrended TEC maps so far which could distinguish MSTIDs from irregular ionospheric disturbances intelligently, leading to controversy for external dependency (e.g. solar activity) and deficiency for overall analysis of long-term MSTIDs characteristics variation. Moreover, previous researches always focus on nighttime MSTIDs because daytime MSTIDs are more difficult to identify. In this work, we propose a cutting edge deep learning instance segmentation model based on Mask R-CNN model to detect wavelike perturbations automatically with the precision of 81%, then by new Filtering Criterion, we eliminate isolated perturbations and only waveforms of MSTIDs are remained to derive instantaneous characteristics (e.g. wavelength), finally by new Matching Criterion, matching waveforms between two consecutive frames are retrieved for derivation of dynamic characteristics (e.g. propagation velocity). With this procedure, we analyze up to 1,209,600 detrended Japanese TEC maps in 1997-2019 automatically and for the first time to figure out instantaneous and dynamic characteristics of daytime and nighttime MSTIDs every 10 minutes, which provides accurate observation data for the verification of MSTIDs generation theory. Our research also reveals the external dependency of instantaneous and dynamic characteristics by monthly and yearly characteristics average in 23 years, especially the seasonal and solar activity composite dependency of nighttime MSTIDs occurrence rate is confirmed, which has been an academic controversy for a long time.

中規模伝搬性電離圏擾乱（MSTIDs）は、電離圏 F 領域における電子密度の波長数百 km 程度の波状変動である。トレンド除去された TEC マップは典型的な MSTIDs の観測方法の一つであり、GPS 地上受信機ネットワークを介した信号伝搬遅延によって全電子数 (TEC) が計算される。しかし、これらの TEC マップから得られる MSTIDs を不規則な電離層擾乱から知能的に区別できる自動処理方法はまだないため、発生傾向の外部要因に対する依存性（太陽活動など）や長期的な発生特性については明らかにされていない。さらに、従来の研究では昼間 MSTIDs の同定がより困難であるため、主に夜間 MSTIDs に焦点が当てられてきた。本研究では、Mask R-CNN モデルに基づいて新たな深層学習インスタンスセグメンテーションモデルを構築し、81 %の精度で MSTID の波状変動を自動的に検出することに成功した。次に、新しいフィルタリング基準により孤立した不規則な変動を除去し、波状の MSTIDs の波形から静的特性（波長など）を導出する。最後に，新しいマッチング基準によって二つの連続するフレームの間にマッチングしている二つの波形を検索して、MSTIDs の動的特性（伝搬速度など）を導出する。この手順により、1997 年から 2019 年まで 1,209,600 枚の日本上空の TEC マップを自動的に分析し、10 分ごとに昼間および夜間の MSTIDs の静的および動的特性を導出し、MSTIDs 生成理論を検証できるデータベースの作成が可能となった。このデータベースから、23 年間の MSTIDs 特性の月平均および年平均変動による MSTIDs 各特性の外部要因に対する依存性を調べ、夜間 MSTIDs 発生率の季節と太陽活動に対する複合的な依存性を確認できた。

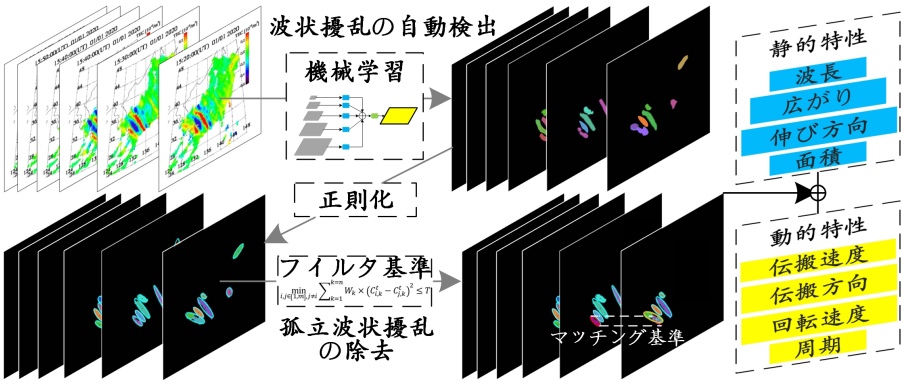

R005-16
Zoom meeting C ：11/1 PM1 (13:45-15:30)
14:45〜15:00

イオノゾンデ観測による電離圏電子密度プロファイル導出

#西岡 未知 [1)], 前野 英生 [2)], 山川 浩幸 [1)], 津川 卓也 [1)], 斎藤 享 [3)]
[(1] 情報通信研究機構,[(2]NICT,[(3] 電子航法研

Derivation of ionospheric electron density profile by VIPIR2 ionosonde observation

#Michi Nishioka[1)],Hideo Maeno[2)],Hiroyuki Yamakawa[1)],Takuya Tsugawa[1)],Susumu Saito[3)]
[(1]NICT,[(2]NICT,[(3]ENRI, MPAT

An ionosonde transmits radio waves of short-wave towards the ionosphere while sweeping frequencies and measures delay time until the transmitted radio waves are reflected to the ionosonde by the ionosphere. Normally, the observation data is recorded as “ionogram” in which the signal strength is indicated with the horizontal axis of the frequency and the vertical axis of virtual height. The virtual height is derived by multiplying the speed of light by flight time and dividing by two. The virtual height is different from true height since the propagation speed of the transmission radio wave is a function of the electron density distribution and the geomagnetic field. In order to obtain the electron density distribution with respect to the “true height” from the ionogram, a procedure is required in which an echo trace is performed to read the frequency and delay time of the reflected echo one by one, and the propagation speed is considered and converted to the electron density with respect to the true height.

National Institute of Information and Communications Technology has been conducting routine ionosonde observations for many years. In this project, some parameters such as critical frequencies and virtual heights of the E- and F- layers are automatically derived, however, the echo trace has not been conducted yet. Recently, we developed a technique to trace ionospheric echoes using machine learning. The traced echoes were subjected to a procedure of deriving electron density profile against true height using the POLynominal Analysis program (POLAN). In this presentation, we will introduce the echo trace technique and discuss quantitative evaluations of the POLAN analysis.

電離圏観測手法の一つであるイオノゾンデ観測では、短波帯電波の周波数を掃引させながら上空に送信し、送信電波が電離圏で反射されて地上に戻ってくるまでの時間（遅延時間）を計測するものである。通常、観測データは、横軸を周波数、縦軸を遅延時間より算出した「見かけの高さ」として、電波の受信強度を色で示すイオノグラムとして記録される。一方、送信電波の伝播速度は、電子密度分布や磁場の関数となっているため、イオノグラムから「真の高さ」に対する電子密度分布を得るためには、反射エコーの周波数と遅延時間を逐一読取るエコートレースを行い、伝播速度を考慮し、真の高度に対する電子密度に変換する手順（NH 解析）が必要となる。情報通信研究機構における国内定常イオノゾンデ観測では、得られたイオノグラムから自動で各種パラメータを抽出する技術は開発してきたものの、反射エコーの周波数と遅延時間を逐一読み取りはこれまで行ってこなかった。そこで、近年開発した機械学習を用いたパラメータの自動抽出手法を発展させ、電離圏エコーのエコートレースを試みた。トレースされたエコーは POLynominal ANalysis program (POLAN) を用いて HN 解析され、真の高度に対する電子密度プロファイルが導出されている。本発表では、エコートレースの現状および、信楽の MU レーダーデータ等を用いて、導出された電子密度プロファイルの定量的評価を行う。

R005-17
Zoom meeting C ：11/1 PM1 (13:45-15:30)
15:00〜15:15

MU レーダーによる電子密度の長期統計解析と信楽イオノゾンデ自動読み取りシステムの開発

#増田 秀人 [1)], 横山 竜宏 [2)], 山本 衛 [3)]
([1] 生存圏研究所,[2] 京大生存研,[3] 京大・生存圏研

Long-term analysis of electron density observed by the MU radar and auto-scaled ionosonde data

#Shuto Masuda[1)],Tatsuhiro Yokoyama[2)],Mamoru Yamamoto[3)]
([1]RISH,[2]RISH, Kyoto Univ.,[3]RISH, Kyoto Univ.

The MU radar, located in Shigaraki-Cho, Koka City, Shiga Prefecture, is a large atmospheric radar designed to observe the middle and upper atmosphere, and has been observing the ionospheric F region as an Incoherent Scatter (IS) radar regularly since 1986. The IS radar emits radio waves into the upper atmosphere and is capable of estimating various physical quantities in the ionosphere that contribute to the intensity and spectrum of the scattered waves. Electron and ion temperatures, plasma drift velocities and echo power are regularly observed by the MU radar (http://www.rish.kyoto-u.ac.jp/mu/isdata/).
First, we focus on the statistics of the echo power, which is proportional to the electron density.
The peak echo power measured by the MU radar is calibrated as the electron density that corresponds to the foF2 measured by Kokubunji ionosonde.
We compare the electron density observed by the MU radar with the International Reference Ionosphere (IRI) model.
Second, we are planning to build a system that reads ionospheric parameters from ionograms obtained by Shigaraki ionosonde, most of which remains unanalyzed.
After removing noise and interference signals, a machine learning model will be developed to process ionogram images automatically.

滋賀県甲賀市信楽町に位置する MU レーダーは、中層大気と超高層大気を観測するために作られた大型大気レーダーであり、1986 年から非干渉散乱 (Incoherent Scatter; IS) レーダーとして現在まで定常的に電離圏の F 領域観測が続けられている。IS レーダーは上層大気に電波を放射し、その散乱波の強度及びスペクトルに寄与している電離圏の各種物理量を推定することができる。MU レーダーによる電離圏観測では、電子・イオン温度、プラズマドリフト速度及びエコー強度を定常的に観測し公開されている (http://www.rish.kyoto-u.ac.jp/mu/isdata/)。本研究では、エコー強度、すなわち電子密度に焦点を当てて解析を行った。

まず電子密度に比例するエコーパワーの統計データに焦点を当てた。各時刻におけるエコー強度の最大値が国分寺のイオノゾンデにより得られた foF2 に対応すると仮定して、エコー強度から電子密度の絶対値へと較正を行った。そして MU レーダーによって観測された電子密度と IRI モデルとの比較を行った。IRI モデルと比べると MU レーダーの最大電子密度の値は全体的に小さく、また最大となる電子密度の高度も低くなることがわかった。

次に、観測は継続して実施されているものの読み取り作業が行われないまま蓄積されている
信楽のイオノゾンデの観測データの活用を検討する。イオノグラムの画像データから、

各種電離圏パラメータを自動的に読み取るシステムを構築中である。ノイズと干渉信号を除いた後に機械学習モデルを用いてイオノゾンデの画像データから自動で処理出来るようにする。

本講演では、自動読み取りシステム開発の現状について報告する。

R005-18
Zoom meeting C ：11/1 PM2 (15:45-18:15)
15:45〜16:00

Observation of ionospheric irregularity by using scintillation of VHF to UHF satellite signals

#Toru Takahashi[1)],Susumu Saito[2)]
([1]ENRI, MPAT,[(2]ENRI, MPAT

The ionosphere plays an important role as a communication path between a ground-ground and satellite-ground. The irregularity of the plasma density in the ionosphere is often generated from a few tens of kilometers to a few meters. Notably, irregularities on the scale of hundreds of meters to a few kilometers cause fluctuation in the radio wave transmitted from the Global Navigation Satellite System (GNSS) satellites. Previous studies presented small-scale ionospheric irregularities were generated by cascading of the large-scale irregularities. Therefore, it is important to observe large (few km) scale irregularities simultaneous with small (100 m-few km) scale irregularities.

We receive the VHF (150 MHz) and UHF (400 MHz) beacon signals transmitted from Low Earth Orbit satellites by receivers based on the software-defined radio (SDR). We plan to install the satellite beacon receiver to observe the scintillation and conduct a simultaneous observation with the GPS receivers from high to low latitude regions. We developed a SDR-based beacon receiver based on the GRBR (GnuRadio Beacon Receiver) and installed at Electronic Navigation Research Institute, Chofu, Tokyo (35.68 N, 139.56 E).

To test the receiver we observe scintillation caused by the sporadic E (Es) layer. The Es layer is known to include kilometer-scale irregularities to cause quasi-periodic scintillations in the VHF/UHF beacon signals which reflects the spatial structure. Recently, structures of the Es layers have also been studied with two-dimensional ROTI (the rate of TEC (Total Electron Content) index) maps and precise TEC measurements based on GNSS signals. We compare the VHF/UHF scintillations with the Es layer structure inferred from ROTI and TEC analysis. The beacon satellite measurement could be not only an independent validation of the ROTI/TEC analysis but also provide better view of Es layer irregularities.

In this presentation, we will show initial observation results as well as the comparison of the VHF/UHF scintillation and ROTI map and discuss the spatial structure of Es layer.

R005-19
Zoom meeting C ：11/1 PM2 (15:45-18:15)
16:00〜16:15

3-D imaging of daytime mid-latitude sporadic E over Japan with ground-based GNSS data

#Weizheng Fu[1)],Nicholas Ssessanga[1)],Tatsuhiro Yokoyama[1)],Mamoru Yamamoto[1)]
[1)]RISH, Kyoto Univ.

Sporadic-E (Es) is electron density inhomogeneities manifested in the ionospheric E-region (˜100 km), exhibiting a high correlation of occurrence with intense trans-ionospheric signal scintillation. Due to the characteristics of its thin-layer (˜2 km) and small contributions (˜1 TECU) in total electron content (TEC), the three-dimensional (3-D) imaging of Es structure is challenging. This paper presents a novel two-step computerized ionospheric tomography (CIT) technique to reconstruct the 3-D structures of mid-latitude daytime Es based on TEC measurements from ground-based Global Navigation Satellite System (GNSS). To facilitate digital CIT at a high spatiotemporal resolution, we have adopted TEC measurements from a dense receiver network, GEONET, which contains more than 1000 receivers over Japan.

In the first step, we reconstruct a more accurate F-region structure on a coarse grid, by using a multiplicative algebraic reconstruction technique (MART) from a smooth background calibrated by empirical orthogonal functions (EOFs). In the second step, on a fine grid and using singular value decomposition (SVD), the 3-D Es structure is estimated based on the residuals of electron density in the E-region covering 80˜180 km in altitude. To vertically constrain the solution, we use time-dependent EOFs generated from a Chapman model function tuned to manually scaled Es observations from a network of four ionosondes over Japan. In step-1 (step-2), the resolution is set to 1 ° (0.4 °) in horizontal, 20 km (1 km) in altitude, and 15 min (1 min) in time. Three event days of daytime sporadic-E are investigated. Results from simulation and real observations show that the technique can reconstruct Es structure with a high degree of fidelity, specifically during strong Es (foEs $>$20 MHz). From the 2-D horizontal slices at the height of maximum Es, the size, shape, and migration of this fine structure Es are obtained and found in good agreement with earlier results. The east-west (E-W) aligned frontal structures of daytime Es are observed to span over several hundred kilometers, last for ˜30 min, and migrate northwestward in the morning and southwestward in the afternoon. The simultaneous analyses of reconstructed Es and zonal wind data from MU radar, further support the Es wind shear theory: at mid-latitudes, the presence, direction, and magnitude of wind shear play a role in Es morphology. For the first time, CIT based on ground-based GNSS TEC is shown to reproduce the Es-layer altitude time variation.

R005-20
Zoom meeting C ：11/1 PM2 (15:45-18:15)
16:15〜16:30

電離圏数値モデルを用いたアレシボ・レーダー周辺における sporadic E 層の 3 次元構造の解析

#安藤 慧 [1)], 齊藤 昭則 [1)], 品川 裕之 [2)]
([1] 京大理,[2] 情報通信研究機構

Simulations on the three-dimensional structures of the Es layers around Arecibo radar

#Satoshi Andoh[1)],Akinori Saito[1)],Hiroyuki Shinagawa[2)]
([1]Graduate School of Science, Kyoto Univ.,[2]NICT

In this study, we investigated the three-dimensional structure of the sporadic E layer (Es layer) around Arecibo radar by combining the newly developed three-dimensional ionospheric model with Mg ions and the neutral winds of the global atmospheric model.

The Es layer is a dense plasma layer occurring in the ionospheric E region. It is widely recognized that the vertical shear of the horizontal winds is important for formation of the Es layers. In a previous study, we investigated the temporal evolution of three-dimensional structures of the Es layers around Japan and argued that, below 110 km altitude, the structure of the Es layer does not reflect the structure of the vertical shear of the horizontal winds because the semi-diurnal tides, which create vertical shear of the horizontal winds, are weak.

Arecibo radar is located in the geomagnetic mid-latitude zone like Japan (29 degrees geomagnetic latitude north). However, it is geographically located in the lower latitudes (˜18 degrees geographic latitude north), and the behavior of the winds in the lower ionosphere is different. Therefore, it is necessary to investigate the three-dimensional structures of the Es layers, because the behavior of the sporadic E can be different.

In this study, we first compared the temporal variation of the electron density profiles observed by the Arecibo radar with the numerical results. Consequently, it was confirmed that the present numerical model can reproduce the semi-diurnal/diurnal Es layers observed by the Arecibo radar, especially the diurnal Es layers at low altitudes. Next, we investigated the three-dimensional structures of the Es layer from the obtained numerical results. As a result, the Es layer has a thin and elongated frontal structure with a width of ˜100 km and a horizontal scale of more than 1000 km, which reflects the structure of the vertical shear of the horizontal winds, even at an altitude of about 100 km. The vertical shear of the horizontal wind was generated by the diurnal tides prevailing below 110 km altitude in the geographic low latitudes. From the above results, we found that, in the geomagnetic mid-latitudes where the Es layer tends to occur, the Es layer can show different three-dimensional structures depending on the geographic latitude corresponding to the geomagnetic latitude where the layers appear.

本研究では, 新たに開発した Mg イオンを組み込んだ 3 次元電離圏モデルと, 全球大気モデルの中性風場を組み合わせることにより, アレシボ・レーダー周辺における sporadic E 層 (Es 層) の 3 次元構造を調査した.

Es 層は電離圏 E 領域に発生する高密度プラズマ層である. その発生には, 水平風の鉛直シアが重要であることが広く認識されている. 過去の研究で発表者らは日本付近の Es 層の 3 次元構造の時間発展を調査し, 高度 110 km 以下では半日潮汐波が弱まるため, Es 層の構造は水平風の鉛直シアの構造を反映しなくなっていくことを主張した.

アレシボ・レーダー周辺は日本と同じく地磁気中緯度帯に位置する (29 ° N geomagnetic latitude). しかし, 地理的には低緯度帯に位置するため (〜18 ° N geographic latitude), 電離圏下部の風の振る舞いが異なる. そのため, 発生する Es 層の振る舞いも異なりうるため, その 3 次元構造を調査する必要がある.

本研究では始めに, アレシボ・レーダーによって観測された電離圏電子密度高度分布の時間変化と数値計算結果との比較を行なった. その結果, 本電離圏数値モデルが, アレシボ・レーダーで観測された半日周期/日周期の Es 層を再現し, 特に低高度の日周期の Es 層を再現できることを確認した. 次に, 得られた数値計算結果から Es 層の三次元構造を調査した. その結果, Es 層は高度 100 km 付近においても, 水平風の鉛直シアの構造を反映した, 幅が˜100 km で水平規模が 1000 km 以上の細く伸びた前線構造を有していた. この水平風の鉛直シアは, 地理低緯度帯の高度 110 km 以下で卓越している日周期潮汐波によって生じていた. 上記の結果から, Es 層が発生しやすい地磁気中緯度帯において, 地磁気緯度と対応する地理緯度に依存して, Es 層は異なる 3 次元構造を示しうることを見出した.

R005-21
Zoom meeting C ：11/1 PM2 (15:45-18:15)
16:30〜16:45

Automated detection of mid-latitude sporadic E using GPS-TEC ROTI and aeronautical navigation radio wave data

#Masahiro Takahi[1)],Keisuke Hosokawa[1)],Jun Sakai[1)],Susumu Saito[2)]
([1]UEC,([2]ENRI, MPAT

The sporadic E (Es) layer is a thin layer having dense electron density that appears at an altitude around 100 km. The Es layer mainly appears at mid-latitudes during the summer months. When the Es layer appears, radio waves in VHF frequencies, sometimes above 100 MHz, may be reflected by the Es layer and propagate over anomalously long distances. It may cause interference on radio systems such as FM broadcast and aeronautical navigation systems. Therefore, it is necessary to clarify the mechanism and dynamics of the Es layer. Although the vertical shear in the neutral wind has been accepted as a basic mechanism of the Es layer generation, the dynamics of the Es layer is still unclear and is still being studied by observations and numerical simulations.

Recently, two types of mapping techniques, such as Global Positioning System (GPS) Total Election Content (TEC) and Rate Of TEC Index (ROTI), have been used to detect the Es layer. Recent studies using these mapping techniques indicated that the Es layer often has a frontal structure extending roughly in the east-west direction during the daytime. More recently, measurements of aeronautical radio navigation signals have been conducted to reveal the location of the Es layer using abnormal radio propagation phenomena. Combining these observations, it is possible to visualize the spatial structure of the Es layer. However, detection of the Es events and estimation of their parameters such as front direction and velocity rely on manual processing. Therefore, it is required to establish a method to automatically detect and analyze the Es layer characteristics.

In this study, we propose a method to automatically detect the Es layer and retrieve the information on the spatial structure of the Es layer by applying the Hough transform, which can extract lines in an image to the ROTI map. This method demonstrated that the detected line segment well captured characteristics of the elongation direction of the Es layer. Furthermore, we used a map of reflection points of the VHF anomalous propagation to improve detection accuracy in the ROTI map. The reflection points of the Es layer are selected by setting minimum received powers (-110, -115, -120 dBm). We confirmed that adding the reflection points of the Es layer to the ROTI map could improve the performance of the Es layer extraction.

R005-22
Zoom meeting C ：11/1 PM2 (15:45-18:15)
16:45〜17:00

Equinoctial Asymmetry of Plasma Bubble Occurrence and Electro-Dynamics in South-East Asia

#Yuichi Otsuka[1)],Prayitno Abadi[2)],Kornyanat Hozumi[3)]
([1]ISEE, Nagoya Univ.,([2]LAPAN,([3]NICT

At the Asian longitudinal sector, plasma bubble and GPS scintillation frequently occur in equinox, when the solar terminator is parallel to the geomagnetic field line. Otsuka et al. (2016), who have analyzed GPS scintillation data observed at Kototabang (0.20^{o}S, 100.32^{o}E; geomagnetic latitude 10.6^{o}S), Indonesia in 2003-2004, have shown equinoctial asymmetry of plasma bubble occurrence. Scintillation occurs more frequently in Mar. equinox than Sep. equinox. Eastward scintillation drift velocity also shows equinoctial asymmetry. The eastward velocity is larger in Mar. equinox than Sep. equinox. They have suggested that the eastward drift corresponding to the downward electric field at post-sunset may be related to the prereversal enhancement of eastward electric field, which could play an important role in generating plasma bubble. To measure zonal drift velocities of a few hundred meter-scale irregularities associated with equatorial plasma bubbles, we have operated three single-frequency GPS receivers with their mutual distance of 116, 127, and 152 m at Kototabang, Indonesia since January 2003. Drift velocities of irregularities were measured using cross-correlation analysis with the time series of the GPS signal intensity obtained from the three receivers. In this study, the drift velocity data obtained during a period from 2003 to 2021 have been analyzed, and found that the eastward drift velocity is larger in Mar. equinox than Sep. equinox. This result is consistent with the previous study. We also investigated the solar activity dependence of the eastward drift velocity, and found that the eastward drift velocity depends on the solar activity largely in Mar. equinox than Sep. equinox, indicating the equinoctial asymmetry of the eastward drift velocity is intensified with increasing solar activity. To compare the vertical drift velocity at sunset, virtual height obtained with an ionosonde at Chumphon (10.73^{o}N, 99.37^{o}E; geomagnetic latitude 1.3^{o}N), Thailand, which is located near magnetic equator is analyzed. The result shows that vertical drift depends on the solar activity largely in Mar. equinox than Sep. equinox. These result indicates close relationship between the eastward drift and vertical drift (eastward electric field) at sunset terminator, and suggests that the zonal drift velocity (vertical electric field) may affect generation of plasma bubbles.

R005-23
Zoom meeting C ：11/1 PM2 (15:45-18:15)
17:00〜17:15

Analysis of Different Spread-F types and GPS Scintillation Occurrence over Bac Liu

#SEPTI PERWITASARI[1)],Kornyanat Hozumi[1)],Michi Nishioka[2)]
([1]NICT,[2]NICT

Equatorial spread-F (ESF) is one of the most important features in space weather because of its significant effect on communication and navigation. Therefore, real-time information on the ESF occurrence will be useful to detect the degradation of radio propagation conditions. We have developed a method to detect spread-F automatically for SEALION FMCW ionogram as a part of the plasma bubble alert system project. We used the 4th-degree polynomial fit and median filter to remove the noise in the ionogram and edge detection to determine the hF and foF2. We calculated the threshold of the non-spread-F ionogram within 100x100 pixels from the edge of hF and foF2. The Spread-F signature is classified into three categories: range type (Q), frequency type (F), and mixed-type (M). The validation using manual scaling data shows ˜80% match. The seasonal variation shows that all types of ESF are higher at equinoxes. We further analyze the relationship between the spread-F types and the scintillation by comparing the different spread-F types with the occurrence of GPS scintillation using the s4 index over Bac Liu (9.30N, 105.71E) in 2019. The analysis is still ongoing, and the detailed result will be discussed during the presentation.

R005-24
Zoom meeting C ：11/1 PM2 (15:45-18:15)
17:15〜17:30

Dependence of the occurrence of storm-time plasma bubbles extending to the mid-latitudes on solar wind dynamic pressure

#Takuya Sori[1)],Atsuki Shinbori[2)],Yuichi Otsuka[3)],Takuya Tsugawa[4)],Michi Nishioka[4)]
([1]ISEE, Nagoya Univ.,([2]ISEE, Nagoya Univ.,([3]ISEE, Nagoya Univ.,([4]NICT

We performed a superposed epoch analysis of solar wind, interplanetary magnetic field,

geomagnetic index, and the rate of total electron content (TEC) index (ROTI) derived from global navigation satellite system (GNSS)-TEC data during geomagnetic storms from 2000 to 2018 (616 events) in order to clarify the dependence of latitudinal extension of plasma bubbles on solar wind dynamic pressure and interplanetary electric field. In this analysis, we defined the time of the SYM-H minimum as the zero epoch time. The 616 events were classified according to whether the integrated value of the dawn-dusk (Ey) component of interplanetary electric field (IEF) for 12 hours before the zero epoch time exceeded 1000 mV/m・min (high IEF Ey: 308 events) or not (low IEF Ey: 308 events). As a result, it is found that the ROTI enhancement in the dusk sector extended to more than 30^o in geomagnetic latitude (GMLAT) for the high IEF Ey subset during the main phase of geomagnetic storms. On the other hand, the ROTI enhancement in the dusk sector for the low IEF Ey subset extended to only 20-25^o in GMLAT during the main phase of geomagnetic storms. This result suggests that the ROTI enhancement associated with plasma bubbles can extend to higher latitudes for high IEF Ey subset than for low IEF Ey, indicating that penetration electric field during geomagnetic storms in the equatorial region increases with IEF Ey.

Furthermore, the 308 events showing the integrated IEF Ey value of more than 1000 mV/m・min (high IEF Ey) were also classified according to whether the integrated value of solar wind dynamic pressure for 12 hours before the zero epoch time exceeded 2350 nPa・min (high pressure: 154 events) or not (low pressure: 154 events). The ROTI enhancement in the dusk sector extended more than 30^o in GMLAT for the high pressure subset during the main phase of geomagnetic storms while that for the low pressure subset extended up to only 25^o in GMLAT. The time-integrated values of IEF Ey for 12 hours before the zero epoch time were 1777 mV/m・min for the high pressure and 1722 mV/m・min for the low pressure. This observational fact implies that the ROTI enhancement associated with plasma bubbles can extend to higher latitudes for high pressure subset than for low pressure although the time-integrated values of IEF Ey for two subsets were comparable. It is suggested that the intensity of penetration electric field during geomagnetic storms can be stronger as the solar wind dynamic pressure becomes large. Therefore, not only IEF Ey but also solar wind dynamic pressure play an important role in the plasma bubble extension to middle latitudes.

R005-25
Zoom meeting C ：11/1 PM2 (15:45-18:15)
17:30〜17:45

COSMIC-2衛星搭載２周波ビーコン観測による東南アジア域のプラズマバブルに繋がりうる電離圏の長波長変動に関する研究

#寺田 一生 [1)], 山本 衛 [2)]
([1] 京大・生存研,[2] 京大・生存圏研

Study of ionospheric large-scale wave structure related to equatorial plasma bubble from COSMIC-2 dual-band beacon experiment

#Issei Terada[1)],Mamoru Yamamoto[2)]
([1]RISH, Kyoto Univ.,[2]RISH, Kyoto Univ.

Plasma bubbles (electron density depletion regions) occur in the ionosphere at low latitudes. They are known to occur immediately after sunset around the vernal and autumnal equinoxes. As a precursor to their occurrence, large-scale east-west electron density fluctuations with wavelengths ranging from 100 to 1000 km, called Large Scale Wave Structure (LSWS), are known to appear in the ionosphere. In previous studies, we succeeded in detecting the LSWS using the dual-band beacon (DBB) experiment with C/NOFS satellite. The orbital inclination of C/NOFS was 13 degrees, which was suitable to the study. However, it was difficult to capture the temporal and spatial structures of the LSWS because the number of satellites was only one and the observation frequency was limited as less than once every 90 minutes. In the present study, we use the DBB experiment with COSMIC-2 that is a constellation of six satellites with the orbital inclination of 24 degrees. COSMIC-2 increases the frequency of observations to about once every 15 minutes, allowing us to reveal changes in the temporal and spatial structures of the LSWS. In calculating the ionospheric Total Electron Content (TEC) from the DBB signals, it is necessary to estimate the instrumental bias. We use the two-station method to find the bias. Our DBB receivers are located in Bangkok, Ho Chi Minh City, and Chumphon, and their observation range is from East longitude 90 degrees to East longitude 120 degrees and from North latitude 20 degrees to South latitude 2 degrees at the IPP (Ionospheric Piece Point) altitude of 350 km. Assuming that a satellite path is the event when the satellite is located over the horizon from one station, about 800 satellite paths are observed per month at each observation site. The number of satellite paths is reduced to about 400 if we count events of successful two-station absolute TEC determination. We are finding the LSWS occurrence from the data, but there are still a lot of room for further study, such as the window function of the moving average and how many points should be averaged. We will report the structure of the LSWS by summarizing the analysis up to the time of presentation.

低緯度帯の電離圏では、プラズマバブル (電子密度の空乏域) が発生する。プラズマバブルは、春分や秋分の日没直後に発生することが知られており、また、発生の前兆現象として電離圏に Large Scale Wave Structure(LSWS) と呼ばれる波長 100km から 1000km に及ぶ大規模な東西方向の電子密度の変動が現れることが知られている。先行研究では、軌道傾斜角 13 度の C/NOFS 衛星を用いて LSWS を検知することに成功したが、機体数が 1 機で約 90 分に 1 回の観測であったため、LSWS の時間的・空間的構造を捉えるのには限界があった。今回の研究では、軌道傾斜角 24 度、機体数 6 機の COSMIC-2 衛星を用いることで約 15 分に 1 回の観測頻度に増え、LSWS の時間的・空間的構造の変化を観測することができる。２周波数から電離圏 Total Electron Content(TEC) を算出する際に、計器バイアスを推定することが必要である。このバイアス推定手法は 2 観測点法を用いている。2 観測点法は、各受信地で計器バイアスの最頻値を算出する 1 観測点法を行い、その最頻値の周辺を 2 観測点で TEC がフィットするように総当たりで調べ、決定している。受信機はバンコク、ホーチミン、チュンポンにあり、その観測範囲は、IPP (Ionospheric Piece Point) 高度 350km において東経 90 度から東経 120 度, 北緯 20 度から南緯 2 度ほどの範囲である。地平線に衛星が現れてから再び地平線に消えて行くまでを 1 衛星パスとすると、各観測地で月間約 800 個の衛星パスが観測され、その中の観測緯度に重なりがある衛星パスどうしで 2 観測点法を行うため、バイアス推定ができ TEC を求めることができた衛星パスは約 400 個に減る。現在までの解析から、LSWS によると思われる緩やかな絶対 TEC の変動が確認できているが、移動平均の窓関数や何点の平均を取るかなど、まだ検討の余地は大きい。発表時点までの解析をまとめて LSWS の構造について報告する。

R005-26
Zoom meeting C ：11/1 PM2 (15:45-18:15)
17:45〜18:00

主成分分析による地上磁場データの成分分離

#高山 久美 [1)], 吉川 顕正 [2)]
(1 九大,(2 九州大学地球惑星科学専攻

Principal component analysis for Component Separation of Geomagnetic field data

#Kumi Takayama[1)],Akimasa Yoshikawa[2)]
(1Kyushu Univ.,(2ICSWSE/Kyushu Univ.

Principal Component Analysis (PCA) is a statistical method that converts and reduces correlated multivariate data into a small number of uncorrelated variables called ”principal components”. In this study, we used this method to derive the basis functions for each station and for each month from the ground magnetic field data of the MAGnetic Data Acqusition System/Circum-pan Pacific Magnetometer Network (MAGDAS/CPMN) during magnetic quiet days in 1992-2004, and constructed a method to reconstruct daily variations using these basis functions.

By using this basis function, the magnetic field variation can be separated into the ”fundamental component” which indicates the daily variation of the geomagnetic field and the ”higher-order component” which indicates the disturbance component. In this study, the fundamental component is extracted by superimposing the first to fifth principal components, and the higher-order component is defined as the disturbance component observed by subtracting the fundamental component from the original data and superimposing it on the daily variation component. The global structure of each component was successfully extracted by visualization using the equivalent current method.

As a result of visualizing the each principal component in the fundamental component, we found that the first principal component has a structure similar to that of the daily variation of the geomagnetic field (Sq-EEJ current system), the second principal component and the third principal component has a structure similar to that of the (2, 2)-mode of the atmospheric tide with wind upwelling and suction near the equator and the (2, 4)-mode with wind upwelling and suction near mid-latitudes. These results strongly suggest that the principal component analysis is a useful method to elucidate the ionosphere-atmosphere vertical coupling.

主成分分析（PCA）とは、相関のある多変量データを『主成分』と呼ばれる相関のない少数の変数に変換し縮約する統計手法の一つである。本研究ではこの手法を用いて、1992〜2004 年の全球的地磁気観測ネットワーク (MAGDAS/CPMN) の磁気的静穏日における地上磁場データから、各観測点、各月の基底関数を導出し、この基底関数を用いて日変動を再構成する手法を構築した。

この基底関数を用いることで、磁場変動を地磁気変動の日変化を示す『基本成分』と擾乱成分を示す『高次成分』に分離することができる。本研究では、基本成分を、第 1 主成分から第 5 主成分までを重ね合わせて抽出し、高次成分を元のデータから基本成分を差し引き、日変化成分に重畳した形で観測される擾乱成分と定義して様々な解析を行った。更に等価電流法を用いた可視化法により、それぞれの成分のグローバルな構造を抽出することに成功した。

更に基本成分に含まれる主成分を可視化したした結果、第 1 主成分は地磁気の日変動（Sq-EEJ 電流系）、第 2 主成分、第 3 主成分は赤道付近に風の湧き出しと吸い込みがある大気潮汐の (2, 2) モード及び緯度 30 ° 付近に風の湧き出しと吸い込みがある (2, 4) モードのどちらかもしくはその両方によってそれぞれ駆動される電流構造と似た構造を持つ事をあきらかにした。これらの結果は、主成分分析が電離圏―大気圏上下結合を解明する際に役立つ手法であることを強く示唆している。

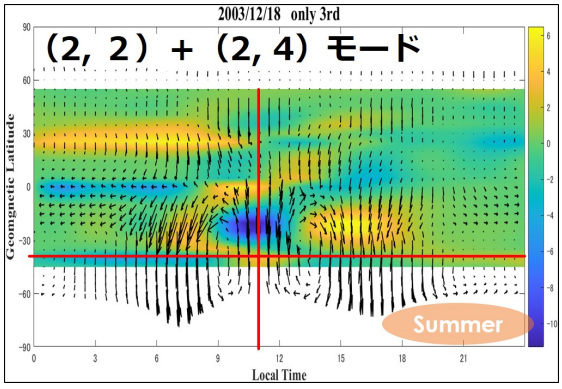

R005-27
Zoom meeting C ：11/2 AM1 (9:00-10:30)
9:00～9:15

A study of plasmaspheric electron content variations during a magnetic storm using the GPS total electron content data

#Zhiyu Chen[1)],Yuichi Otsuka[1)],Kazuo Shiokawa[1)],Atsuki Shinbori[1)],Takuya Sori[1)],Takuya Tsugawa[2)],Michi Nishioka[2)]
([1]ISEE, Nagoya Univ.,([2]NICT

By using dual-frequency Global Positioning System (GPS) data, the value of total electron content (TEC), which is an integration of the electron density along a ray path from satellite to receiver, can be measured. However, the measured TEC contains not only TEC values but also the inter-frequency biases inherent with satellites and receivers. In order to obtain absolute TEC, these biases need to be removed. Previous research (Otsuka et al., 2002) has developed a technique to estimate the absolute TEC using a least square fitting technique with an assumption of a single layer. However, the estimated absolute TEC sometimes shows negative values at equatorial region. This may be caused by the estimation error for the absolute TEC. In the current technique, the plasmasphere is not considered. The plasmaspheric electron content (PEC) could be included in the estimated biases. Therefore, in this study, we have analyzed the bias data obtained from approximately 9,000 receivers in the world to investigate PEC during a magnetic storm on March 17, 2013. The Dst index reached a minimum of -132 nT at 21 UT on March 17, 2013. Ten days' average of bias data during magnetic quiet days on March is calculated as reference value for each receiver to investigate effects of the magnetic storm. Standard deviations of biases during quiet days are used to investigate the stability of biases. The standard deviation of the biases for most of the receivers ranges 0-2 TECU, denoting that the biases are stable for day-to-day variation and that PEC variation during magnetic storm can be investigated. By subtracting reference value from the biases on the day during the magnetic storm, PEC variations at different longitudes and latitudes during the magnetic storm are investigated. The results show that during the main phase of magnetic storm, the PEC, on average, decreased by 1.69 TECU in Japan, by 0.95 TECU in Europe, by 0.77 TECU in Australia and by 0.61 TECU in North America, indicating that the PEC decrease has longitudinal dependence. Most of the PEC recovers during the period from March 18, 2013 to March 20, 2013.

Key words: total electron content; global positioning system; bias; plasmasphere

R005-28
Zoom meeting C ：11/2 AM1 (9:00-10:30)
9:15〜9:30

20 年間の GNSS-TEC データに見られる CIR/CME 駆動型磁気嵐時の大規模電離圏擾乱の統計的振る舞い

#新堀 淳樹 [1)], 惣宇利 卓弥 [2)], 大塚 雄一 [3)], 津川 卓也 [4)], 西岡 未知 [4)]
([1] 名古屋大学宇宙地球環境研究所,[2] 名大　ISEE,[3] 名大・宇地研,[4] 情報通信研究機構

Statistical behavior of large-scale ionospheric disturbances during CIR/CME-driven storms as seen in 20-year GNSS-TEC data

#Atsuki Shinbori[1)],Takuya Sori[2)],Yuichi Otsuka[3)],Takuya Tsugawa[4)],Michi Nishioka[4)]
([1]ISEE, Nagoya Univ.,[2]ISEE, Nagoya Univ.,[3]ISEE, Nagoya Univ.,[4]NICT

To investigate the differences of statistical behavior of global electron density in the ionosphere during geomagnetic storms driven by different solar wind structures of corotating interaction region (CIR) and coronal mass ejection (CME), we conducted a super epoch analysis of interplanetary magnetic field (IMF), solar wind, geomagnetic indices (AE and SYM-H), and global navigation satellite system (GNSS) - total electron content (TEC) data for 20 years (2000-2019). In this study, we analyzed the ratio of the TEC difference (rTEC) for 663 geomagnetic storms with the minimum SYM-H value of less than -40 nT. The rTEC is defined as a difference between the storm-time TEC and averaged quiet-day TEC normalized by the quiet-day one. Further, we identified 318 and 345 geomagnetic storms driven by CIR and CME, respectively. As a result, the characteristics of global rTEC variations did not show a significant difference between CIR-driven storms and CME-driven storms, but the magnitude of the rTEC variations and their duration time were different. Specifically, the rTEC enhancement related to the mid-latitude storm-enhanced density (SED) base and plume was much smaller for CIR-driven storms than that for CME-driven storms. The amplitude of the rTEC depletion at mid-latitudes and high latitudes also was larger for CME-driven storms. The main reason is that the large amount of electromagnetic energy inputs to the high-latitude ionosphere during CME-driven storms because the magnitude of the Bz component of the IMF and SYM-H index is larger for CME-driven storms than for CIR-driven storms. On the other hand, the duration time of the rTEC enhancements in the nighttime auroral zone and equatorial region was much longer for CIR-driven storms than for CME-driven storms. The mid-latitude trough also continued to appear equatorward of auroral oval for a long time for CIR-driven storms. However, the duration time of the rTEC enhancements related to the SED base and plume in the daytime mid-latitude ionosphere was shorter for CIR-driven storms than for CME-driven storms. The main reason is that high-speed stream with the Alfvenic oscillation of the Bz component of the IMF after the passage of CIR persists for several days and electromagnetic energy continues to input to the magnetosphere and ionosphere, which causes the consecutive occurrence of substorms during the recovery phase of CME-driven storms. This implies that the condition of negative storms persists for a long time and it takes longer time to recover the pre-storm condition for CME-driven storm events.

R005-29
Zoom meeting C ：11/2 AM1 (9:00-10:30)
9:30〜9:45

観測ロケットから地上までの電離圏全電子数観測システムの開発

#山本 衛 [1)], 黒川 浩規 [2)]
(1 京大・生存圏研,(2 京都大学生存圏研究所

Development of measurement system of rocket-ground total electron content (TEC)

#Mamoru Yamamoto[1)],Koki Kurokawa[2)]
(1RISH, Kyoto Univ.,(2RISH

This presenation reports the development of measurement systems of ionospheric total electron content (TEC) from the sounding rocket to the ground. It is to transmit two radio signals at coherent but different frequencies. In the ionospheric plasma, the radio wave's propagation velocity is related to the frequency. By detecting the phase variation between two signals, we estimate TEC along the radio propagation path. This time we developed a transmitter and antennas of the dual-band beacon (DBB) experiment at 150MHz and 400MHz frequencies. The transmitter generates 1W at both frequencies based on a unique phase-locked loop LSI Si5338 that can generate at most four different timing signals that are almost perfectly phase coherent. We developed a compact inverse-L type antenna that is attached on the skin of the JAXA ISAS soudning rocket S-520-32. One unit transmits both 150MHz and 400MHz signals. By attaching four antennas around the rocket, we transmit a circular polarized DBB signals to the ground. On the ground, we will use GNU Radio Beacon Receivers (GRBR) that is the very successful inplimentation of software radio for the measurement of satellite-ground TEC. The rocket experiment is planned in July/August 2022 from JAXA Uchinoura Space Center. In the presentation we will show design of the rocket instruments and preparation status of the experiment.

観測ロケットから地上までの電離圏全電子数（Total Electron Content; TEC）の観測システムの開発について報告する。電波はプラズマ中において真空中に比して電波の位相速度は速くなり、一方で群速度は低下する。その変化の程度は周波数の二乗に反比例するため、同じ経路に複数の周波数の電波を伝搬させ、その位相変化あるいは変調波の伝搬速度を測定することによって、TEC が測定できる。今回、我々は JAXA 宇宙科学研究所の観測ロケット S-520-32 号機を用いて 150MHz と 400MHz の 2 周波ビーコン（Dual-Band Beacon; DBB）観測を実施する。これに用いられるロケット搭載用の送信機とアンテナを開発した。送信機は両方の周波数でそれぞれ 1W 出力であり、発振器として、最大で 4 つの位相の揃ったタイミング信号が発生できる LSI である Si5338 を用いている。アンテナは、1 台から 2 つの周波数が放射できる逆 L 型アンテナを設計した。ロケットの周囲に 4 台のアンテナを均等配置することで、円偏波の DBB 波を地上に向かって放射する。一方で、地上においては、これまで衛星＝地上の DBB 観測に利用してきた GNU Radio Beacon Receiver (GRBR) 受信機を活用する。この観測ロケットは 2022 年 7〜8 月に JAXA 内之浦宇宙空間観測所から打上げが予定されている。現在、送信機とアンテナのフライト品の製作を行っている。発表では、これらの設計と性能について報告する。また観測全体の準備状況についても触れる予定である。

R005-30
Zoom meeting C ：11/2 AM1 (9:00-10:30)
9:45〜10:00

複数の GNSS 衛星群を用いる低コストな TEC 観測システム開発

#河上 晃治 [1)], 山本 衛 [2)], 斎藤 享 [3)],Ssessanga Nicholas[2)]
(1 京大,(2 京大・生存圏研,(3 電子航法研

Development of low-cost TEC observation system of using multiple GNSS constellations

#Koji Kawakami[1)],Mamoru Yamamoto[2)],Susumu Saito[3)],Nicholas Ssessanga[2)]
(1Kyoto Univ.,(2RISH, Kyoto Univ.,(3ENRI, MPAT

The ionosphere is located at about 100 to 1000 km altitudes. It is part of the atmosphere that is partially ionized. The electron density is fluctuated owing to the perturbations from the lower atmosphere and/or the solar activity. Depending on the distribution of electrons, the ionosphere causes reflection and absorption of medium- and short-wavelength radio waves, and cause delay of propagation at very high and ultra high frequency radio waves. Severe fluctuations of the ionospheric density can cause positioning failures by the Global Navigation Satellite System (GNSS) such as GPS, or other satellite-to-ground communications. They also cause problems short-wave radio communication as it depends on the reflection of the radio wave by the ionosphere. In order to avoid obstacles of those, it is necessary to observe and analyze the electron density in the ionosphere and build a highly accurate prediction model.

The electoron density is observed by analyzing the total electron content (TEC) that the radio waves passed from the satellite to the receiver. However, GNSS modules that can receive two-frequency signals are required for the measurement of the TEC. Such GNSS modules used to be very expensive (about a few millions of Japanese Yen). In recent years, on the other hand, an inexpensive, but multi-channel GNSS module appeared in the market at about tens of thousands of yen for the purpose of high-accuracy positioning.

In this presentation, we report the accuracy of this inexpensive module (u-blox F9P module) in TEC observation. However, the accuracy of TEC obtained by the module has not been well evaluated. Since the internal structure is not disclosed, we evaluated the accuracy by conducting actual observations. We compared the results with those from the GEONET receivers operated by the Geospatial Information Authority of Japan. In actual TEC observation, we developed a system to estimate TEC from the observation data. In order to highly accurate data, we have implemented a function that removes low elevation angle data, which is greatly affected by multipath error, and detects or corrects cycle slips.

In GPS, the estimation error of phase TEC was 5.7 TECU or less. Since the F9P module supports multiple GNSS constellations, we collect similar results with different GNSS constellations, i.e., QZSS, GLONASS, Galileo, Beidou, etc.

上空約 60km から 1000km に位置する電離圏では大気の一部が電離しており，電子密度が下層大気や太陽活動の影響によって活発に変動する．電子の分布によって電離圏は中波・短波帯電波の反射や吸収，超短波・極超短波帯電波の遅延を引き起こす．そのため，GPS 等の全球測位システム (GNSS) や衛星放送，電離圏による電波の反射を利用した短波通信などを利用するシステムに障害をもたらす要因となる．障害を回避するために，電離圏の電子密度の観測，解析および高精度な予測モデルの構築が必要となる．

電子密度の観測は主に人工衛星からの電波が受信機に到達するまでに通過した全電子数 (TEC) を解析することにより行われるが，二周波を同時に受信できるモジュールが必要である．この受信モジュールが数百万円と非常に高価であったのに対し，近年になって数万円程度の安価なものが自己位置推定用途で登場している．

本発表では，この安価なモジュール (u-blox F9P モジュール) の TEC 観測における精度の評価結果を報告する．モジュールの内部構造が明らかにされていないため，実際に観測を行い，その結果を国土地理院が日本全国に展開する GEONET 受信機網のデータと比較することで精度を評価する．実際に TEC 観測を行うにあたり，観測データから TEC を導出するシステムの開発を行った．高精度なデータを得るために，マルチパス誤差の影響が大きい低仰角のデータを除去し，位相の追尾の途切れを検出あるいは補正する機能を実装している．

GPS において，今回の環境では位相 TEC の誤差平均は 5.7(TECU) 以下であるという結果が得られた．F9P モジュールは GPS 以外にも複数の GNSS に対応しているため，受信から TEC の出力までを一元化した自律的に TEC 観測を行うシステムを開発し，それに組み込むことで安価に大量のデータを収集することが期待される．

R005-31
Zoom meeting C ：11/2 AM1 (9:00-10:30)
10:00〜10:15

南極観測船「しらせ」における大気光・全電子数観測

#山科 佐紀[1)], 齊藤 昭則[1)], 坂野井 健[2)], 津田 卓雄[3)], 青木 猛[3)], 江尻 省[4)], 西山 尚典[4)], 直井 隆浩[5)], 永原 政人[5)], 穂積 裕太[5)]
([1] 京都大・理・地球物理,[2] 東北大・理・PPARC,[3] 電通大,[4] 極地研,[5] 情報通信研究機構

Airglow and Total Electron Content observations on the Antarctic research vessel ”Shirase”

#Saki Yamashina[1)],Akinori Saito[1)],Takeshi Sakanoi[2)],Takuo Tsuda[3)],Takeshi Aoki[3)],Mitsumu K Ejiri[4)],Takanori Nishiyama[4)],Takahiro Naoi[5)],Masato Nagahara[5)],Yuta Hozumi[5)]
([1]Dept. of Geophysics, Kyoto Univ.,[2]PPARC, Grad. School of Science, Tohoku Univ.,[3]UEC,[4]NIPR,[5]NICT

Optical observations of the ionosphere have been conducted by ground-based all-sky imagers, and the ionosphere located over the ocean have not been observed sufficiently, so there are observational gaps over the ocean. In the southern hemisphere, where the ocean account for a large proportion, the gaps have been particularly large. We conducted optical observations of the ionosphere from the ocean using vessels in order to eliminate these gaps and to evaluate the differences in phenomena between the northern and southern hemispheres and the effects of land and ocean on the ionosphere. In the 61st and 62nd Japanese Antarctic Research Expedition (JARE), the all-sky imagers were installed on the Antarctic research vessel ”Shirase”, and optical observations were conducted on its route. The observation period was from November 2019 to March 2020 for the 61st JARE, and from November 2020 to February 2021 for the 62nd JARE. In the 61st JARE, one imager was installed to capture the 630.0nm wavelength emission with an exposure time of 19 seconds, and in the 62nd JARE, two imagers were installed to capture the 630.0nm and 670.0nm wavelength emission with an exposure time of 9 seconds. These two wavelengths respectively correspond to the atomic oxygen emission in the F-region of the ionosphere, and the aurora emission from nitrogen molecules and airglow emission from OH molecules in the E-region. In the 63rd JARE from November 2021 to March 2022, we plan to observe airglow and aurora with two imagers at 630.0nm and 760.0nm, using the same system as the 62nd JARE, except for some improvements in the observation system. This 760.0nm wavelength emission also corresponds to the emission from nitrogen molecules. ”Shirase” makes a round trip once a year between Japan and the Syowa Station in Antarctica, always passing through the equatorial anomaly zone at low latitudes and sailing under the southern auroral zone for a long time. In the 61st JARE we succeeded in observing airglow in the low latitudes and aurora in the Antarctic Ocean. In the 62nd JARE, however, “ Shirase” changed its route due to COVID-19 and hardly passed under the auroral zone, so observations of aurora were not conducted. On the other hand, airglow was observed in the 62nd JARE as well as in the 61st JARE. Although some route changes from previous years are planned for the 63rd JARE, it is expected that both of airglow and aurora will be observed. A GNSS receiver was newly installed in our system in the 62nd JARE, so Total Electron Content (TEC) observation was also carried out. The mesospheric gravity wave was observed from 670.0nm wavelength airglow, the ionospheric electron density structure at 250km altitude was observed from 630.0nm wavelength airglow, and the ionospheric electron density structure was observed from GNSS TEC. By comparing these observations with other satellite and ground observations, we evaluated observations of the upper atmosphere from the vessel with our system and analyzed the changes in the upper atmosphere over the ocean.

電離圏光学観測は地上に設置された全天イメージャーによって行われてきたため、海上に位置する電離圏の光学観測は十分に行われず、観測空白領域が生じていた。特に海洋の占める割合の多い南半球で観測空白領域が大きくなっていたが、これらの観測空白領域を解消し、南北半球間での現象の相違や、海陸が電離圏に与える影響の違いなどを評価することを目的に、船舶を利用した海上からの電離圏光学観測を実施した。第 61 次及び第 62 次南極地域観測（JARE）において、南極観測船「しらせ」に全天イメージャーを搭載し、その航路上で観測を行なった。観測期間は、第 61 次 JARE は 2019 年 11 月から 2020 年 3 月、第 62 次 JARE は 2020 年 11 月から 2021 年 2 月であった。第 61 次 JARE では 1 台のイメージャーを用いて露出時間 19 秒で 630.0nm 波長の発光を撮影し、第 62 次 JARE では 2 台のイメージャーを用いて、露出時間 9 秒で 630.0nm と 670.0nm 波長の発光を撮影した。この 2 波長はそれぞれ、電離圏 F 領域での酸素原子発光と、E 領域での窒素分子由来のオーロラ発光や OH 分子由来の大気光発光に対応する。また、2021 年 11 月から 2022 年 3 月までの第 63 次 JARE においても、一部観測システムの改良を行った点を除いて第 62 次 JARE と同様のシステムを用いて、2 台のイメージャーによってそれぞれ 630.0nm、760.0nm の波長帯域で大気光・オーロラの観測を行なう予定である。この 760.0nm 波長の発光も窒素分子由来の発光に対応するものである。「しらせ」は日本と南極昭和基地を 1 年に 1 度往復し、低緯度地域において赤道異常帯下を通過し、復路では南側のオーロラ帯下を長期間航行するような航路を取る。そのため第 61 次 JARE では低緯度地域での大気光観測と、南極近海でのオーロラ観測に成功した。しかし第 62 次 JARE では COVID-19 の影響から「しらせ」は大幅なルート変更を行い、オーロラ帯下をほとんど通過しなかったためオーロラの観測は実施されなかった。一方で大気光に関しては第 62 次 JARE でも、第 61 次 JARE と同様に観測が実施された。第 63 次 JARE では例年から多少のルート変更が計画されているが、大気光・オーロラどちらも観測できることが期待される。第 62 次 JARE では新たに観測システムに GNSS 受

信機を導入し、全電子数観測も行った。670.0nm 波長大気光から中間圏重力波、630.0nm 波長大気光から高度 250km の電離圏電子密度構造、GNSS 全電子数から電離圏電子密度構造が観測され、これらと他の衛星観測・地上観測との比較を行い、本システムによる船舶からの超高層大気観測の評価と海洋上空超高層大気の変動の解析を行なった。

R005-32
Zoom meeting C ：11/2 AM2 (10:45-12:30)
10:45〜11:00

はやぶさ２カプセル再突入（2020 年) における ELF/VLF 電波観測

#渡邉 堯 [1)], 小林 美樹 [2)], 加藤 泰男 [3)], 大矢 浩代 [4)], 塩川 和夫 [3)], 鈴木 和博 [2)], はやぶさー２ カプセル回収チーム [5)]
([1] 情報通信研究機構,[2] 日本流星研究会,[3] 名古屋大学宇宙地球環境研究所,[4] 千葉大学大学院工学研究院,[5] 宇宙航空研究開発機構

ELF/VLF Monitoring of the Hayabusa-2 Sample Return, 2020

#Takashi Watanabe[1)],Miki Kobayashi[2)],Yasuo Katoh[3)],Hiroyo Ohya[4)],Kazuo Shiokawa[3)],Kazuhiro Suzuki[2)],Team Hayabusa-2[5)]
([1]NICT,[2]Nippon Meteor Society,[3]Institute for Space-Earth Environment Research,[4]Graduate School Engineering, Chiba University,[5]Japan Aerospace Exploration Agency

Keay (1980) proposed that anomalous “sound” upon display of a very bright meteor (fireball) will be caused by the electrophonic hearing of strong ELF/VLF radio noise apparently coming from the fireball appearing in the upper atmosphere. He also proposed that anomalous hearing reported upon re-entry of spacecraft will be caused also by ELF/VLF radio noise of the descending spacecraft. No observational evidence of the radio emission was reported yet for the several re-entries of spacecraft. We planned this observational project to detect the ELF/VLF radio emission and associated anomalous sound for the re-entry of the Hayabusa-2 return capsule, taking place in the southern part of Australia on 6 December 2020 (JST). A loop antenna with a set of ELF/VLF amplifiers, a digital audio recorder (TASCAM DR-70D, 48000 samplings per sec), and a GPS time signal generator was used. The actual observation was performed by members of JAXA’s Hayabusa-2 team. The environmental ELF/VLF noise was successfully recorded for about 1 hour including the “fireball phase” of the capsule return, taking place in the interval of 02:28 - 02:29 (JST) at an altitude approximately ranged from 100 to 40 km. The linear distance of the return capsule from the observational site was ranged from 400 km to 60 km in this phase.

Several examples of weak radio bursts with a typical duration of 10 msec having a relatively flat spectrum were found in the fireball phase. The waveform and the frequency spectrum of an example are shown in Fig. 1. These radio bursts also showed a very weak dispersive nature. These characteristics suggest that the radio bursts were originated near the observational site, in a range of 100 - 200 km. Strong electric discharges of the highly charged capsule and turbulent slipstream of the ionized ablated gas formed in the fireball phase are suggested to generate observed ELF/VLF radio bursts.

Keay, C. S. L., Anomalous sounds from the entry of meteor fireballs. Science, 210, p 11, 1980.

Fig. 1: An ELF/VLF burst observed at 02:56 (JST) in the fire-ball phase of the Hayabusa-2 return capsule (indicated by a red box in the left-hand panel), and the spectrum of the burst (right-hand panel).

宇宙機の地球大気再突入に伴う ELF/VLF 電波放射の存在は、明るい流星（火球）に伴う異常聴音との関連で；早くから示唆されている（Keay, 1980)。しかしこれまでの宇宙機再突入に於いて試行された電波観測においては、通常の雷起源空電と異なる性質を示す電波放射の存在は報告されていない（Beech and Murray, 2005)。そこで 2020 年 12 月 6 日 02 時 (JST) に実施されたはやぶさ２カプセル再突入に関わる地上観測プログラムの一環として、ELF/VLF 電波観測を行った。しかし Covid-19 による移動制限により、観測器機はループアンテナ（単一方向)、ELF/VLF 受信機、データロガー（TASCAM DR-70、48000 サンプリング/秒)、GPS 時刻信号生成器等の必要最小限の機器のみとし、JAXA カプセル回収班メンバーによる代理観測として実施された。観測地の電波環境は極めて静穏であり、再突入の火球フェイズ（02 時 28 分 48 秒〜29 分 22 秒 JST）を含む約 30 分間にわたって、優れた観測データが得られた。

観測当日は観測地の北方に気圧の谷があり、オーストラリア西岸と東岸に強い温帯低気圧と前線が存在したため、これらの領域が起源と思われる空電が数多く受信されている。しかし今回は方探による直接的な空電源位置の測定は行っていないため、通常の雷活動起源の空電とは異なった特性を持つ、ELF/VLF ノイズの検出を試みた。その結果、Fig.1 左図にあるように立ち上がりが緩やかで継続性のある、弱い ELF/VLF ノイズが数個検出された。また同右図に示すように、このノイズは比較的フラットなスペクトルを持ち、当日約 1.7 kHz にあった電離層・地表導波管の遮断周波数域での強度の増加や、遠距離からの伝播を示す分散・減衰傾向も余り見られず、観測時間帯におけるカプセルの位置に相当する <200 km の、比較的近距離の発生であることが推測される。カプセルの火球フェイズでは遮熱物質のアブレーションが激しく起こっており、カプセルも秒速 10 km 近い高速で地球大気中を移動していることなどから、カプセル本体の強い帯電や飛跡中の電荷分布の偏りが発生し、カプセルとその周辺領域における断続的な放電によって、受信可能なレベルの ELF/VLF 電波が放射されたことが示唆される。

Keay, C. S. L., Anomalous sounds from the entry of meteor fireballs. Science, 210, p 11, 1980.
Beech, M. & Murray, I., VLF monitoring of the Genesis Sample Return Capsule re-entry, WGN, Journal of the International Meteor Organization, vol. 33, no. 2, p. 59, 2006

Fig. 1:(左)2016 年 12 月 6 日 02 時 54 分 (JST)、はやぶさ２カプセル再突入の火球フェイズに観測された ELF/VLF

継続性ノイズ波形、（右）周波数スペクトル。横軸：周波数 (Hz)、縦軸：電波強度 (db)。

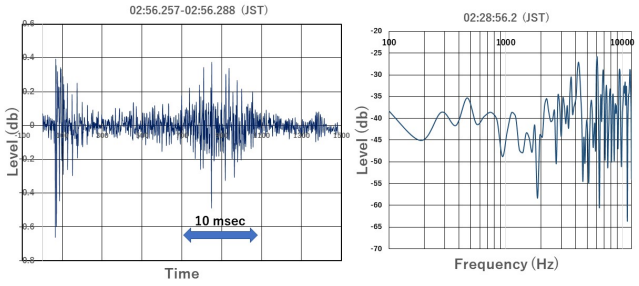

R005-33
Zoom meeting C ：11/2 AM2 (10:45-12:30)
11:00〜11:15

D-region ionospheric effects of fireballs occurred in Hokkaido using VLF/LF transmitter signals

#Takeru Suzuki[1)],Hiroyo Ohya[2)],Fuminori Tsuchiya[3)],Kazuo Shiokawa[4)],Hiroyuki Nakata[5)]
([1]Science and Engineering, Chiba University,[2]Engineering, Chiba Univ.,[3]Planet. Plasma Atmos. Res. Cent., Tohoku Univ.,[4]ISEE, Nagoya Univ.,[5]Grad. School of Eng., Chiba Univ.

Meteors and fireballs are known to ionize the D-region and lower E-region ionospheres at 80-120 km heights [Davies, 1966]. The fireballs are meteors whose magnitude of brightness is larger than -4 based on the IAU (International Astronomy Union) definition. TID (traveling ionospheric disturbance) associated with the Chelyabinsk meteoroid in Russia was reported based on GPS-TEC (total electron content) observations [Perevalova et al., 2015]. The amplitude and averaged period of the TEC variations were 0.07-0.5 TECU (1TECU=10^{16} electrons/m^2), and 10 minutes, respectively. The epicenter of the TID was airburst point at 20-30 km heights of the meteoroid, and the TID velocities were 250-660 m/s. As for D-region variations associated with meteoroids/meteors/fireballs, periodic variations in the phase of the transmitter signal (the frequency of RBU transmitter:66.67 kHz, Moscow, Russia) were observed after the Chelyabinsk meteoroid [Chernogor, 2015]. However, few quantitative studies for the D-region ionosphere associated with meteors and fireballs have been reported. In this study, we investigate the variations in the D-region ionosphere during a fireball occurred in Hokkaido at 11:55:55 UT on 18 October 2018, using VLF (very low frequency, 3-30 kHz) / LF (low frequency, 30-300 kHz) transmitter signals. The transmitter signals are reflected in the D-region ionosphere and intensities of the received signals are sensitive for variations in electron density in the lower ionosphere. The transmitters used in this study were JJY40kHz (Fukushima, Japan, 37.37 N, 140.85 E), JJY60kHz (Saga, Japan, 33.47 N, 130.18 E), and JJI (Miyazaki, Japan, 22.2 kHz, 32.05 N, 130.82 E). The receiver was located at RKB (Rikubetsu, Hokkaido, Japan, 43.45 N, 143.77 E). Periodic variations of 100-200 s were identified by a wavelet transformation of the signal intensities for the JJY40kHz-RKB, JJY60kHz-RKB, and JJI-RKB paths at about five minutes (12:01 UT) after the fireball. We consider that these variations of intensity were caused by the D-region variations due to acoustic waves in the atmosphere excited by the fireball. If the acoustic waves were excited at the beginning point (118 km altitude) or end point (25 km altitude) of the fireball, the propagation times of the acoustic waves from the exited point to the LF reflection point at 90 km height over RKB were calculated to be 138 s or 311 s, respectively. The arrival time (311 s) of the acoustic waves excited from the end point at the 25 km altitude agreed with the time lag between the fireball and onset of the VLF/LF variations with the period of 100-200 s. From the onset of the VLF/LF variations, we estimated the location where the variations in the D-region initiated along the paths. The estimated location was close to the RKB. The VLF/LF variations would be caused by acoustic waves excited at the end point. The acoustic waves obliquely propagated from the end point (25 km altitude) up to the D-region height (90 km altitude) at the south point of the RKB receiver.

R005-34
Zoom meeting C ：11/2 AM2 (10:45-12:30)
11:15〜11:30

D-region ionospheric signatures associated with the 2015 Nepal earthquake using LF transmitter signals

#Tekkan Akashi[1)],Hiroyo Ohya[2)],Fuminori Tsuchiya[3)],Kenro Nozaki[4)],Hiroyuki Nakata[5)]
([1]Engineering, Chiba Univ.,[2]Engineering, Chiba Univ.,[3]Planet. Plasma Atmos. Res. Cent., Tohoku Univ.,[4]UEC,[5]Grad. School of Eng., Chiba Univ.

In the D-region ionosphere, oscillations of LF (low frequency, 30-300 kHz) transmitter signals with a period of 100 s were reported about five minutes after mainshock of the 2011 Tohoku earthquake [Ohya et al., JGR, 2018]. This is only one report for coseismic disturbances in the D-region ionosphere. In this study, we investigate the D-region ionospheric variations associated with the 2015 Nepal earthquake using LF transmitter signals that reflect in the D-region ionosphere. The mainshock of the Nepal earthquake (Mw 7.9) occurred at 06:11:26 UT on April 25, 2015. The propagation path was BPC (68.5 kHz, 34.63N,115.83E) - TKN (Takine, Fukushima, 37.34N, 140.67E). Intensity and phase were observed with a sampling time of 0.1 s. We compared time variations between the LF transmitter signals and vertical velocity data of seismometers provided by IRIS (Incorporated Research Institutions for Seismology), USA. It was found that the received LF signal showed changes in the amplitude of +/-0.1 dB and phase of +/-1 degree change, respectively, after 1294 s after the mainshock of the earthquake. Based on wavelet analysis, a periodic component of about 100-300 s was seen in both the LF signals and seismic velocity at arrival time of acoustic waves excited by Rayleigh waves. The coherences between the LF variation and the seismic velocity were 0.90 and 0.77 for amplitude and phase, respectively, which were significant at the 95% confidence level. If the acoustic waves were excited at the midpoint of BPC-TKN propagation path by the Rayleigh waves that propagated horizontally from the epicenter, and propagate upward up to the D-region height 70 km, the propagation time from the ground to 70 km height would be 225 s. The propagation time of the Rayleigh wave calculated from seismograph data was 1057 s, and the whole propagation time of the Rayleigh and acoustic waves was 1282 s. The arrival time of the acoustic waves is 06:32:48 UT. This is in good agreement with the start time of the LF oscillation. We also used the wave-hop method to estimate the change in the reflection altitude. The results showed that the reflection altitude changed by $\pm$ 40 m, which corresponded to changes in the amplitude of +/-0.1 dB and phase of +/-1 degree change, respectively.

R005-35
Zoom meeting C ：11/2 AM2 (10:45-12:30)
11:30〜11:45

GPS 電波掩蔽観測を用いた東北地方太平洋沖地震に伴う津波による電離圏擾乱の高度分布解析

#伏見 亮祐 [1)], 中田 裕之 [2)], 大矢 浩代 [3)]
[(1 千葉大・融合理工,(2 千葉大・工,(3 千葉大・工・電気

Vertical profiles of ionospheric disturbances caused by the tsunami of the Tohoku earthquake using GPS occultation observation

#Ryosuke Fushimi[1)],Hiroyuki Nakata[2)],Hiroyo Ohya[3)]
[(1Science and Engineering , Chiba Univ,(2Grad. School of Eng., Chiba Univ.,(3Engineering, Chiba Univ.

It is reported that ionospheric disturbances are caused by large earthquakes. One of the causes is the infrasound wave excited by surface waves and/or tsunami. The horizontal propagations of the ionospheric disturbances after large earthquakes and tsunami have been examined by using a network of ground-based GPS receivers. As concerns the vertical propagation of ionospheric disturbances, on the other hand, gravity waves excited by the tsunami were detected using TEC data obtained by GPS radio occultation observations [Coisson et al., 2014]. However, there are still several unknowns about the variation of the vertical profiles of the ionospheric disturbances. In this study, to examine the vertical propagation of the ionospheric disturbances due to tsunamis, we have examined electron density profiles observed by GPS radio occultation measurements of FORMOSAT-3/COSMIC satellites. The data is provided by CDAAC (COSMIC Data Analysis and Archive Center). We analyzed the ionospheric disturbances caused by a tsunami associated with Tohoku Earthquake (M9.0) occurred at 5:46:18 on 11th March 2011 (UTC). Based on the simulation result of tsunami propagation provided by the NOAA, we selected density profiles observed within 3 hours after the passage of the tsunami. In the previous study, we used the Chapman model to extract the fluctuating components. On the other hand, in this study, we applied the wavelet transform directly to the vertical profiles of the electron density to determine the spectrum intensity of the ionospheric disturbance as a function of wavelength. In the data points observed in the northeast direction from the epicenter near the Kamchatka peninsula, the spectrum intensity in the wavelength range of 8 to 32 km was enhanced more strongly over the altitude range of 200 to 450 km compared to the quiet days. In the data points observed in the southeast direction from the epicenter, the spectrum intensity was smaller than that of the data observed in the northeast direction from the epicenter, but the spectrum with a wavelength of 32 km was strongly detected over the altitude range of 200-450 km compared to the quiet days. In the previous analysis method, it was difficult to see the long-wavelength fluctuations associated with the tsunami due to the fitting error with the Chapman model, especially for the data observed in the southeast direction from the epicenter, but the analysis method in this study makes it easier to see the fluctuations for the wavelength longer than 32km.

大規模な地震の発生後に電離圏擾乱が発生することが報告されている。これは、地面変動や津波により生じた音波や大気重力波が電離圏高度まで伝搬するためである。津波発生後の電離圏変動の水平方向の伝搬特性は、TEC 観測などを用いて明らかにされつつある。これに対し、鉛直方向の伝搬については、GPS 電波掩蔽観測により得られた高度方向の TEC データを用いて、津波によって励起された大気重力波の観測が報告されている [Coisson et al. , 2014]。しかし津波の伝搬に伴う変化についてはまだ不明な点が存在する。そこで、本研究では、東北沖地震により発生した津波に伴う電離圏擾乱の高度方向の変化について解析を行った。用いたデータは、CDAAC(COSMIC Data Analysis and Archive Center) により提供されている FORMOSAT-3/COSMIC 衛星による GPS 電波掩蔽観測で得られる電子密度の高度プロファイルデータである。解析対象とした事例は 2011 年 3 月 11 日 5 時 46 分 18 秒（協定世界時）に東北沖で発生した M9.0 の東北地方太平洋沖地震による津波である。NOAA により提供されているシミュレーション結果に基づき、津波第一波到達後 3 時間以内に観測されたデータを取得し、解析を行った。以前は、チャップマンモデルとの差を変動成分として抽出していた。それに対し、今回は高度方向の電子密度データに直接ウェーブレット変換を施し、変動の波長に対するスペクトルを求め、静穏時のデータと比較することで、変動の検出を行った。震央から北東方向のカムチャッカ半島付近で観測されたデータでは、静穏日と比較して、高度 200˜450km にわたって波長 8˜32km のスペクトルが強く検出された。また震央から南東方向の地点で観測されたデータでは、北東方向のデータよりスペクトルの強度は小さかったが、静穏日と比較して、高度 200˜450km にわたって波長 32km のスペクトルが強く検出された。以前の解析方法では、特に震央から南東方向の地点で観測されたデータにおいて、チャップマンモデルとのフィッティング誤差により、より長波長の変動が見えづらかったが、今回の解析手法では、波長 32km の変動がより明瞭になった。

R005-36
Zoom meeting C ：11/2 AM2 (10:45-12:30)
11:45〜12:00

HFD を用いた地震に伴う電離圏擾乱の 3 次元空間分布の解析

#堀切 友晃 [1)], 中田 裕之 [2)], 大矢 浩代 [3)], 細川 敬祐 [4)]
([1] 千葉大学院融合理工学府,[2] 千葉大・工,[3] 千葉大・工・電気,[4] 電通大

Analysis of 3-dimensional spatial distributions of coseismic ionospheric disturbances using HFD

#Tomoaki Horikiri[1)],Hiroyuki Nakata[2)],Hiroyo Ohya[3)],Keisuke Hosokawa[4)]
([1]Graduate School of Science and Engineering, Chiba Univ.,[2]Grad. School of Eng., Chiba Univ.,[3]Engineering, Chiba Univ.,[4]UEC

Since acoustic waves and/or atmospheric gravitational waves generated by ground motions and/or tsunamis associated with large earthquakes propagate upward, the coseismic ionospheric disturbances occurs. The horizontal propagation of ionospheric disturbances is examined by using GPS observations. On the other hand, the vertical propagations of the coseismic disturbances are rarely reported. Since HF Doppler sounding system(HFD), which is operated by the University at Electro-Communications, is enable to receive the four radio waves (5.006, 6.055, 8.006 and 9.595 MHz) simultaneously, three-dimentional distributions of various ionospheric disturbances can be examined by this system. In this study, therefore we examined the 3-dimentional distribution of ionospheric disturbances associated with earthquakes by using the HF Doppler sounding system. In this study, we examined the ionospheric disturbances associated with the earthquake occurred at Hamadori, Fukushima Prefecture on April 11, 2011(the location of epicenter is at latitude 36 degrees 33 minute north, 140 degrees 24 minutes of east longitude). The largest disturbances of Doppler frequencies ware observed at Iitate which is the closest to the epicenter. The vertical velocities of neutral atmospheric particles at the ionospheric reflection height were estimated as, 59.3 m/s for 5.006 MHz and 56.3 m/s for 8.006 MHz. The variation of Doppler frequency at Kakioka was about 1.2Hz which corresponds to 34.9 m/s for the vertical velocity. The magnitude of the disturbance decreased as the distance form the epicenter increased. By using the International Reference Ionosphere (IRI), the reflection altitudes of the radio waves received at Sugadaira were found to be about 193 km at 5.006 MHz, 230 km at 6.055 MHz, and 240 km at 8.006 MHz. To determine the propagation path of the disturbance, we calculated the arrival times of the disturbances in the case that the disturbances arrived directly from the epicenter as an acoustic wave and the case that the an acoustic wave generated by the Rayleigh wave propagated from the epicenter excite the ionospheric disturbance. As a result, the observed disturbances in the HFD are considered to be caused by the latter case. From these results, it is confirmed that the disturbances propagated over an distance of about 240 km from the epicenter of a M7 earthquake.

大規模な地震の発生後に地面変動や津波により生じた音波や大気重力波が電離圏高度まで伝搬し電離圏擾乱が発生することが知られている。地震に伴う電離圏擾乱の伝搬特性は GPS 観測等を用いた研究により、水平方向の伝搬については詳細に調べられてきたが、鉛直方向の伝搬に関する解析はきわめて少ない。現在電気通信大学を中心に行われている HF ドップラー観測 (HFD) は、日本全国に広がる観測点で複数の電波が受信できる観測システムであり、様々な電離圏変動の空間的な広がりを調べることが可能である。そこで本研究では地震に伴う電離圏擾乱の鉛直方向の伝搬特性に特に注目し解析を行った。研究で用いた HF ドップラー観測では、異なる送信周波数 (5.006, 6.055, 8.006, 9.595 MHz) の電波を用いることで複数の高度で変動を観測できる。本研究では福島県浜通りで 2011 年 4 月 11 日に発生したマグニチュード 7.0 の地震 (震源の位置 36.56 ° N , 140.40 ° E) に伴う変動について解析を行った。HFD 反射点が地震源に一番近い飯舘で取得されたデータでは、他の受信局と比べ変動が大きかった。HFD での変動を電離圏反射高度においての中性大気粒子の上下動速度に換算すると、5.006 MHz で 59.3 m/s、8.006 MHz では 56.3 m/s 程度の変動が確認された。また、6.055 MHz のデータの中で震源に近い柿岡では 34.9 m/s 程度の変動であった。このように HFD 反射点での中性大気粒子の上下動速度比較では、震央から距離が離れるにつれ擾乱が小さくなる様子が見られた。さらに、国際標準電離圏モデル (IRI) を用いて 各周波数の電離圏反射高度を求めたところ、5.006 MHz で 200 km、6.055 MHz で 230 km、8.006 MHz で 240 km 程度の反射高度となった。変動の伝搬経路を明らかにするため、変動が音波として震源から直接到達する場合と、震源で発生したレイリー波によって大気波動が生じそれが電離圏に到達した場合での変動到達時間の比較を行った。結果として、HFD で観測された変動はレイリー波による影響であると考えられる。M7 の地震で震源を中心に約 240km にわたる範囲に変動が伝搬していく様子が確認できた。さらに事例を追加し、マグニチュードと変動の広がりについての関係を明らかにしていく。

R005-37
Zoom meeting C ：11/2 AM2 (10:45-12:30)
12:00〜12:15

電離圏イオンドリフト測定器開発のための低エネルギーイオン加速装置の開発

#尾原 咲穂 [1)], 阿部 琢美 [2)], 三宅 亙 [3)]
([1] 東海大,[2] ＪＡＸＡ宇宙科学研究所,[3] 東海大・工

Development of a low energy ion source for ion drift measurements

#Sakiho Ohara[1)],Takumi Abe[2)],Wataru Miyake[3)]
([1]Tokai Univ,[2]ISAS/JAXA,[3]Tokai Univ.

The ionosphere is the region from about 70 km to 1000 km above the Earth's surface. It is composed of neutral particles without charge, and charged particles (plasmas) generated by extreme ultraviolet and X-ray radiation from the Sun. The motion of plasma particles in the ionosphere is influenced by the Earth's magnetic field, while collisions between ions and neutral particles are also important. Such collisions result in a momentum transport between ion particles and neutral particles, and are related to various phenomena such as ionospheric disturbance in the ionosphere.

In the F region of the ionosphere, the F1 layer has the largest electron density, while ion and electron tend to diffuse through the atmosphere in the F2 layer. Ambipolar diffusion occurs because of the unbalance of gravity and pressure. Ions in this region have a drift motion in the direction perpendicular to the electric and magnetic fields. Thus, ions are known to make complex movement due to momentum transport occurring in this region.

The purpose of this study is to develop an advanced instrument to measure 3D ion drift velocity in the lower ionosphere. ISAS/JAXA has been developing such an instrument which can be installed on sounding rocket. To calibrate a performance of the instrument, it is necessary to prepare plasma environment in which ion particles are coming into the instrument with a speed of several km/s, which corresponds to the speed of a sounding rocket or satellite.

The average temperature of ion particles in the ionosphere is known to be about several hundred K, which corresponds to several hundred m/s in terms of thermal velocity. Considering the speed of the sounding rocket is about 1~2 km/s during its ballistic flight, it is an assumed situation that the ions are coming into the instrument with a bulk velocity of 1~2 km/s. Therefore, for this purpose, we will have to develop a source that can generate drifting ions with a velocity of several km/s (kinetic energy of several eV).

We have so far tried to generate drifting ions by applying a voltage to a mesh grid in the ion accelerator, and to make measurements of the ion current with a Langmuir probe. As a result, when the voltage applied to the accelerator was changed, the electron temperature and density obtained from Langmuir probe current-voltage characteristics seemed unchanged, but the saturated electron current changed significantly depending on the applied voltage. Since ions with relatively large energy (more than 1 eV) may affect the saturation electron current, the change observed in the saturation electron current region may be due to the accelerated ions. To further study this possibility, we are going to measure the energy distribution of the accelerated ions in detail using the instrument under development.

Next, we ate going to use a simulation program to investigate the reason why the saturation electron current changed with the applied voltage and to simulate a trajectory of the ions accelerated by the electric field which is generated by applying the voltage to the mesh grids. In addition, we will discuss in detail the conditions on which an ion drift velocity becomes close to that of the sounding rocket.

電離圏は高度約 70km から約 1000km までの空間で, 電荷を持たない中性大気と, 太陽からの極端紫外線や X 線放射等によって生成されたイオンと電子により構成される電離大気から成る. 電離圏に存在するプラズマ粒子の運動は地球の磁場によって支配され, 更にイオン粒子と中性大気の衝突が顕著にある. このため,2 種類の粒子間衝突による運動量の輸送現象が起こる. この輸送現象は, 電離圏における電子擾乱をはじめとする多様な現象に係っている.

電離圏 F 領域では, 最大の電子密度を持つ F1 層と, イオンや電子が中性大気中を拡散し, 重力と圧力勾配を釣り合わせようとする両極性拡散が起こる F2 層が存在する. この領域に存在するイオン粒子は, 電場と磁場に垂直な方向で (E × B)/B^2 ドリフトを始める. 中性大気はイオン粒子の抗力によってイオン粒子と同じ速さ, 同じ向きで運動をしようとするが, イオンの密度成分により急速に抑制され, 運動は水平方向成分が卓越する. このような運動量輸送により電離圏 F 領域ではイオン粒子は複雑な運動を行なっている.

本研究の目的は上記の諸現象が顕著である電離圏下部において, イオンドリフトを直接観測出来るような精度の高い測定器の開発である. 電離圏中のイオンドリフト運動を測定するために海外ではイオンドリフトメータが用いられてきた.JAXA 宇宙科学研究所ではこの類の飛翔体搭載用の測定器開発を行っている. 測定器の性能を確認するためには, 飛翔体上でのイオン測定時に予測される環境, すなわち飛翔体の速度である数 km/s の速度でイオン粒子が測定器に向かって飛び込んでくる状況を作り出す必要がある.

電離圏中に分布するイオンの平均的な温度は数 100K であることが知られており, 熱速度に換算するとおよそ数 100m/s に相当する. これに対し, 観測ロケットの飛翔速度はおよそ 1~2km/s であり, ロケット上では見かけ上, イオンが 1~2km/s のバルク速度をもって測定器に向かってくると捉えることができる. よって本研究では数 km/s の速度 (数 eV の運動エネルギー) を持ち, ドリフト運動をするイオンの生成が可能な加速装置の開発を行う.

これまで, イオン加速装置内のメッシュグリッドに電圧を印加し, 設置してあるラングミュアプローブで電流を測定

する基礎実験を行ってきた. その結果, 加速装置の印加電圧を変えた場合にラングミュアプローブの電流電圧特性から得られる電子温度, 密度に変化は見られなかったが, 印加電圧に応じて飽和電子電流領域に変化が見られた. エネルギーが比較的大きな (1eV 以上) イオンは飽和電子電流に影響を及ぼす可能性があることから, これまでの実験で確認された飽和電子電流領域の変化は加速されたイオン粒子による影響である可能性が考えられる. これを確認するため, 開発中の測定器を用いて加速されたイオンのエネルギー分布を詳しく測定することにしている.

また, 今後はシミュレーションプログラムを用いて加速装置に印加する電圧毎にプローブによって得られる電流値の変化を調べると共に, 電極に電圧を印加した際に電界により加速されるイオン粒子の軌道シミュレーションを行う. 更に, 飛翔体上で観測するときの条件に近いイオン流れを生成するための条件について詳しく解析していく予定である.

R005-38
Zoom meeting C ：11/2 PM1 (13:45-15:30)
13:45〜14:00

火星熱圏電離圏にみられる密度擾乱の励起源

#中川 広務[1)], 吉田 奈央[2)], 堺 正太朗[3)], 原田 裕己[4)], 寺田 香織[5)], 寺田 直樹[6)], 藤原 均[7)], 今村 剛[8)], 関 華奈子[9)]
([1] 東北大・理・地球物理,[2] 東北大・理・地物,[3] 東北大・理・地球物理,[4] 京大・理・地球惑星,[5] 東北大・理・地物,[6] 東北大・理・地物,[7] 成蹊大・理工,[8] 東京大学,[9] 東大理・地球惑星科学専攻

Relative importance of possible sources on density perturbations in the Martian thermosphere and ionosphere

#Hiromu Nakagawa[1)],Nao Yoshida[2)],Shotaro Sakai[3)],Yuki Harada[4)],Kaori Terada[5)],Naoki Terada[6)],Hitoshi Fujiwara[7)],Takeshi Imamura[8)],Kanako Seki[9)]
([1]Dep. Geophysics, Grad. Sch. Sci., Tohoku Univ.,[2]Geophysics, Tohoku Univ.,[3]Dept. Geophys., Science, Tohoku Univ.,[4]Dept. of Geophys., Kyoto Univ.,[5]Geophys., Tohoku Univ.,[6]Dept. Geophys., Grad. Sch. Sci., Tohoku Univ.,[7]Faculty of Science and Technology, Seikei University,[8]The University of Tokyo,[9]Dept. Earth & Planetary Sci., Science, Univ. Tokyo

Atmospheric waves are recognized as an important part of the upper atmospheric system. This work offers the in-depth compositional study of wave perturbations in density profiles in the Martian thermosphere and ionosphere. Recent missions revealed highly variable nature of the Martian upper atmosphere, which is the reservoir region for atmospheric escape to space. Large-amplitude perturbations (>50 %) of density and temperature ubiquitously exist in the Martian thermosphere (Bougher et al., 2015; Yigit et al., 2015; Terada et al., 2017; England et al., 2017; Nakagawa et al., 2020) and ionosphere (Mayyasi et al., 2019). The excitation sources of density perturbations in the Martian thermosphere and ionosphere are still open question. There are two possible sources to drive the perturbations: (1) atmospheric waves propagating from lower atmosphere, and (2) energy injected from above by external forcing, such as solar wind (SW), and solar energetic particle (SEP). In order to constrain the possible sources to drive perturbations, we examine the in-situ observations of CO2, N2, O, CO2+, and O+ density perturbations by NGIMS onboard MAVEN. Longer-wavelength perturbations caused by atmospheric gravity waves presumably from below are dominant in both dayside and nightside in thermosphere. The relative perturbations between CO2 and CO2+ indicates the thermosphere-ionosphere coupling. The effective thermosphere-ionosphere coupling in perturbations can be found in dayside northern hemisphere. On the other hand, ion-specific perturbations can be additionally identified in dayside southern hemisphere. In nightside, ion-specific perturbations are notably significant rather than dayside, especially in southern hemisphere. This is the effect of the crustal magnetic field in southern hemisphere, which possibly leads perturbations by precipitating electrons of the solar wind. Negative correlation between CO2+ and O+ perturbations caused by photochemical reactions can be found only in dayside. Photochemical imprint in dayside ionospheric perturbations suggests slow perturbations, longer than photochemical lifetime at these altitudes (10-100 sec), originated from thermospheric composition, in addition to fast perturbations with well in-phase between CO2+ and O+. Fast perturbations which immediately fluctuate all species in phase, presumably caused by precipitating electrons is the main driver especially in nightside ionosphere. This result coincides with the notable decrease of positive correlations between CO2 and CO2+ perturbations toward nightside, which suggests less coupling in perturbations between thermosphere and ionosphere in nightside.

R005-39
Zoom meeting C ：11/2 PM1 (13:45-15:30)
14:00〜14:15

衛星 GOCE による熱圏の大気密度の日変動について

#中山 沙由香 [1)],Liu Huixin[2)]
(1 九大,(2 九大・理・地惑

Day to day variability of neutral density in the thermosphere observed by GOCE satellite

#Sayuka Nakayama[1)],Huixin Liu[2)]
(1Kyusyu univ,(2None

Day to day variability of neutral density in the thermosphere observed by GOCE satellite

Sayuka Nakayama, Huixin Liu
Earth and planetary science division, Kyushu university, Japan

It is well known that extreme space weather events (e.g., intense geomagnetic storms) cause day-to-day variabilities of neutral density and wind in the ionosphere/thermosphere system (IT system) (Liu et al(2021)). On the other hand, the density and wind in the IT system are variable even during the quiet time. During quiet times, the IT system is strongly influenced by the lower atmosphere. In J.G.Charney(1990), the summer circumpolar anticyclone and the winter circumpolar cyclone in the upper stratosphere and mesosphere are little influenced by lower atmosphere motions. Energy may escape into the mesosphere near the equinoxes, when the upper-atmosphere zonal flow reverses. Therefore, effects from lower atmosphere to upper atmosphere are so important. However, it is poorly understood that quantitative roles of the lower atmosphere and outer space to the IT system variability are during quiet times.

This study will show the day-to-day variation of the neutral density observed by GOCE satellite during quiet times (Kp $\leqq$ 3). Also, we will compare the neutral density with F10.7, Kp, and wind in the lower atmosphere to reveal whether the main driver of the neutral density is impacts from the outer space or the lower atmosphere.

R005-40
Zoom meeting C ：11/2 PM1 (13:45-15:30)
14:15〜14:30

地磁気静穏時に発生したpseudo breakupにおける電離圏変動に対する熱圏風変動

#大山 伸一郎[1,4],Heikki Vanhamaki[2],Cai Lei[2],Anita Aikio[2],Rietveld Michael[3], 小川 泰信[4],Raita Tero[5],Kellinsalmi Mirjam[6],Kauristie Kirsti[6],Kozelov Boris[7], 新堀 淳樹[1], 塩川 和夫[1], 津田 卓雄[8], 坂野井 健[9]
([1] 名大 ISEE,[2]Univ. Oulu,[3]EISCAT,[4] 極地研,[5]SGO, Univ. Oulu,[6]FMI,[7]PGI,[8] 電通大,[9] 東北大・理・PPARC

Thermospheric wind response to ionospheric variations at a pseudo breakup during geomagnetically quiet conditions

#Shin ichiro Oyama[1,4],Heikki Vanhamaki[2],Lei Cai[2],Anita Aikio[2],Michael Rietveld[3],Yasunobu Ogawa[4],Tero Raita[5],Mirjam Kellinsalmi[6],Kirsti Kauristie[6],Kozelov Boris[7],Atsuki Shinbori[1],Kazuo Shiokawa[1],Takuo Tsuda[8],Takeshi Sakanoi[9]
([1]ISEE, Nagoya Univ.,[2]Univ. Oulu,[3]EISCAT,[4]NIPR,[5]SGO, Univ. Oulu,[6]FMI,[7]PGI,[8]UEC,[9]PPARC, Grad. School of Science, Tohoku Univ.

Thermospheric wind response at F-region altitude to a sudden westward turning of the ion velocity at high latitude was studied by analyzing data obtained during a conjunction event with Fabry-Perot interferometer (FPI; 630 nm), Dynasonde and Swarm A/C satellites in northern Scandinavia. The event was found during a period of geomagnetically quiet conditions with Kp of 0 to 1 through the night, but some auroral activity in the north. From the Swarm measurement, the ionospheric trough was identified at 70-72N. The collocated FPI and Dynasonde measured thermospheric winds (**U**) and ionospheric plasma velocities (**V**), respectively, at the equatorward edge of the trough. A notable scientific message that was revealed by this study is a possible role of the thermospheric wind in the energy dissipation process. Negative **U**・**V** indicates that kinetic energy of the thermosphere is dissipated into the ionosphere by particle collisions, and this can occur when the thermospheric wind is not able to follow instantly a sudden **V** change due to inertia. At a pseudo breakup during the conjunction event, the Dynasonde-measured **V** suddenly changed the direction from eastward to westward within 10 min. The FPI-measured **U** was also accelerated westward after the pseudo breakup, but its development was more gradual than that of **V**, so that **U** remained eastward for a while after the pseudo breakup. During this transition interval of about 10 min, **U**・**V** was negative. An irresistible force of the thermosphere such as seen in this study should be found frequently at high latitudes because sudden direction change in **V** is a typical ionospheric feature at the substorm onset. Sign of **U**・**V** may be used as the indicator to find time and location where the thermospheric inertia plays a role in the energy dissipation process.

R005-41
Zoom meeting C ：11/2 PM1 (13:45-15:30)
14:30〜14:45

大気圏電離圏モデルGAIAによる地磁気静穏時の平均的熱圏・電離圏変動の再現性評価と課題

#陣 英克[1)], 三好 勉信[2)], 垰 千尋[1)], 品川 裕之[1)], 藤原 均[3)]
([1] 情報通信研究機構,[2] 九大・理・地球惑星,[3] 成蹊大・理工

Evaluation of climatological features of global thermosphere and ionosphere reproduced by a whole atmosphere-ionosphere model GAIA

#Hidekatsu Jin[1)],Yasunobu Miyoshi[2)],Chihiro Tao[1)],Hiroyuki Shinagawa[1)],Hitoshi Fujiwara[3)]
([1]NICT,[2]Dept. Earth & Planetary Sci, Kyushu Univ.,[3]Faculty of Science and Technology, Seikei University

Temporal and spatial variations in the ionospheric electron density and thermospheric mass density can have significant impacts on radio communications between ground and space, GNSS navigations, orbits of satellites and space debris, and so on. In order to nowcast and forecast upper atmospheric variations and disturbances, a whole atmospheric model, GAIA, has been developed. A number of minor and major revisions have been made to the model since the previous major update in 2013, including addition of ion compositions and chemical reactions, revisions of ion dynamics and energetics equations, replacement of input solar irradiance model, and so on. For validation, we compared monthly averaged variations of thermosphere and ionosphere reproduced by the previous and current versions of GAIA with global observations of upper thermospheric mass density by satellites (CHAMP, GRACE and SWARM) as well as with global and local ionospheric observations by GNSS-TEC and ionosondes. The results suggest that the current version of GAIA generally reproduce better climatological variations of thermosphere and ionosphere as compared with the previous version. However, we also found that there are still disagreements between GAIA and observations, in the ionospheric variations in some regions and local times. We will make some numerical experiments and further comparisons with observations to identify which factors in the model lead to the disagreements with observations. We will report how the latest version of the model can reproduce averaged features of thermosphere and ionosphere, and discuss subjects to be improved in the future.

熱圏や電離圏の大気・電子密度の変動は、地上-衛星間の通信や衛星測位、衛星・スペースデブリの軌道などを変えるため、これらを利用する我々の社会活動に影響する。我々は熱圏および電離圏の変動や乱れの現況把握や予測のため、全球の大気圏と電離圏を扱うことのできる大気圏電離圏モデルGAIAを開発してきた。2013年以降、我々はGAIAに様々な大小の改良を加えてきた（イオン成分や化学反応の追加、ダイナミクスやエネルギー式の改良、太陽放射光モデルの入れ替え等）。我々はGAIAの検証のため、GAIAによる地磁気静穏時の平均的な熱圏と電離圏の変動について、全球の熱圏質量密度分布の衛星観測（CHAMP、GRACE、SWARM）および全球・国内電離圏観測（GNSS-TEC、イオノゾンデ）と比較し、再現性の評価を行った。その結果、GAIAの新バージョンは熱圏と電離圏の平均的な変動について、これまでより全体的に再現性が向上したが、未だ一部の季節や時間、領域においてはGAIAと観測による電離圏の変動に不一致が残ることも分かった。今回、更に数値的な実験や他の観測との比較解析を行うことにより、モデルと観測のずれの原因を調査する。そして、改良したモデルによる熱圏と電離圏の平均的描像の再現性能を報告し、また今後の課題について議論する。

R005-42
Zoom meeting C ：11/2 PM1 (13:45-15:30)
14:45〜15:00

2019年9月南半球成層圏突然昇温が熱圏・電離圏に及ぼす影響

#三好 勉信[1)], 山崎 洋介[2)]
[(1] 九大・理・地球惑星,[(2]GFZ/Potsdam

Impacts of the 2019 September SSW event on the thermosphere/ionosphere

#Yasunobu Miyoshi[1)],Yosuke Yamazaki[2)]
[(1]Dept. Earth & Planetary Sci, Kyushu Univ.,[(2]GFZ/Potsdam

A sudden stratospheric warming event occurred in September2019 in the Antarctic region. During the SSW event, the quasi 6-day wave was enhanced in the middle atmosphere, and strong6-day oscillations are observed in the thermo-sphere and ionosphere. Using an atmosphere-ionosphere coupled model GAIA and GPS/TEC data, impacts of the 6-day wave on the 6-day oscillation in the thermosphere/ionosphere. Our results indicate that a westward-moving 11-h wave with zonal-wave number 3 and a westward-moving 13-h wave with zonal-wave number 1 are generated by the non-linear interaction between the migrating semidiurnal tide and the 6-day wave. These secondary waves play an important role on the 6-day oscillation in the thermosphere/ionosphere. Furthermore, a 29-h standing oscillation, which is generated by the non-linear interaction between the migrating diurnal tide and the 6-day wave, is also important. The detailed mechanism of the 6-day oscillation in the ionosphere will be shown.

2010年9月に発生した南半球突然昇温により引き起こされた熱圏・電離圏変動を、大気圏―電離圏結合モデルGAIAシミュレーションおよびGPS/TECデータにより調べてみた。2019年9月の成層圏突然昇温時には、成層圏から下部熱圏にかけての領域では6日波が顕著となり、熱圏・電離圏で6日変動がみられる。熱圏・電離圏での6日変動と6日波の関係について、GAIAシミュレーション結果を解析することにより明らかにした。その結果、熱圏・電離圏の6日変動は、6日波と太陽同期半日潮汐波の非線形相互作用により生成された東西波数1の約13時間周期の波と東西波数3の約11時間周期の波が重要な役割を演じていることが明らかとなった。さらに、GPS/TECデータを用いて、この結果を検証した。TECに、東西波数1の約13時間変動と東西波数3の約11時間変動がみられた。また、太陽同期1日潮汐波と6日波との非線形相互作用により生成された、東西波数0の約29時間周期変動も確認できた。これらの結果から、熱圏・電離圏の6日変動にとって、潮汐波と6日波の非線形相互作用が重要であることが明らかとなった。

R005-43
Zoom meeting C ：11/2 PM1 (13:45-15:30)
15:00～15:15

Impacts of CO2 doubling on momentum balance in the thermosphere.

#Masaru Kogure[1)],Huixin Liu[1)],Chihiro Tao[2)]
([1]Kyushu University,[2]NICT

A CO2 increase causes global cooling in the thermosphere. Numerical models predict that a doubling of the CO2 mixing ratio leads to ˜50 K neutral temperature cooling and ˜50 % neutral density drop in the thermosphere (e.g., Dickinson, 1989; Solomon et al., 2018). Also, observation studies support this cooling thermosphere due to the CO2 increase (Ogawa et al., 2014). While the CO2 increase impact on the neutral temperature is understood well, its impact on the thermospheric dynamics is poorly understood. Liu et al. (2020) investigated the impacts of CO2 doubling on the dynamics of thermosphere using the whole atmosphere model Ground-to-topside Atmosphere Ionosphere model for Aeronomy (GAIA). The zonal mean zonal wind in the lower thermosphere is accelerated eastward in June except for middle latitudes. The meridional circulation in June, the summer to winter circulation (southward) in an altitude range of 120-300 km is strengthened. However, the dynamic mechanisms for these changes in the thermospheric circulation are still unclear.

This presentation will show the change in the momentum balance and discuss the mechanism responsible for the dynamical response to the CO2 doubling by investigating changes in the momentum balances in June between the 350 ppm CO2 and 700 ppm CO2 run data, which are the same data as Liu et al. (2020).

R005-44
Zoom meeting C ：11/2 PM2 (15:45-18:15)
15:45〜16:00

磁気リップルおよび電子密度変動の振幅と衛星軌道直下の降雨との統計的関連

#家森 俊彦 [1)], 青山 忠司 [2)], 横山 佳弘 [3)]
(1 京大,(2 エフ・ファクトリー,(3 スウェーデン宇宙物理学研究所

Statistical relationship between amplitude of magnetic ripples or electron density fluctuations and rainfall below the Swarm orbit

#Toshihiko Iyemori[1)],Tadashi Aoyama[2)],Yoshihiro Yokoyama[3)]
(1Kyoto Univ.,(2F-Factory,(3Swedish Institute of Space Physics

In the mid- and low-latitude ionospheric F layer on the dayside, magnetic field and electron density (Ne) fluctuations with a spatial scale of several tens of kilometers to several hundreds of kilometers are almost always observed. The amplitudes of fluctuations are as small as 1 to 2 nT and 1 to 2% or less of Ne, respectively, and it is presumed from the analysis so far that the cause is the waves caused by the lower atmosphere. However, the type of wave (sound wave or internal gravity wave) and its generation and propagation are not clear. The origin of atmospheric waves is not only meteorological phenomena, but also earthquakes and volcanic eruptions, but from the fact that they are observed almost all the time, it is presumed that meteorological phenomena are the main origin. Among them, cumulus convection and associated rainfall are considered to be the main candidates for atmospheric wave generation. Because there is no global atmospheric wave observation that can be compared with satellite observations, we use the global rainfall map (GSMaP) published by JAXA as a proxy of atmospheric wave activity and compare with the amplitude of magnetic ripples and electron density fluctuations observed by the Swarm satellites. Hourly data of global rainfall directly below the satellite orbit are compared with amplitude of magnetic ripples and electron density fluctuations. On the dayside, there are similarities between the global distribution of these amplitudes and the distribution of rainfall, but it cannot be concluded whether or not they are related only by the similarity of the distributions. Therefore, the amplitudes of magnetic ripple and electron density fluctuation along the Swarm satellite orbit with and without rainfall were compared. As a result, statistically, the amplitude tend to be about 10% larger in the case with rainfall than in the case without rainfall.

中低緯度電離圏 F 層では数十 km〜数百 km の空間スケールの磁気リップルとよばれる磁場変動や電子密度 ”Ne” の変動がほぼ常時観測される。変動の振幅はそれぞれ 1〜2nT、Ne の 1〜2%程度かそれ以下の微小なもので、これまでの解析からは、下層大気に起因する波動が原因であると推測されている。しかし波動の種類、すなわち、音波か内部重力波かや、その生成と伝搬については明確になっていない。大気波動の成因は気象現象だけではなく、地震や火山噴火などもあるが、ほぼ常時観測されることからは、気象現象が主要な起源であると推測される。中でも積雲対流やそれに伴う降雨が大気波動発生の有力な候補と考えられるが、衛星観測と比較できる全球的な大気波動の観測はないので、ここでは、JAXA が公開している全球降雨マップ ”GSMaP” の毎時値データをそのプロキシと仮定して、Swarm 衛星により観測された磁気リップルおよび電子密度変動の振幅と比較した。昼間側ではそれら振幅のグローバルな分布と降雨の分布には類似点が見られるが、分布の類似だけでは関連の有無は結論できない。そこで、降雨がある場合と無い場合のその上空での磁気リップルおよび電子密度変動の振幅を比較した。その結果、統計的には降雨のある場合の方がない場合より振幅が 10%程度大きくなる傾向が見られた。

R005-45
Zoom meeting C ：11/2 PM2 (15:45-18:15)
16:00〜16:15

観測ロケット搭載超高層大気密度測定用真空計の開発

#田中 勇人 [1)], 阿部 琢美 [2)], 三宅 亙 [1)]
([1] 東海大・工,[2]JAXA 宇宙科学研究所

Development of a pressure gauge for study of upper atmosphere on sounding rocket

#Yuto Tanaka[1)],Takumi Abe[2)],Wataru Miyake[1)]
([1]Tokai Univ.,[2]JAXA/ISAS

We are developing a pressure gauge for installing on the sounding rocket to estimate a number density of neutral atmospheric particles in the lower thermosphere. A brief overview of our instrument development will be presented in this paper.

Both charged particles and neutral particles are known to coexist in the lower thermosphere. Many characteristic phenomena occur because of those different behaviors against electromagnetic force. While radar and other remote sensing technique measure the upper atmosphere indirectly, sounding rocket is the only way which enables in-situ measurement. We are developing two types of vacuum gauge containers with structures such that are sensitive/insensitive to the relative velocity of the neutral atmosphere observed on the sounding rocket. The values obtained from these containers will be compared to estimate the number density of neutral atmosphere. In general, the velocity of the sounding rocket is faster than the thermal speed of the thermospheric neutral particles, and therefore the container structure must be designed so that the translational energy of the particles produced by the rocket movement can be lost.

The first container is designed on basis of Patterson probe, which is known as a close-type spherical container with long tube. In this shape, the translational energy can be lost once the incoming gas collides with the inner wall of the tube. If it can be assumed that the temperature of the incoming particles is the same as that of the container, we can estimate the number density of neutral atmosphere from the pressure by using the gas state equation. The second container is open-type cylindrical container. This container is designed so that the pressure obtained by ion gauge inside the container can change depending on incident angle of the gas to the orifice on the container surface. The possibility of estimating the direction of the neutral gas with this pressure gauge system is now being considered. In this presentation, the second container design will be discussed in detail.

To determine the shape of the cylindrical container, we carried out the pressure measurement using Space Science Chamber in JAXA Sagamihara Campus. This facility provides an environment of the lower thermosphere with a pressure of 10^{-5} Pa. The container was placed inside the chamber and nitrogen gas flow was blown towards the orifice of the container. Then, the pressure inside the container was continuously monitored while it was rotated on a spin table to examine the pressure variation with a change in the incident angle of gas. If the pressure change is relatively large, it will be useful for estimating the incident angle. Then, we have made three prototypes of cylindrical containers to find a suitable structure.

Crystal ion gauge consisting of crystal gauge and B-A gauge is adapted as the pressure gauge in our development. Crystal gauge can measure pressure above 4 Pa. When the pressure decreases down to 4 Pa, the pressure gauge changes from crystal gauge to B-A gauge mode automatically. The B-A gauge is a vacuum gauge suitable for observation in high vacuum environments and can measure down to 10^{-6} Pa. This vacuum gauge can be used for a wide range of measurements from atmospheric pressure environments to high vacuum environments.

These pressure gauge will be installed on the top side of payload section of the sounding rocket. In this presentation, We will focus on results of pressure measurements.

我々は観測ロケットに搭載し、熱圏下部領域の中性ガス密度の測定ができる真空計の開発を行っている。本稿では、この開発概要について述べる。　熱圏下部領域は中性粒子と電離粒子が混在している。中性大気は電磁気的な力を受けないが、電離大気は影響を受けることからこの領域には様々な特有の現象が発生している。本研究では、観測ロケットへの搭載を前提にした真空計を開発する。熱圏下部の大気観測手法として地上に設置されたレーダーによる手法や人工衛星のリモートセンシング技術を用いた方法などがあるのに対し、観測ロケットはこの領域をその場観測する唯一の手段である。ここでは、ロケット上で観測される中性大気の総裁速度を受けにくい/受けやすい構造の２種類の真空計容器を搭載し、それぞれから中性ガスの数密度の推定を行うこととした。一般に観測ロケットの飛行速度は熱圏大気粒子の熱速度よりも速いが、ロケットの飛行により生じる粒子の並進エネルギーが圧力測定に影響を与えないような容器の設計を行わなければならない。

真空計容器の一つはパターソンプローブを参考にし、球形容器に粒子の流入口を持つパイプが球形容器に連結された形で流入口以外は閉じられている。この形では流入してくるガスが一度パイプの壁に当たることで、並進方向の運動エネルギーが失われ、内部の大気温度が容器の温度と等しいと仮定すれば、中性ガス密度の正確な測定が可能になる。もう一つは円筒形で、先端部が漏斗のようにすぼまっている形状である。前者とは異なり、ガスの入射角度による圧力変化が測定できる。このような設計を行うことで、中性風の方向の推定可能性について議論したい。今回のプレゼンテーションでは後者の円筒形の設計について詳細に述べる。

真空型センサを収納する容器形状を決定するため JAXA 相模原キャンパス内の熱圏下部環境である 10^{-5}Pa を再現

できるスペースサイエンスチャンバーを利用し実験を行った。高真空にしたチャンバー内に容器を設置し、容器正面からガスを噴射させて容器内の真空計で圧力を測定する。容器を回転させて、ガスの入射角度による圧力変化を調べた。圧力変化が大きいほうが入射角度の推定には有利と考えられるが、適した構造を見つけるためにこの実験では容器の流入口付近の構造が異なる３種類の円筒形容器を試作してデータを取得した。試作した３種類の容器はいずれも３ D プリンターで作成した。

使用する真空計は、クリスタルゲージと B-A ゲージの２つのセンサで構成されるクリスタルイオンゲージである。クリスタルゲージでは大気圧から 4 Pa までを測定し、圧力が 4Pa 以下になると自動的に B-A ゲージに切り替わる。B-A ゲージは高真空環境の観測に適した真空計で、10^{-6}Pa まで測定可能である。この真空計を用いることで、大気圧環境下から高真空環境まで幅広く測定が可能である。

これらの真空計は観測ロケットの開頭部に搭載される予定である。搭載部分には様々な制約があるため、これを考慮したデザインにする必要がある。発表では圧力の測定結果を中心に述べる。

R005-46
Zoom meeting C ：11/2 PM2 (15:45-18:15)
16:15〜16:30

Detection of polar mesospheric clouds utilizing Himawari-8/AHI full-disk images

#Takuo Tsuda[1)],Yuta Hozumi[2)],Yoshiaki Ando[1)],Keisuke Hosokawa[1)],Hidehiko Suzuki[3)],Ken T. Murata[2)],Takuji Nakamura[4)],Jia Yue[5)],Kim Nielsen[6)],Yasunobu Miyoshi[7)]
[(1]UEC,[(2]NICT,[(3]Meiji univ.,[(4]NIPR,[(5]NASA GSFC,[(6]UVU,[(7]Dept. Earth & Planetary Sci, Kyushu Univ.

To advance polar mesospheric cloud (PMC) observations by Advanced Himawari Imager (AHI) onboard the Japanese geostationary-Earth-orbit (GEO) meteorological satellite Himawari-8, we have developed a PMC detection method for application to the Himawari-8/AHI full-disk images. The PMC detection method consists of two steps, which are for detection in stronger PMC signals by the first step and for detection in weaker PMC signals by the second step. By using this two-step detection, we eliminate false detections as much as possible, and enhance detection sensitivity. As the results, the PMC detection sensitivity by Himawari-8/AHI is well comparable to that by Cloud Imaging and Particle Size (CIPS) onboard Aeronomy of Ice in the Mesosphere (AIM). This suggests that new PMC dataset from Himawari-8/AHI would be of benefit for research on various PMC science in the future.

R005-47
Zoom meeting C ：11/2 PM2 (15:45-18:15)
16:30〜16:45

2020 年および 2021 年における北海道での夜光雲観測状況および補足率向上に向けたイメージャーの開発

#中村 優里子 [1)],Peh Bengau[1)], 鈴木 秀彦 [1)], 石井 智士 [1)], 坂野井 和代 [2)], 坂口 歌織 [3)], 西谷 望 [4)], 岩本 勉之 [5)], 高田 拓 [6)], 津田 卓雄 [7)], 穂積 裕太 [3)], 村山 泰啓 [3)], 小川 忠彦 [3)], 藤吉 康志 [8)]
([1] 明治大,[2] 駒澤大学,[3] 情報通信研究機構,[4] 名大 ISEE,[5] 紋別市役所,[6] 東京都立産業技術高等専門学校,[7] 電通大,[8] 北大・低温研

Results of NLC observations during 2020 to 2021 in Hokkaido and progress on development of the imager for NLC.

#Yuriko Nakamura[1)],Bengau Peh[1)],Hidehiko Suzuki[1)],Satoshi Ishii[1)],Kazuyo Sakanoi[2)],Kaori Sakaguchi[3)],Nozomu Nishitani[4)], Katsushi Iwamoto[5)],Taku Takada[6)],Takuo Tsuda[7)],Yuta Hozumi[3)],Yasuhiro Murayama[3)],Tadahiko Ogawa[3)],Yasushi Fujiyoshi[8)]

([1]Meiji univ.,[2]Komazawa Univ.,[3]NICT,[4]ISEE, Nagoya Univ.,[5]Monbetsu city,[6]Tokyo Metropolitan College of Industrial Technology,[7]UEC,[8]ILTS, Hokkaido Univ

It is important to know an exact occurrence rate and spatial distribution of noctilucent clouds (NLCs) in middle latitude region. An expansion of an NLC region toward lower latitudes is thought to be a result of progress of the global warming. A network of digital cameras has been operated in Hokkaido (43.2 N -44.4N), Japan since Jun 2010 in order to monitor NLCs in the middle latitude region by several research groups of Japanese institutes and universities. They reported the first detection of NLCs from multiple sites in Hokkaido, Japan in Jun 21, 2015 [Suzuki et al. 2016]. However, there had been no reports of NLC detection through 2016 to 2019 from Hokkaido despite continuous observations after the first event. The silence of NLC activity in Japan had been abruptly broken by 4 times detections from multiple sites in Hokkaido in 2020. Successively, very faint NLC signature are captured simultaneously from two sites of Hokkaido on Jun 22, 2021. This is the first case in two senses. First, this is the first case that NLCs had been detected multiple days in single season (2020). Second, this is the first case that NLCs had been detected in two successive seasons (2020 and 2021). We present these results and discuss possible causes by comparing the ground-based observations and global atmospheric parameters from satellites. In addition, we also focused on the single event captured in 2021 (Jun 22). The NLC signal captured in this day was quite faint and hard to recognized by glancing of the image. Fortunately, we could find this feature by careful check of image data. Simultaneous images taken from Rikubetsu and Monbetsu also increased robustness of the NLC detection. Such faint signals are thought to be rather dominant in middle latitude region (i.e., lower latitude limit of NLC occurrence). Thus, we have started to develop a new imaging system which can capture the faint signals from NLCs with high signal to noise ratio even under the bright sky background condition. The design of the imaging system and a result of test observations are also presented in this talk.

夜光雲の出現領域の低緯度側への拡大は地球温暖化の進行によるものと考えられるため、中緯度帯における夜光雲の出現頻度を正確にモニターすることは重要である。日本の MTI 研究者で構成される夜光雲研究チームは 2010 年 6 月頃より北海道の複数地点において地上カメラネットワークによる夜光雲の監視を開始し、2015 年には北海道の 5 地点で初めて夜光雲の同時撮像に成功した [Suzuki et al. 2016]。その後も観測は継続されたが 2016 年から 2019 年にかけて北海道における夜光雲の検出報告はなかった。しかし、2020 年 6 月から 7 月にかけて突如夜光雲が北海道の複数地点で 4 例検出され、翌年の 2021 年も 6 月 22 日において微弱ながら夜光雲が 2 地点から捉えられた。北海道において、単シーズンのなかで複数例夜光雲が検出されたこと（2020 年）、連続したシーズンで夜光雲が観測されたこと（2020 年および 2021 年）は、いずれも初めてのケースである。本研究ではこれらの夜光雲観測結果を報告し、その大出現のメカニズムについて衛星データとの比較により議論する。さらに、本研究では 2021 年に得られた微弱な夜光雲画像に着目した。北海道などの中緯度帯は夜光雲出現領域の低緯度側の極限であると考えられるため、北海道などに出現する夜光雲の信号の多くはこのイベントのように微弱である可能性がある。このような微弱な夜光雲の信号は、明るい背景光や下層の雲の影響に埋もれがちであり、今回のように諸条件が整わないと検出が難しいと考えられる。そこで、本研究ではより微弱な夜光雲の信号も捉えることが可能なカメラシステムの開発に着手している。本発表ではこのカメラシステムの開発状況や試験観測結果に基づく性能についても報告する。

R005-48
Zoom meeting C ：11/2 PM2 (15:45-18:15)
16:45〜17:00

ダーウィンで得られた大気光画像の3次元スペクトル解析に基づく中間圏・熱圏波動の水平位相速度分布の初期統計解析

#坪井 巧馬 [1)], 塩川 和夫 [1)], 大塚 雄一 [1)], 中村 卓司 [2)], ネウデグ デイビッド [3)]
(1 名大 ISEE,(2 極地研,(3 アデレード大学

Spectral analysis of the phase velocity distribution of AGWs and MSTIDs in airglow images at Darwin: Initial results

#Takuma Tsuboi[1)],Kazuo Shiokawa[1)],Yuichi Otsuka[1)],Takuji Nakamura[2)],Daivid Anthony Neudegg[3)]
([1]ISEE, Nagoya Univ.,([2]NIPR,([3]Adelaide Univ.

Atmospheric gravity waves and medium-scale traveling ionospheric disturbances (MSTIDs) in the upper atmosphere affect the atmospheric circulation and the radio-wave transmission, respectively. These waves can be observed in nocturnal airglow images. Thus, spectral analysis of airglow images provides propagation direction and power of these waves. However, such spectral analysis of airglow images have not been done yet for stations in the southern hemisphere except for Antarctica. In this study, we studied the horizontal phase velocity distribution of atmospheric gravity waves and MSTIDs, by applying the 3-dimensional spectral analysis method of Matsuda et al. [2014] to the airglow images obtained at Darwin (12.4^{o}S, 131.0^{o}E) in Australia from 2001 to 2007 and from 2011 to 2019. Horizontal phase velocity spectra of mesospheric gravity waves in airglow images at a wavelength of 557.7 nm show that the power spectral density is strongest in summer, with a strong tendency to the south in the meridional direction and to the east in the zonal direction. This may be due to the variation in the location of intertropical convergence zone (ITCZ) in the troposphere, which is a possible source of atmospheric gravity waves. Horizontal phase velocity spectra of MSTIDs in airglow images at a wavelength of 630.0 nm show that the power spectral density is stronger during solar quiet periods and for waves propagating northwestward. These features can be explained if the observed MSTIDs are caused by the ionospheric Perkins instability. We speculate that the MSTIDs propagating other directions can be generated by atmospheric gravity waves.

超高層大気中を伝搬する大気重力波や中規模伝搬性電離圏擾乱（MSTID）は、大気の大循環や短波通信に影響を与える。これらの波動現象は地上から大気光イメージャで撮像観測され、そのスペクトル解析から、これらの波動の伝搬方向やパワーを見積もることができるが、南極を除けば南半球の観測点でこのような大気光画像のスペクトル解析はこれまで行われていなかった。本研究では南半球のオーストラリアのダーウィン観測点（12.4 ° S, 131.0 ° E）で得られた大気光画像に Matsuda et al. [2014] の３次元スペクトル解析手法を適用し、2001 年から 2007 年および 2011 年から 2019 年の大気重力波と MSTID の統計解析を行った。その結果、波長 557.7nm の大気光画像に見られる中間圏大気重力波の水平位相速度スペクトルの解析から、夏のパワースペクトル密度が最も強く、南北方向では南、東西方向では東に強い傾向をもつことがわかった。これは、大気重力波の波源となり得る対流圏の熱帯収束帯の位置の変動が影響していると考えられる。波長 630.0nm の大気光画像に見られる MSTID の水平位相速度スペクトルの解析から、MSTID は太陽活動が静穏な期間のパワースペクトル密度が強く、また、北西方向に伝搬する傾向を持つことがわかった。北西方向の高まりや太陽活動度依存性については、MSTID が電離圏のパーキンス不安定で生成されると考えると説明できるが、それ以外の伝搬方向を持つ MSTID については、大気重力波によって MSTID が生成されている可能性が考えられる。

R005-49
Zoom meeting C ：11/2 PM2 (15:45-18:15)
17:00～17:15

Atmospheric instabilities in the polar upper mesosphere (2)

#Satonori Nozawa[1)],Takuya Kawahara[2)],Norihito Saito[3)],Satoshi Wada[3)],Takuo Tsuda[4)],Tetsuya Kawabata[1)],Chris Hall[5)]
([1]ISEE, Nagoya Univ.,[2]Faculty of Engineering, Shinshu University,[3]RAP, RIKEN,[4]UEC,[5]TGO, UiT

The sodium LIDAR at Tromsoe (69.6N, 19.2E) has been operated for 9 years since October 2010. For the first two winters, we have observed neutral temperature and sodium density between about 80 and 110 km. Since October 2012, wind measurements have been made together with the both measurements. Utilizing these temperature and wind data, we have calculated Brunt-Vaisala frequency (N) and Richardson number (Ri) to study the atmospheric instabilities between about 80 and 110 km above Tromsoe. Using those values, we have calculated probabilities of the static instability ($N<0$) and the dynamic instability ($0=<Ri<0.25$) that can be used for proxies for evaluating the atmospheric instability. We have addressed what makes the atmosphere unstable: possible relationship with gravity wave activity, semidiurnal tidal amplitude, solar activity (F10.7 index), and geomagnetic disturbance (local K-index) is investigated.

In this talk, in particular we will focus on (1) horizontal spatial extent and duration time of the static unstable region, and (2) dependence of the static and dynamic instabilities on the semidiurnal tidal amplitude.

R005-50
Zoom meeting C ：11/2 PM2 (15:45-18:15)
17:15〜17:30

極域下部熱圏における地磁気活動度に対する半日潮汐波の変動

#小山 裕貴 [1)], 野澤 悟徳 [2)], 小川 泰信 [3)],Brekke Asgeir[4)]
(1 名大・宇地研,(2 名大・宇地研,(3 極地研,(4 トロムソ大・理工

Variability of the semidiurnal tide in the polar lower Thermosphere at various geomagnetic activities

#Hirotaka Koyama[1)],Satonori Nozawa[2)],Yasunobu Ogawa[3)],Asgeir Brekke[4)]
(1ISEE, Nagoya Univ.,(2ISEE, Nagoya Univ.,(3NIPR,(4Science and Technology, UiT

We will present variability of the semidiurnal tide in the polar lower Thermosphere (93-119 km) above Tromsoe, Norway (69.6N, 19.2E) based on 33 years of EISCAT UHF radar data at various geomagnetic activities under different seasonal (summer and winter) and solar activity (F10.7<75, 75<F10.7<150, 150<F10.7) conditions. The neutral wind velocity data are used with time and altitude resolutions of 6 minutes and 3-4 km, respectively. The wind data are averaged according to time and altitude for different conditions, and semidiurnal tides re derived using the averaged wind data under various conditions, and then are compared with each other. Main results are as follows: (1) As the solar activity is higher, the amplitude of the semidiurnal tide increases regardless of season and solar activity. (2) Local time of maximum of the semidiurnal tide under conditions of 5<Kp is about 2-hr ahead of that under conditions of Kp<3. (3) Geomagnetic activity dependence in winter is stronger than in summer.

下部熱圏 (高度 90-130 km) において、中性大気の運動は圧力勾配力、コリオリ力、粘性力、ローレンツ力などによって支配されている。そして、下方からの上方伝搬する大気波動 (大気潮汐波、大気重力波、プラネタリー波) は、この領域のダイナミクスに大きな影響を与える。極域においては、オーロラ電子による粒子加熱、ペダーセン電流によるジュール加熱、磁気圏起源の（強い）電場によるイオンドラッグ力が加わり、風系はいろいろな条件で変動する。極域下部熱圏は、磁気圏からの電磁気的作用と下層大気からの力学的作用を時に同時に受ける特異領域である。そのため、磁気圏―電離圏―熱圏結合を理解する上で、この領域の大気ダイナミクスの理解は非常に重要である。

極域下部熱圏では、半日潮汐波が大気ダイナミクスにおいて支配的であることが示されている [Nozawa and Brekke, 1999a; Wu et al., 2003]。先行研究 [Brekke et al., 1994; Nozawa and Brekke, 1995, 1999a, b] では、56 日分の EISCAT UHF レーダデータを用いて、季節依存性、太陽活動度依存性、地磁気活動依存性が調べられたが、用いたイベント数が十分ではなかったため、それぞれの依存性を区別して調べることができなかった。本研究では、半日潮汐波の地磁気活動度依存性を、夏と冬、および異なる太陽活動度に分類して、明らかにすることを目的としている。

本研究では、ノルウェー北部に位置するトロムソ (69.6 ° N, 19.2 ° E) で稼働されている EISCAT UHF レーダで得られた 33 年間 (1986-2019 年) の高度 93-119 km のイオン速度データから導出した中性風速度データ (時間分解能：6 分、高度分解能 3-4 km) を用いた。季節、太陽活動度、地磁気活動度を下記のようにそれぞれ分類を行った。

季節：夏 (4 月 23 日-8 月 22 日)、冬 (10 月 23 日-2 月 22 日)

太陽活動度：F10.7 ≦ 75、75<F10.7<150、150 ≦ F10.7

地磁気活動度：Kp ≦ 3、3<Kp<5、5 ≦ Kp

季節、太陽活動度、地磁気活動度の各条件に合った中性風速度データを各時刻、各高度で平均し、ロムスカーグル法 [Lomb ,1976; Scargle, 1982] を用いて 12 時間成分を抽出した。ここでは、12 時間成分を、半日潮汐波として扱う。得られた 12 時間成分の振幅を用いて sin 関数で最小二乗法フィッティングを行い、風速が正（東向き、および北向き）に最大となる時の地方時 (以下、LTM: Local Time of Maximum) を求めた。振幅および LTM の地磁気活動度依存性において、シグニフィキャンスレベルを超える点のみ議論の対象とした。

極域下部熱圏における半日潮汐波の地磁気活動度依存性の結果は以下の通りである。（１）季節、太陽活動度に関わらず、地磁気活動度が高くなるにつれ、振幅が大きくなる (例：75<F10.7<150、冬、北向き成分では、Kp ≦ 3 と比較して 5 ≦ Kp は約 20 m/s 大きくなっている)。（２）冬は夏よりも Kp ≦ 3 の時に対する 5 ≦ Kp の時の振幅の増加量が約 10m/s 強くなっており、夏よりも冬の地磁気活動度依存性が強い。（３）LTM は季節、太陽活動度に関わらず Kp ≦ 3 と比較して 5 ≦ Kp は約 2 時間進んでいる。

イオンドラッグに対してロムスカーグル法を用いて 12 時間成分を抽出すると、5 ≦ Kp において、最大 5.0 × 10^(-11) N(LTM は、07 時) となり、この時の電場は約 40mV/m であった。イオンドラッグの 12 時間成分と半日潮汐波の振幅および LTM の比較から、北向き成分に関して、イオンドラッグの振幅のピーク高度は 105〜111 km であり、この高度の半日潮汐波の振幅はその他の高度よりも Kp ≦ 3 の時に対する 5 ≦ Kp の時の振幅の増加量が約 10 m/s 大きくなっている。Kp ≦ 3 の時、半日潮汐波の高度 105 km における LTM は 02 時である。5 ≦ Kp の時、半日潮汐波の LTM は 02~04 時となっており、イオンドラッグの LTM(07 時) の方へシフトしている。これらの結果よりイオンドラッグは半日潮汐波の励起源の 1 つとして働いていると解釈することができる。

本講演では、半日潮汐波の地磁気活動度依存性の詳細について報告する。

REFERENCES:

Brekke, A., Nozawa, S., Sparr, T. (1994), Studies of the E region neutral wind in the quiet auroral ionosphere. J. Geophys. Res. 99, 8801-8825. https://doi.org/10.1029/93JA03232

Lomb, N.R. (1976), Least squares frequency analysis of unequally spaced data, Astrophys. Space Sci., 39, 447-462. https://doi.org/10.1007/BF00648343

Nozawa, S., Brekke, A. (1995), Studies of the E-region neutral wind in the disturbed auroral ionosphere. J. Geophys. Res. 100, 14,717-147,34. https://doi.org/10.1016/S1364-6826(99)00016-4

Nozawa, S., Brekke, A. (1999a), Studies of the auroral E-region neutral wind through a solar cycle: Quiet days. J. Geophys. Res. 104, 45-66. https://doi.org/10.1029/1998JA900013

Nozawa, S., and A. Brekke. (1999b), Seasonal variation of the auroral E region neutral wind for different solar activities, J. Atmos. Sol. Terr. Phys., 61, 585- 605, 1999b. https://doi.org/10.1016/S1364-6826(99)00016-4

Scargle, J. D (1982), Studies in astronomical time series analysis. II. Statistical aspects of spectral analysis of unevenly spaced data. Astrophys. J. 263, 835. https://doi.org/10.1086/160554

Wu, Q., T. L. Killeen, S. Nozawa, D. McEwen, W. Guo, and S. C. Solomon (2003), Observations of mesospheric neutral wind 12‐hour wave in the Northern Polar Cap, J. Atmos. Sol. Terr. Phys., 65(8), 971- 978. https://doi.org/10.1016/S1364-6826(03)00116-0

R005-51
Zoom meeting C ：11/2 PM2 (15:45-18:15)
17:30〜17:45

MF レーダー観測に基づく南極 MLT 領域風速場の水平構造の推定

#堤 雅基 [1)], 橋本 大志 [1)], 西村 耕司 [2)], 佐藤 亨 [3)], 高麗 正史 [4)], 佐藤 薫 [4)]
[(1] 極地研,[(2] 京大・生存圏,[(3] 京大・国際高等教育院,[(4] 東大・理

Estimation of horizontal wind structure in the Antarctic MLT region based on MF radar

#Masaki Tsutsumi[1)],Taishi Hashimoto[1)],Koji Nishimura[2)],Toru Sato[3)],Masashi Kohma[4)],Kaoru Sato[4)]
[(1]NIPR,[(2]RISH, Kyoto Univ.,[(3]ILAS, Kyoto Univ.,[(4]Graduate School of Science, Univ. of Tokyo

MF (Middle Frequency) radars have been used to measure wind velocity in mesosphere and lower thermosphere based on correlation analysis techniques [e.g., Reid, 2015]. The motion of atmosphere weakly ionized by solar insolation is measured in the technique. The ionized atmosphere is usually horizontally stratified, and radar echoes from such layered atmosphere are mostly obtained in the vertical direction. However, there also exist echoes coming back from large off-vertical angles. Meteor echoes are such type of echoes often detected at night (winter time in the polar region) mostly above 80 km. Because of the low radio frequency (2-3 MHz) the duration of MF radar meteor echoes is two orders longer than that of VHF meteor echoes. Thus, meteor echoes can sometimes dominate the MF radar echoes when the background atmospheric ionization is relatively low. These meteor echoes have been used to compensate the known problem of MF radar correlation technique above about 90 km [Tsutsumi and Aso, 2005].

We have recently scrutinized the MF radar meteor measurement technique and found that wind velocity can be estimated with a time resolution as good as 10 min under preferable ionospheric conditions. Such a resolution is remarkably high as meteor wind measurements. Horizontal structure of wind field can be further estimated within the horizontal region of 200 x200 km (see Figure). Estimation of momentum flux deposition may be possible using the method proposed by Hocking [2005].

The obtained results are to be verified by comparing with those observed by the co-locating PANSY radar [Sato et al, 2014].

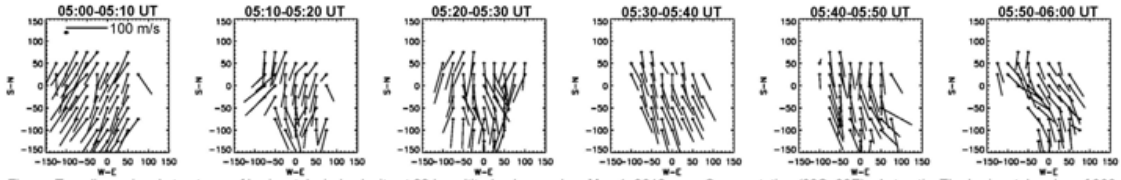

Figure: Two-dimensional structures of horizontal wind velocity at 88 km altitude observed on May 1, 2018, over Syowa station (69S, 39E), Antarctic. The horizontal region of 300 x 300 km is shown. Each wind vector is estimated using echoes detected within the corresponding sub-region with dimensions of 50 x 50 km.

R005-52
Zoom meeting C ：11/2 PM2 (15:45-18:15)
17:45〜18:00

Development of the meteor radar functionality on the PANSY radar to reinforce wind measurements in the Mesosphere

#Taishi Hashimoto[1)],Masaki Tsutsumi[1)],Koji Nishimura[2)],Toru Sato[3)],Masashi Kohma[4)],Kaoru Sato[4)]
([1]NIPR,[2]RISH, Kyoto Univ.,[3]ILAS, Kyoto Univ.,[4]Graduate School of Science, Univ. of Tokyo

Program of Antarctic Syowa MST/IS radar (PANSY radar) is a large VHF atmospheric radar installed at the Syowa Station (69.0S, 39.6E). The PANSY radar measures three-dimensional wind fields through the Troposphere to Mesosphere using the Doppler Beam Swing (DBS) technique, converting the radial wind velocities from four oblique beams and one vertical beam into vertical, zonal, and meridional wind velocities. However, since the primary source of radar echoes in the Mesosphere is the ionized atmosphere generated by solar radiation, the availability of the wind measurements is mostly limited to daytime, especially in winter.

To reinforce wind measurements in the Mesosphere, a supplemental meteor-radar functionality has been developed and installed on the PANSY radar in March 2021. Generally, meteor radars do not have as high temporal or range resolution as MST radars but provide more continuous horizontal wind measurements regardless of time and seasons. Also, this system uses subsidiary meteor echoes scattered in sidelobes of the transmitted radio waves while in the wind measurement using the DBS method. Hence, wind fields estimated by the standard DBS method and meteor radar functionality are simultaneously available and complement each other.

In this presentation, the system description of the new meteor radar functionality on the PANSY radar will be reported, followed by some preliminary results.

R005-53
Zoom meeting C ：11/3 AM1 (9:00-10:30)
9:00〜9:15

ノルウェー・トロムソにおけるミリ波分光観測装置を用いた中層大気微量分子観測

#中島 拓 [1)], 後藤 宏文 [1)], 長濱 智生 [1)], 野澤 悟徳 [1)], 大山 伸一郎 [1)], 三好 由純 [1)], 川端 哲也 [1)], 鈴木 和司 [1)], 児島 康介 [1)], 藤森 隆彰 [1)], 水野 亮 [1)]
[1 名大・宇地研

Observation of minor constituents in the middle atmosphere with millimeter-wave spectroradiometer in Tromsoe, Norway

#Taku Nakajima[1)],Hirofumi Goto[1)],Tomoo Nagahama[1)],Satonori Nozawa[1)],Shin ichiro Oyama[1)],Yoshizumi Miyoshi[1)],Tetsuya Kawabata[1)],Kazuji Suzuki[1)],Yasusuke Kojima[1)],Ryuji Fujimori[1)],Akira Mizuno[1)]
[1ISEE, Nagoya Univ.

Energetic particle precipitation (EPP) due to solar activity such as the solar proton event or magnetic storm occur in polar region. These particles create odd nitrogen (NOx) and odd hydrogen (HOx), which can affect the neutral chemistry of the middle atmosphere, and will in turn impact ozone concentration (e.g., Turunen et al., 2009). We developed and installed a millimeter-wave spectroradiometer in Syowa station, Antarctica in 2011 under the collaboration with NIPR, and so far, the monitoring observation of ozone and nitric oxide (NO) has been implemented. In this research, we found the short-term sporadic enhancement of NO column density due to mainly energetic electron precipitation as well as seasonal variation due to photochemical reaction by sunlight (Isono et al., 2014). Moreover, the peak values of NO column density, which are observed every winter season, has large variation based on the long-term monitoring observation (Nagahama et al., SGEPSS, 2018). However, we cannot separate the effects of the EPP, photochemistry, and atmospheric transportation from these variations. Therefore, we have planned the simultaneous observation in the northern hemisphere and comparison of changing in both polar atmosphere for approaching this problem. The initial observation of ozone and NO in Tromsoe, Norway located at Arctic region have been already reported (Ito et al., SGEPSS, 2016; Mizuno et al., JpGU, 2018). Although the long-term monitoring observation has not been currently started in Tromsoe due to some troubles in observational instruments, we obtained a pilot observational data of NO from December 26, 2018 to March 10, 2019 (Goto et al., SGEPSS, 2021).

In this presentation, we will report a briefly introduction of observation plan and current situation in Tromsoe. Moreover, a new research project ”Eneargetic Particle Chain” in ISEE, Nagoya University for 7 years beginning this fiscal year will be explained.

極域では、太陽陽子イベントや磁気嵐などの太陽活動に伴う高エネルギー粒子が、磁力線に沿って地球大気に降り込む現象が知られている。それらは中性大気とのイオン分子反応によって窒素酸化物ラジカル（NOx）や水素酸化物ラジカル（HOx）を増加させ、結果的に中層大気のオゾン減少を引き起こすと考えられている（e.g. Turunen et al., 2009）。我々は、2011 年から国立極地研究所と共同して南極・昭和基地に 250 GHz 帯の分光観測装置を設置し、オゾンと一酸化窒素（NO）のモニタリング観測を継続してきた。ここでは、極域中間圏の NO カラム量について、主に高エネルギー電子の降り込みに対応する短期的な変化と、日照による光化学反応に対応する季節変化を見出した（Isono et al., 2014）。また、NO カラム量は光化学反応が起こらない冬季に増大するが、そのピーク値は年によって大きく異なることも分かった（長濱他、2018 年講演会）。しかし一方で、南極における観測だけでは、光化学反応や輸送による間接的な影響と、高エネルギー粒子の降り込みに伴う変化を区別することは難しかった。

我々は、2015 年から日照のフェーズが半年間異なる北極域（ノルウェー・トロムソ）にも同様の観測装置を設置し、南極とのオゾン・NO 同時比較観測を行うことで、この問題へのアプローチを試みていることを既に報告した（伊藤他、2016 年講演会；水野他、2017 年 JpGU）。その後は残念ながら装置のトラブルが続き、連続的なモニタリング観測の開始にはまだ至っていない。しかしそのような中で、2018 年 12 月 26 日から 2019 年 3 月 10 日に比較的まとまった期間の観測データが試験的に取得でき、現在この間の NO カラム量変動と降り込み電子との関係性の解明を進めている（後藤他、本年講演会参照）。

本講演では、トロムソにおける中層大気微量分子観測の概要と現在の状況を説明するとともに、本研究所のプロジェクトとして本年度より 7 年計画で開始された北極域における荷電粒子降り込みの中層・下層大気への影響に関する新たな研究計画について紹介する。

R005-54
Zoom meeting C ：11/3 AM1 (9:00-10:30)
9:15〜9:30

ノルウェー・トロムソにおけるNO柱密度の導出と、高エネルギー電子の降り込みとの関係性の考察に関する研究

#後藤 宏文[1)], 中島 拓[1)], 長浜 智生[1)], 野澤 悟徳[1)], 児島 康介[1)], 川端 哲也[1)], 藤森 隆彰[1)], 鈴木 和司[1)], 小川 泰信[2)], 水野 亮[1)]
([1] 名大 ISEE,[2] 国立極地研究所

A study on the relationship between NO column density and high-energy electrons based on the mm-wave observation at Tromsoe

#Hirofumi Goto[1)],Tac Nakajima[1)],Tomoo Nagahama[1)],Satonori Nozawa[1)],Yasusuke Kojima[1)],Tetsuya Kawabata[1)],Ryuji Fujimori[1)],Kazuji Suzuki[1)],Yasunobu Ogawa[2)],Akira Mizuno[1)]
([1]ISEE, Nagoya Univ.,[2]National Institute of Polar Research

We have carried out millimeter-wave spectroscopic observation of minor constituents in the middle atmosphere such as nitric oxide (NO) and ozone at Syowa Station (69.00^{o}S, 39.85^{o}E) in Antarctica since 2012 to study the effects of energetic particle precipitation into the polar regions induced by the solar activity. In addition, similar steady observation is about to start at Tromsoe, Norway (69.35^{o}N, 19.14^{o}E) in the Arctic region to obtain further understanding of the differences between the two polar regions (Nakajima et al., SGEPSS, 2021).

In this presentation, we will present the results of short-term test observation of NO at Tromsoe, Norway over 17 days from January 23 to February 4 and February 17 to February 20, 2019. Then we will report the results of correlation study between the observed NO column density and proxies of geomagnetic activities and energetic particle precipitations. To calculate the NO column density, two emission lines of F = 5/2-3/2 (250.815594 GHz) and F = 3/2-1/2 (250.816954 GHz) of the hyperfine structure lines $^2\Pi_{1/2}$J = 5/2-3/2 were used. F = 7/2-5/2（250.796436 GHz）emission line used for the analysis of NO at Syowa Station (Isono et al. 2014) was not used in this analysis due to outside interference. The atmospheric temperature in the region where NO is present was assumed to be a constant 200 K as well as the previous research. The average error in the column density estimated from the random noise in the data is 0.6 $*10^{14}$ cm^{-2}. During this period, there were two increases in column density for about three days, with peaks on January 27 and February 2 at 6.5 $*10^{14}$ cm^{-2} and 9.7 $*10^{14}$ cm^{-2}, respectively.

In comparison with the Dst index, there was a sharp decrease in the Dst index from January 31 to February 1, before the peak of the NO column density on February 2, suggesting that NO may have increased due to electrons accelerated by the geomagnetic disturbance. Next, we compared the NO column density with the electron flux data obtained by the MEPED 0^o telescope in the six POES/METOP satellites. For the comparison, we used the L-value and MLT of the satellite observations to select the electron flux data that were most likely to precipitate onto Tromsoe. As a result, it was found that the NO column density increased after the increase in electron flux observed by the satellite. Furthermore, the electron fluxes at energies of $>$40 keV, $>$130 keV, $>$287 keV, and $>$612 keV were analyzed for correlation with the NO column density, and the correlation coefficients were found to be 0.5, 0.4, 0.6, and -0.1, respectively, indicating that $>$287 keV has the highest correlation. This suggests that the range of $>$287 keV has the most influence on the variation of the NO column density.

太陽活動に伴って極域に降り込む高エネルギー粒子がNOx(窒素酸化物) やオゾンなどの中層大気中の微量分子に及ぼす影響を観測的に調べるため、我々は2012年から南極・昭和基地 (69.00^{o}S, 39.85^{o}E) でミリ波分光観測を行ってきた。さらに、両極域での差異を明らかにするため、2016年から北極域のノルウェー・トロムソ (69.35^{o}N, 19.14^{o}E) で同様の観測を進めつつある（詳細は中島他、本年講演会参照)。本研究は、トロムソで2018年12月26日から2019年3月10日までの75日間にわたって実施したNOのテスト観測のデータをもとにNO柱密度の時間変化と地磁気擾乱の指標であるDst指数、衛星観測から得られた電子フラックスデータとの関係を調べた。

上記75日間の観測データについては、スペクトルデータのバックグラウンドのランダムノイズと下層大気の光学的厚みの時間変動などを元にしてスクリーニングと電波強度の補正を行った結果、2019年1月23日〜2月4日と2月17日〜2月20日の17日間について、連続的に質の良いデータを抽出した (Goto et al., JPGU 2021で報告)。今回は、この17日間分のデータについてさらに解析を進めた結果を報告する。$^2\Pi_{1/2}$J = 5/2-3/2の超微細構造線 F=5/2-3/2（250.815594 GHz）と F=3/2-1/2（250.816954 GHz）の2本の輝線スペクトルを用いた。昭和基地での観測においてNOの解析に用いられた F=7/2-5/2（250.796436 GHz）の輝線 (Isono et al. 2014) は外部からの混信があったため今回の解析には用いていない。先行研究と同様に、NOが存在する領域の大気温度は一様に200 Kで、NO輝線は光学的に薄いと仮定した。データのランダムノイズから見積もった柱密度の誤差は、平均0.6 $\times$ 10^{14} cm^{-2} である。この間のNOの変動としては、1月27日と2月2日にピークがみられ、このときの柱密度はそれぞれ6.5 $\times$ 10^{14} cm^{-2} と9.7 $\times$ 10^{14} cm^{-2} であった。

Dst指数との比較では、NO柱密度のピークがみられる2月2日より前、1月31日から2月1日にかけてDst指数の急激な減少が見られ、磁場の擾乱により加速された電子によりNOが増加した可能性が考えられる。そこで、６機のPOES/METOP衛星に搭載されたMEPED検出器0度望遠鏡で得られた電子フラックスのデータと比較した。比較

に当たっては、L 値および MLT の値で条件を与えトロムソに降り込んでくる可能性の高い電子フラックスデータを選定した。その結果、衛星で観測される電子フラックスの増加の後に、それぞれ NO 柱密度が増加していることがわかった。さらに>40 keV、>130 keV、>287 keV、>612 keV の 4 つのエネルギー別の電子フラックスについて、それぞれ NO 柱密度との相関を調べたところ、それぞれ相関係数が 0.5、0.4、0.6、-0.1 となり>287 keV が最も相関が高いことがわかった。これより、>287 keV の範囲で最も NO 柱密度の変動に影響を与えていると考えられる。

R005-55
Zoom meeting C ：11/3 AM1 (9:00-10:30)
9:30〜9:45

Exploring interannual and long-term variability of the stratospheric ozone using the Aura/MLS Level3 dataset

#Tianliang Yang[1,2],Tomoo Nagahama[2]
([1]Graduate School of Engineering, Nagoya University,[2]ISEE, Nagoya Univ.

We present the interannual and long-term characteristics, especially the over-two-years components, of the global stratospheric ozone and the variation mechanism by using the Aura/MLS Level3 Ozone dataset. Among the stratospheric interannual variations, QBO (quasi-biennial oscillation) is a well-known phenomenon that the stratospheric zonal wind upon the equatorial region changes its direction in about every 13 months (e.g. Baldwin et al., 2001). In this study, using the Aura/MLS Level3 ozone data (version 4.2) which is the daily binned zonal average every 4 degree in latitude, the temporal variations of ozone were separated into three components with different time periods of less than 2 years, 2-to-5 years and more than 5 years, using the digital filter method by Nakazawa et al. (1997), and their characteristics of the time variability were obtained for each pressure level and latitude.

The obtained 2-to-5-years component of ozone in the equatorial region shows a significant feature of temporal variation whose amplitude is estimated as 7.4% of the average in 2010, associated with the zonal wind QBO. In addition, a remarkable phase reversal of the ozone variation at around the pressure level of 15 hPa (25 km) was clearly seen, being consistent with previous results (e.g. Bai et al., 2021). This indicates that the present analysis method was found to produce results comparable to those of the previous studies. In addition to the equatorial region, a prominent QBO-like signal was detected in the polar region around the latitude of 80 degree in north and south, and these maximum and minimum occur during the polar summer. We found that the amplitude of the polar QBO-like signal varies from year to year: the signal over the Arctic region is amplified in 2009-2014 period and 2018-2020 period with an amplitude of about 3.6%˜9.1% of the average in 2010, although that in the Antarctic region was in 2007-2011 and 2016-2020 with an amplitude of about 4.2%˜9.3% of the 2010 average.

In the presentation, the further details of the characteristics of the interannual and long-term variations of the stratospheric ozone, their connection with the QBO in the equatorial region and other contributors such as solar activities and Arctic Oscillation to the QBO-like signal will be discussed.

References

Baldwin, M. P., et al. (2001), The quasi-biennial oscillation, Rev. Geophys., doi:10.1029/1999RG000073.

Nakazawa, T., et al. (1997), Two curve fitting methods applied to CO{/sub2} FLASK data, Environmetrics, doi:10.1002/(SICI)1099-095X(199705)8:3<197::AID-ENV248>3.0.CO;2-C.

Bai, X. Y., et al. (2021), Anomalous changes of temperature and ozone QBOs in 2015 ー 2017 from radiosonde observation and MERRA-2 reanalysis, doi:10.26464/epp2021028.

R005-56
Zoom meeting C ：11/3 AM1 (9:00-10:30)
9:45〜10:00

Sporadic, large gravity wave events over Syowa Station -Comparison between the PANSY radar and the ERA5 reanalysis-

#Lihito Yoshida[1)],Yoshihiro Tomikawa[1,2)],Mitsumu K Ejiri[1,2)],Masashi Kohma[3)],Kaoru Sato[3)]
([1]Polar Science, SOKENDAI,([2]NIPR,([3]Graduate School of Science, Univ. of Tokyo

Gravity waves (GWs) are atmospheric waves whose restoring force is buoyancy. They are originated mainly from mountains, jet-front systems, and convection, and can modify a global wind structure through momentum transport and deposit. They do not only decelerate the upper part of the mesospheric jets, but also affect the horizontal winds in the lower stratosphere, and contribute to drive the global meridional circulation. However, GW observations are usually not enough to verify their behaviour in the Antarctic, due to the harsh environment. In addition, GWs have a wide range of horizontal wavelength (i.e., from several km to several thousand km) and period (i.e., from Brunt-Vaisala period (approximately 5 minutes) to inertial period (over 12 hours), which makes it difficult to reproduce GWs in the entire frequency range even in the state-of-the-art atmospheric models in spite of the recent increase of the model resolution. In order to implement the effect of subgrid-scale phenomena into the models, which are not explicitly represented, GW parameterizations are introduced. In general, nonorographic GW parameterization assumes nearly constant wave sources and instantaneous upward propagation, but in reality the wave sources are not constant and GWs propagate horizontally as well (Sato et al., 2009; Geller et al., 2013; Plougonven et al., 2020). Thus it is required to constrain the GW effect in the models based on observations which cover the whole frequency range of GWs and estimate the GW momentum transport in the Antarctic.

Intermittency, a measure of how transient or intermittent a GW event is, has recently received much attention. Even if the total amount of momentum flux is the same, continuous, small amplitude events deposit momentum to higher altitudes, while sporadic and large amplitude events deposit momentum to lower altitudes. As a result, the structure and strength of the driven meridional circulation depend on the GW intermittency (Hertzog et al., 2008). In Antarctica, intermittency has been studied using super pressure balloons (Hertzog et al., 2012) and the Program of the Antarctic Syowa MST/IS radar (PANSY radar) at Syowa Station (Minamihara et al., 2020), suggesting differences in the characteristics of intermittency due to different wave generation mechanisms and wave filtering.

Our purpose of this study is to investigate the characteristics of GWs for sporadic and large amplitude events that can have a large impact on the overall momentum transport, and also to investigate how well the reanalysis data reproduces the GWs events in the Antarctic. We used the PANSY radar for the observation data and the ERA5 reanalysis for the reanalysis data. The PANSY radar, which was installed at Syowa Station (69^{o}S,40^{o}E) in 2011, observes vertical profiles of three dimensional winds in the troposphere and lower stratosphere with high accuracy and fine temporal and vertical resolution (Sato et al., 2014). It is the only instrument in the Antarctic that enables us to capture GWs in the almost entire frequency range. The ERA5 reanalysis is the latest meteorological reanalysis dataset provided by the European Centre for Medium-Range Weather Forecasts. The ERA5 data is distributed at 137 vertical levels from the surface to 0.01 hPa with a horizontal spacing of 0.25 degree every 1 hour.

We use three dimensional winds of the PANSY radar and the ERA5 reanalysis during the period of October 2015 to September 2016, in which the PANSY radar was continuously operated (Minamihara et. al.,2018). The inertia-GWs are extracted by applying a bandpass filter with a cutoff period of 4-24 h and a cutoff vertical wavelength of 0.8-8 km. As a result, we found many similar wave-like structures between the PANSY radar and the ERA5 reanalysis.

In order to examine the propagation characteristics of inertia-GWs, we use a hodograph analysis. It utilizes the feature that the hodograph (i.e., vertical change of the horizontal wind vector drawn in the zonal and meridional wind space) becomes an ellipse, in which the amplitude, intrinsic period, vertical wavelength, phase velocity, and group velocity of GWs can be estimated. Although the hodograph analysis generally has an ambiguity of horizontal propagation direction by 180^{o}, we exclude it by comparing direct estimates of the ground-based wave period from the time and altitude section.

We will discuss the similarities and differences between the PANSY radar and ERA5 and seasonal variations of sporadic GW events over Syowa Station.

R005-57
Zoom meeting C ：11/3 AM1 (9:00-10:30)
10:00〜10:15

Revisiting models of TKE dissipation rates from UHF and VHF Doppler radar spectrum width from theory and UAV data

#Hubert LUCE[1)],Hiroyuki Hashiguchi[2)],Lakshmi Kantha[3)],Abhiram Doddi[4)],Dale Lawrence[3)],Masanori Yabuki[2)]
([1]RISH,([2]RISH, Kyoto Univ.,([3]Univ. of Colorado,([4]University of Colorado Boulder

Shortly after the development of Stratosphere-Troposphere VHF radars and UHF wind profilers, analytical models have been proposed to estimate turbulence kinetic energy (TKE) dissipation rate from Doppler spectrum width. TKE dissipation rate is a fundamental parameter indicative of the strength of turbulence. The commonly used models were recently assessed from comparisons with Unmanned Aerial Vehicles (UAV) data collected during Shigaraki-UAV-Radar EXperiment (ShUREX) campaigns (2016-2017) at Shigaraki MU observatory (Japan). Applied to the VHF Middle and Upper atmosphere (MU) radar and to the UHF LQ7 wind profiler, these models failed to reproduce accurately UAV-derived dissipation rates and a simple model based on dimensional analysis provided the best agreements. However, the latter raises conceptual issues and its applicability must be understood. New insights have been obtained by expending theoretical derivations based on energy budget equations for expressing the temperature structure parameter in terms of outer scales of turbulence (Basu and Holtslag, 2021). These derivations lead to a possible interpretation of the efficiency of the simple model and to a generalized expression of the dissipation rate models allowing us to identify the domain of applicability of the commonly used model for turbulence in stratified conditions.

R005-58
Zoom meeting C ：11/3 AM2 (10:45-12:30)
10:45〜11:00

夜間の空の連続画像から晴天領域の時空間分布ログを自動生成する手法の開発

#石井 智士 [1)], 鈴木 秀彦 [2)], 西谷 望 [3)]
([1] 明大・理工・物理,[2] 明治大,[3] 名大 ISEE

Development of an automatic procedure to make a log of a sky condition from successive images of night sky.

#Satoshi Ishii[1)],Hidehiko Suzuki[2)],Nozomu Nishitani[3)]
([1]Meiji Univ.,[2]Meiji univ.,[3]ISEE, Nagoya Univ.

For optical observations from ground, it is important to precisely know a temporal and spatial distribution of clouds to judge the data quality. In this study, we developed an automatic procedure to make a log of the sky condition (distribution of lower clouds which obstacle signals from upper sky) from successive images of night sky. Since the field of view (FOV) of photometers and spectrometers tends to be narrow, it is difficult to distinguish the actual fluctuations in signals from the occultation effect by the lower clouds. Thus, a sky condition is often checked by an image data acquired by collocated imagers for nocturnal luminous phenomena such as aurora and airglow. However, it costs too much by means of time and effort to manually check huge data set. Moreover, a criterion to judge a sky condition highly depends on an inspector. If an outstanding method to judge a condition of night sky by using image data taken by a fixed imager is established, it is useful to extract valid data from huge data set and be a powerful tool for statistical analysis with long-term data. Unlike daytime, night sky images have poor color contrast between clear and cloudy areas. It means that a method using color information is difficult to be applied. Therefore, we have developed a method to determine the spatial and temporal distribution of clear sky using stars. In ground based image observations, the elevation and azimuth angle of the FOV are fixed. If the information for an observation situation (latitude, longitude, and observation time) is known, the positions of stars in the FOV can be estimated from the star chart (star positions in an equatorial coordinate system). Then, it is possible to determine the presence or absence of clouds from night sky images, by checking presence of a star image in predicted area. Since star images present in almost whole sky, a spatial distribution of cloud can be determined with a resolution corresponding to mean angular distance between available stars. In this talk, we present the method to automatically make a log of a sky condition from successive images of night sky. We also show initial result of this method obtained by applying the procedure to images of night sky acquired by an imager operating to monitor the SuperDARN radar system in Rikubetsu, Hokkaido. Comparison between results by our method and results based on a manual inspection is also performed to shows robustness and effectiveness of the developed method.

夜間の地上光学観測のデータ品質を判定するためには，視野内におけるデータ取得時の晴天域の時空間分布情報が重要である。狭視野のフォトメーターや分光計では空間情報が得られないことも多く、観測対象とする現象の実際の信号強度変動と、下層雲の増減による掩蔽や吸収の効果を後処理により精密に判別するのは困難である。現在、南極昭和基地で稼働中である OH 分光計のデータ解析においてもこの問題が存在する。これまでは、夜間の自動観測で得られたスペクトルデータから水蒸気の吸収に起因すると考えられるスペクトル形状を検出した場合は観測視野内に雲が発生していたと判断し、そのデータを無効と判定している。これに加え、最終的な天候の判定には大気光やオーロラのイメージ観測で取得される画像を目視で確認し、雲の分布情報を得ることで行われるが、画像データは膨大な量があるため選別は多大な労力を必要とし、さらに判定基準が判定者に依存してしまうなど客観性に欠ける。一方、定点観測で得られた夜間の画像データから自動的に晴天の空の分布や割合を導出することができれば、データ選別が機械的にできて長期データの統計解析などに役立つ。青空と雲域が明瞭に判別できる昼間と違って、夜空の画像には色味にコントラストがなく、雲に反射する光も地上からの人工光や月明かりの有無によって色味や見え方が異なるため、単純にカラー情報から雲域と晴天域を切り分けることは難しい。そこで本研究では星を使って晴天域の時空間分布を判定する手法を開発した。定点イメージ観測では観測視野の高度角、方位角が固定されるため、観測地点の緯度、経度、観測時間といった情報があれば、星の赤道座標からある時刻にその星が観測視野内でどこに位置するのか推定することが可能である。この推定位置において、実際の画像に点光源とみなせる星像が存在するかどうかを判定できれば、その位置における雲の有無を判定することができる。この手法では、夜間に取得された一連の画像データがあればその場における晴天の時空間分布のログを機械的に生成することが可能である。本研究では北海道陸別町で SuperDARN システムを監視するために稼働している定点観測カメラの夜間画像を用いて、晴天域の時空間分布を客観的に求め、手動による天候ログと比較した結果を報告する。

R005-59
Zoom meeting C ：11/3 AM2 (10:45-12:30)
11:00〜11:15

Estimation of cloud base height and cloud cover from all-sky cloud imagers

#Atsuya Nemoto[1)],Hiroyo Ohya[2)],Toshiaki Takano[3)],Tamio Takamura[4)],Alessandro Damiani[4)],Hiroyuki Nakata[5)]
([1]Science and Engineering, Chiba University,[2]Engineering, Chiba Univ.,[3]Chiba Univ.,[4]CEReS Chiba Univ.,[5]Grad. School of Eng., Chiba Univ.

Cloud base height has been observed by radiosondes, radars, and lidars (ceilometer). Radiosonde observation is carried out only twice a day at 00:00 and 12:00 UT over the world, and observation sites are limited (for example, 16 sites in Japan). Wilheit and Hutchison [2000] also proposed a method to retrieve the cloud base height by combining passive microwave brightness temperature and infrared cloud top temperature. Lidars can be obtained relatively accurate cloud base heights locally [Takano and Takamura, 2014]. However, they detect only the overhead cloud base height. The advantage of satellites is that two-dimensional distributions of the microphysical and macrophysical properties of clouds may be retrieved on a global scale with high resolution [Huang et al., 2006]. However, the acquisition of cloud base height cannot be obtained directly from satellite observations. On the other hand, column resistance of global electric circuit increases by 10 % with increasing cloud cover based on simulation[Zhou and Tinsley, 2010], although quantitative verification has not been performed by observations yet. In this study, we propose a method for estimating cloud base height and cloud cover using all-sky imagers at two sites. The advantage of all-sky imagers is that they are cheaper than radars and lidars. Cloud observations have been performed by the two all-sky imagers on the roofs of Engineering Research Building 1 (35.6246N, 140.1037E) and 2 (35.6266N, 140.1040E) in Nishi-Chiba campus in Chiba University, Japan. The distance between the two all-sky imagers is 216 m. The all-sky imagers have equisolid angle projection. The estimation method of the cloud base height is described below. When the cloud base height is assumed in the range of 500-2500 m with step of 50 m, the two cloud images are projected to each map. Then we calculate cross-correlation of RGB and binarized values between the two maps. The height that the cross-correlation coefficients show maximum value is adopted as the cloud base height. We verified the estimation accuracy of the cloud base height by simulation. When we made several pseudo-cloud images in the cloud base height range of 500 - 3000 m with a step of 500 m, the estimation errors were 0 - 30 m. The errors are very low, because spatial resolutions of visible spectra for the Himawari-8 satellite and X-band radar network are 1 km and 250 m, respectively. Applying our estimation method for observation data, the cloud base height was estimated to be 1987 m and 1937 m in the cases of the RGB and binarized values at 11:45:13 JST on 16 March, 2020, respectively. The cloud base height was observed to be 1860 m by a lidar installed by the National Institute for Environmental Studies (NIES) in the same campus in Chiba University at 11:45:00 JST. On the other hand, we improved an automatic procedure to estimate nighttime cloud cover from cloud optical images using the RGB color values. The nighttime judgement conditions of the RGB values for clouds were changed from daytime one. In the session, we will show the results of verification for the accuracy of the estimation method and relationship between cloud cover and atmospheric electric field in details.

R005-60
Zoom meeting C ：11/3 AM2 (10:45-12:30)
11:15〜11:30

Response of thunderstorms, rainfalls and snowfalls to global electric circuit in Kanto area using W-band cloud radar FALCON-I

#Hiroyo Ohya[1)],Masashi Kamogawa[2)],Tomoyuki Suzuki[3)],Toshiaki Takano[4)],Kazuomi Morotomi[5)]
([1]Engineering, Chiba Univ.,([2]University of Shizuoka,([3]Education, Gakugei Univ.,([4]Chiba Univ.,([5]Japan Radio Co., Ltd.

Global electric circuit (GEC) is a huge capacitor between the Earth's surface and lower ionosphere. Thunderstorm is main generator of the GEC (e.g., Rycroft et al., 2000). Air current flows upward from a thunderstorm cloud top toward the ionosphere and flows in the lower ionosphere horizontally. Then the air current flows from the lower ionosphere down to the Earth's surface in fair weather and flows in the Earth's surface. The current flows from the ground into the thunderstorm generator, and the GEC closes. The currents are 0.1-6.0 A, with an average between about 0.5 and 1 A per thunderstorm cell (Blakeslee et al., 1989). Correlation between atmospheric electric field in Antarctica and thunderstorm rainfall was 0.54 (Lavigne et al., 2016). In Kanto area, large oscillations in atmospheric electric field with a period of 78 minutes during snowfalls of 24 November, 2016 were reported, which was caused by vertically convective cells in the snowclouds (Ohya et al., Scientific Reports, 2021). However, it is not still clear how clouds affect the GEC quantitatively. In this study, we reveal response of thunderstorms, rainfalls, and snowfalls to the GEC in Kanto area using W-band (95 GHz) cloud radar, FALCON (FMCW radar for cloud observations)-I. FALCON-I is a cloud radar with high spatial and sampling resolution developed at Chiba University, Japan. The field mills at Chiba University (CHB, 35.63N, 140.10E), Kakioka, Ibaraki (KAK, 36.23N, 140.19E), Koganei, Tokyo (KGN, 35.71N, 139.49E), and Musashino, Tokyo (MSS, 35.72 N, 139.57E); the FALCON-I at CHB; and a X-band phased array weather radar (PAWR) operated by Japan Radio Co., Ltd. (XBR, 35.52N, 140.23E), Japan are used in this study. The distances between CHB and KAK, KGN, and MSS are 64.8, 56.4, and 49.5 km, respectively. There were 79 events that the atmospheric electric field largely varied during thunderstorms and snowfalls from June 2016 to June 2018. Around end of precipitations that continued for 11.5 hours, the atmospheric electric field largely decreased at CHB at 23:30 UT on 4 June, 2016. During precipitations on 21 June, 2016, the atmospheric electric field oscillated with a period of about 20 minutes. During snowfall of 27 March, 2017, the atmospheric electric field largely varied, but not oscillated. At that time, the snowclouds had complex structure at heights of 0.5-6.0 km. In this session, we will show the response of these weather phenomena in detail.

R005-61
Zoom meeting C ：11/3 AM2 (10:45-12:30)
11:30〜11:45

V-POTEKA 観測網で検出された西部北太平洋における雷活動と台風強度発達との関係性

#佐藤 光輝 [1)], 高橋 幸弘 [2)], 久保田 尚之 [3)],Lopez Glenn Vincent C.[4)]
([1] 北大・理・宇宙,[2] 北大・理・宇宙,[3] 北大・理,[4] フィリピン先端科学技術研究所

Relation between lightning activities measured by the V-POTEKA network and typhoon intensity development

#Mitsuteru SATO[1)],Yukihiro Takahashi[2)],Hisayuki Kubota[3)],Glenn Vincent C. Lopez[4)]
([1]Faculty of Science, Hokkaido Univ.,[2]Faculty of Science,Hokkaido Univ.,[3]Faculty of Science, Hokkaido Univ.,[4]ASTI, DOST

Many countries in the western north Pacific region suffer from the attack of tropical cyclones (typhoons) and have a strong demand to predict the intensity development of typhoons by a cost-effective ways. Recent studies revealed that the lightning occurrence number in tropical cyclones shows clear relation to the intensity development of TCs. Thus, we have developed a new automatic weather and lightning observation system (V-POTEKA) and deployed this system in the Philippines, Guam, Palau, Jakarta, Okinawa since September 2017. Using the V-POTEKA data, lightning locations are estimated by using the time-of-arrival geolocation algorithm. We have compared the relation between the lightning activities within the typhoon area measured by the V-POTEKA network and the intensity development of the western north Pacific typhoons in the period of 2018-2020. Although a total of 81 typhoons occurred in these 3 years, we selected 46 typhoons in this study and conducted cross-correlation analysis between lightning activities and typhoon intensity development. We confirmed that the time variations of the detected lightning event numbers and typhoon intensities (maximum wind speed (V_{max}) and minimum pressure (P_{min})) are correlated (R=0.50 for V_{max} and R=0.57 for P_{min}) and that there is clear time lag between lightning activities and typhoon intensities (+33 h for V_{max} and +36 h for P_{min}), which means the peak of lightning activity comes first and the peak of the typhoon intensity comes next. We also found that the time lag in the weaker typhoons is smaller than that in the stronger typhoons. However, as for the super typhoons (category 5 typhoons), this relation is not always clear. At the presentation, we will show the detailed results derived from this cross-correlation analysis and discuss the possible explanation for these characteristics.

西部北太平洋地域の多くの国は熱帯低気圧（台風）の襲来に悩まされており、費用対効果の高い方法で台風の強度発達を予測することが強く求められている。近年の研究では、熱帯低気圧における雷放電の発生数が台風の強度発達と明確な相関関係があることが明らかになっている。そこで我々は、新規に自動気象・雷放電観測システム（V-POTEKA）を開発し、2017 年 9 月からフィリピン、グアム、パラオ、インドネシア、沖縄に配備し、西部北太平洋地域の雷活動を高い検出効率で継続的に観測するネットワークを構築してきた。V-POTEKA の雷放電電波観測データと到来時間差法を用いて雷放電の発生位置を 1 時間おきに自動推定するシステムを構築している。本研究では、2018 年から 2020 年の期間に西部北太平洋で発生した台風の強度発達と、V-POTEKA ネットワークで計測された台風領域内の雷活動との関係を比較し、両者にどのような相関関係があるかを明らかにすることを目的としている。2018 年から 2020 年の 3 年間に合計 81 の台風が発生したが、本研究では 46 の台風を選出し、雷活動と台風の強度発達との相関解析を実施した。 その結果、検出された雷イベント数と台風の強さ（最大風速（V_{max}）と最低気圧（P_{min}））の時間変化には明瞭な相関性が認められ（V_{max} で R=0.50、P_{min} で R=0.57）、雷活動と台風強度の発達曲線には明らかなタイムラグがあることが判明した（V_{max} で+33 時間、P_{min} で+36 時間）。また、弱い台風のタイムラグは、強い台風のタイムラグよりも小さくなることが明らかとなった。講演では、相関解析の結果を詳細に報告するとともに、このような関係性が生じる原因について議論する予定である。

R005-62
Zoom meeting C ：11/3 AM2 (10:45-12:30)
11:45～12:00

Scope and progress of ULAT/SATREPS project for extreme weather monitoring in Asia

#Yukihiro Takahashi[1)],Mitsuteru SATO[1)],Hisayuki Kubota[1)],Jun Matsumoto[2)],Algodon Meryl[1)]
([1]Hokkaido Univ.,[2]Tokyo Metropolitan Univ.

ULAT/SATREPS is for realizing precise real-time monitoring and issuing alert for extreme weather, such as torrential rainfall or typhoon. We are developing a ground observation network with lightning sensors and trying to establish semi real-time operation of micro-satellites to capture the typhoon and thunderstorms. In this project, we apply two technologies, 1) the lightning activity monitoring with the ground-based lightning networks with 12 sites for VLF radio wave measurement in nation-wide of Philippines and with 50 sites for electrostatic field measurement in Metro Manila together with infrasound sensor and automated weather station, and 2) the 3 dimensional capturing of thunderstorms by the on-demand operation of 50-kg micro-satellites. ULAT project was started in 2017 and the installation of the ground lightning observation station with automated weather station was completed by about 70 percent of the original plan and the continuous recording was started. About satellite observation, we succeeded in making detailed 3-D cloud structure model near the center of the typhoon with micro-satellite and aircraft. We plan to carry out the coordinated observation using the ground networks and micro-satellite for the quasi real time monitoring of extreme weather in the next summer season. This research was supported by Science and Technology Research Partnership for Sustainable Development (SATREPS), Japan Science and Technology Agency (JST) / Japan International Cooperation Agency (JICA).